AWARD NUMBER: W81XWH-11-2-0021

TITLE: "Threshold-Switchable Particles (TSP) to Control Internal Hemorrhage"

PRINCIPAL INVESTIGATOR: James H. Morrissey, Ph.D.

CONTRACTING ORGANIZATION: University of Illinois, Urbana, IL 61801-3620

REPORT DATE: December 2014

TYPE OF REPORT: Annual

PREPARED FOR: U.S. Army Medical Research and Materiel Command
Fort Detrick, Maryland 21702-5012

REPORT DOCUMENTATION PAGE

Form Approved
OMB No. 0704-0188

1. REPORT DATE	2. REPORT TYPE	3. DATES COVERED
December 2014	Annual	23 Nov 2013 - 22 Nov 2014

4. TITLE AND SUBTITLE

"Threshold-Switchable Particles (TSP) to Control Internal Hemorrhage"

5a. CONTRACT NUMBER

5b. GRANT NUMBER
W81XWH-11-2-0021

5c. PROGRAM ELEMENT NUMBER

6. AUTHOR(S)
James H. Morrissey, Rustem Ismagilov, Ying Liu, Galen Stucky,

and Christian Kastrup

E-Mail: jhmorris@illinois.edu

5d. PROJECT NUMBER

5e. TASK NUMBER

5f. WORK UNIT NUMBER

7. PERFORMING ORGANIZATION NAME(S) AND ADDRESS(ES)

UNIVERSITY OF ILLINOIS
GRANTS AND CONTRACTSOFFICE
506 S WRIGHT ST, 364 HENRY ADMIN BLDG
URBANA IL 61801-3620

8. PERFORMING ORGANIZATION REPORT NUMBER

9. SPONSORING / MONITORING AGENCY NAME(S) AND ADDRESS(ES)

U.S. Army Medical Research and Materiel Command
Fort Detrick, Maryland 21702-5012

10. SPONSOR/MONITOR'S ACRONYM(S)

11. SPONSOR/MONITOR'S REPORT NUMBER(S)

12. DISTRIBUTION / AVAILABILITY STATEMENT

Approved for Public Release; Distribution Unlimited

13. SUPPLEMENTARY NOTES

14. ABSTRACT

The final goal of this project is to develop smart particles to stop internal hemorrhage at local sites. Four collaborating laboratories are working together under this contract to define threshold levels of activators of blood clotting such that the candidate clotting activators will circulate in the blood at a concentration below the threshold necessary to trigger clotting, but accumulation of the activators at sites of internal injury/bleeding will cause the local concentration of clotting activators to exceed the clotting threshold and restore hemostasis. During the past year we have applied our improved methods for covalently attaching inorganic polyphosphate (a potent initiator and accelerator of blood clotting) to nanoscale solid supports including silica- and gold-based nanoparticles that have been fabricated using a variety of derivitization and passivation methods. We have conducted extensive testing of candidate procoagulant nanoparticles to quantify their ability to trigger and/or accelerate blood clotting and have made significant progress toward the goal of adjustable procoagulant activities of the particles to render them sub- or supra-threshold with regard to initiation of the clotting cascade.

15. SUBJECT TERMS
Internal hemorrhage; Bleeding; Blood clotting; Nanoparticles; Trauma

16. SECURITY CLASSIFICATION OF:			17. LIMITATION OF ABSTRACT	18. NUMBER OF PAGES	19a. NAME OF RESPONSIBLE PERSON
a. REPORT	b. ABSTRACT	c. THIS PAGE			USAMRMC
Unclassified	Unclassified	Unclassified	Unclassified	80	19b. TELEPHONE NUMBER *(include area code)*

Table of Contents

DECEMBER 2014 ANNUAL REPORT FOR WQ81XWH-11-2-0021:

"Threshold-Switchable Particles (TSP) to Control Internal Hemorrhage"

1. INTRODUCTION

The final goal of our research is to develop smart particles to stop internal hemorrhage at local sites. Our research comprises five collaborating laboratories working to develop new types of pro-hemostatic nanoparticles and to define threshold levels of these particles such that the candidate nanoparticles will circulate in the blood at a concentration below the threshold necessary to trigger clotting. On the other hand, when the particles accumulate at sites of internal injury/bleeding, their local concentration should exceed the clotting threshold and restore hemostasis. Our continuing approaches include the development and application of chemistries for attaching inorganic polyphosphate (polyP; a potent trigger and accelerator of blood clotting) to nanoscale solid supports, development of candidate nanoparticles with varying abilities to trigger and/or accelerate blood clotting, and defining the threshold levels under which these particles will or will not trigger blood clotting.

2. KEYWORDS

- Internal hemorrhage
- Bleeding
- Blood clotting
- Nanoparticles
- Trauma

3. OVERALL PROJECT SUMMARY

Comments on Administrative and Logistical Matters

Overview of subcontracts — Five laboratories now participate in this project, headed by Drs. James Morrissey (University of Illinois at Urbana-Champaign), Ying Liu (University of Illinois at Chicago), Rustem Ismagilov (originally at the University of Chicago; now at Caltech), Galen Stucky (University of California at Santa Barbara), and Christian Kastrup (University of British Columbia in Vancouver, BC, Canada.

No-cost extension — Relocating the Ismagilov lab to Caltech delayed progress on certain subtasks, so we obtained a one-year, no-cost extension of this proposal. Unfortunately, granting our request for the new subaward to Dr. Kastrup took over eight months, resulting in further unavoidable delays in this project. We therefore requested and received an additional, one-year, no-cost extension, resulting in a new expiration date of May 22, 2015.

Human Anatomical Substances use approval (Milestone #2) — Some of the studies to be conducted in Dr. Ismagilov's lab were designed to employ blood samples from human volunteer blood donors. Dr. Ismagilov obtained IRB approval from Caltech for these studies (RI-334, approved on December 5, 2011) and Dr. Ismagilov was notified on March 20, 2012 that the protocol was approved by the Office of Research Protections. During 2014, the Ismagilov concluded these studies with samples from human volunteers, and on 28 October 2014 submitted a request to close the protocol to the US Army Medical Research and Materiel Command (USAMRMC), Office of Research Protections (ORP), Human Research Protection Office (HRPO). The final report and supporting documents were reviewed by HRPO and found to be acceptable. The protocol was therefore closed in October 2014 and no additional studies with human subjects will be undertaken for the remainder of this project.

Scientific Progress

BACKGROUND

Inorganic polyphosphates (polyP) are linear polymers of phosphate monomers. Ubiquitous across a diverse range of organisms, its physiological function in humans and other complex eukaryotes has only recently been investigated in detail [1]. PolyP is secreted from activated blood platelets and research from the Morrissey lab and others has shown that polyP acts at various stages of the coagulation cascade, depending on its polymer length [2]. Long-chain polyP (>300 phosphates long) is a potent activator for the contact pathway of blood clotting, while shorter polyP polymers of 60-100 phosphate units (the size secreted by platelets) accelerate the activation of coagulation factor V and slow fibrin clot lysis [2, 3]. With its role now clearly established as a critical hemostatic agent within the body, polyP could potentially serve as a useful and safe procoagulant compound to address multiple bleeding disorders including internal hemorrhage.

When intravenously administered, nanoparticle therapies have been devised to target activated platelets with some success, but the goal of functionally delivering a procoagulant therapy to treat internal hemorrhage in practice has yet to be fully realized [4]. We are developing novel approaches for the targeted delivery of nanoparticles functionalized with controlled amounts of polyP. These tunable particles will then be able to selectively target sites of injury in response to appropriate stimuli such as a drop in temperature without the induction of clotting anywhere else in the body, a property that aqueous polyP unfortunately does not possess. Therefore, the overall goal of this study is to understand the process of particle-induced blood clotting, eventually leading to optimally engineered particles for treating internal bleeding.

Task 1 — Conduct spatially-defined numerical simulations to identify threshold conditions. The simulations will utilize Comsol Multiphysics modeling software to screen concentrations of activators and particles, reaction rates, temporal dynamics, shear and external fields.

To examine how localizing polyP onto surfaces affects thrombin generation, we used a two-dimensional numerical simulation that considered diffusion, convection, and the rates of 41 reactions of the coagulation cascade. An established kinetic model for the coagulation cascade [5] was used with the addition of $polyP_{>1000}$ in three reactions that were previously characterized in kinetic assays [2, 6-9]. PolyP (7.54 x 10^{-9} moles, 30 μM) was either spatially localized onto the surface of a cylindrical channel or dispersed throughout its volume. When polyP was localized onto the surface of the channel with a shear rate of 1 s^{-1}, the local thrombin concentration was 782-fold higher than when polyP was dispersed throughout the volume (1.83 x 10^{-8} M versus 2.34 x 10^{-11} M) (**Fig. 1A-B**). The difference in the concentration of thrombin generated can be attributed to the higher local concentration of polyp, which led to increased positive feedback from the coagulation cascade. However, simulations showed that the effectiveness of localizing polyP decreases as shear rate increases (**Fig. 1C**).

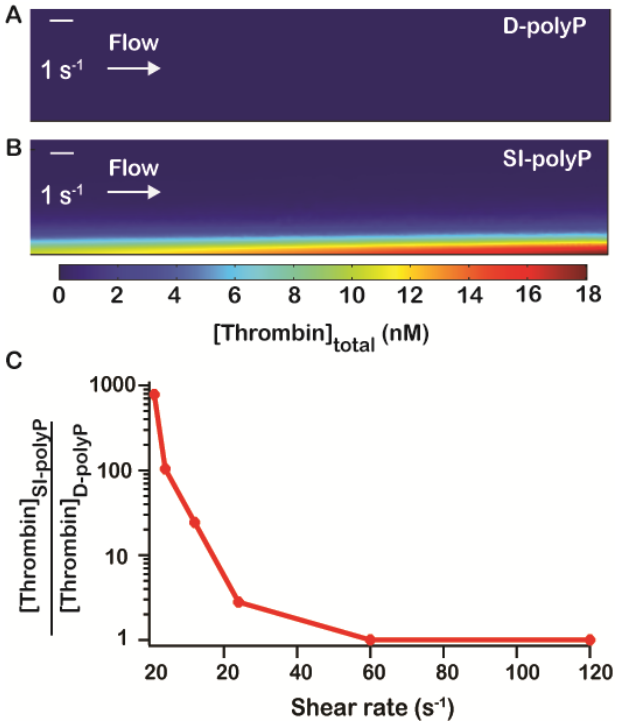

Figure 1. Localization of polyP accelerates thrombin production in the presence of flow. Two-dimensional numerical simulations of the human blood coagulation cascade, comparing the generation of thrombin by polyP dispersed throughout a cylindrical channel versus polyP immobilized on the channel surface. The overall number of polyP molecules was the same in all simulations (7.54x10^{-9} moles). (A) Plots show $[thrombin]_{total}$, the sum of [thrombin] and [meizothrombin], for a two-dimensional longitudinal cut of the cylinder from simulations where polyP was either dispersed throughout the volume or was immobilized onto the surface of the channel. $[Thrombin]_{total}$ was sampled at 500 s in both cases. (B) The fold difference in maximum [thrombin] generated when polyP is surface-immobilized versus dispersed at varying shear rates.

Simulation Methods: Thrombin generation was modeled using the *Transport of Diluted Species* module of Comsol Multiphysics 4.4 by adding diffusion and convection to a previously reported kinetic model by Chaterjee, et. al. [5]. The following modifications were made to the Chaterjee model: i) Reactions 28, 29 and 35 were omitted because our experiments did not include a thrombin detection agent, a surface that activates factor XII, or CTI; ii) Reactions 50-57 describe the fibrinolysis reactions and were omitted to conserve computational resources; and iii) three rate equations were added to describe the activation the clotting cascade by polyP [2, 6-9]:

Reaction 58: TFPI + polyP ↔ TFPI-polyP; k58_on = 1.0x10^{6} $M^{-1}s^{-1}$, k58_off = 1.0x10^{-2} s^{-1}
Reaction 59: V + Xa + polyP → Va + Xa + polyP; k59 = 2.0x1013 $M^{-2}s^{-1}$
Reaction 60: XI + IIa + polyP → XIa + IIa + polyP; k60 = 2.2x1010 $M^{-2}s^{-1}$

In the Chaterjee et al. model, rate constants were modified to include the effect of platelet activation using parameters ϵ and η. As our microfluidic experiments used platelet-poor plasma, these modifications to the rate constants were ignored and original literature values were used (columns 2-4

of Table 1 in reference [5]). The rate constants for the three extra polyP reactions were estimated from kinetic assays in references [2, 6-9].

The diffusion coefficient for all soluble species was 5 x 10^{-11} m^2/s and the velocity profile varied with the shear rate, $v_z(r) = \frac{\gamma_w R}{2}\left(1 - \frac{r}{R}\right)^2$, where v_z is the velocity in the axial direction at each radial coordinate r, R is the cylinder radius, and γ_w is the shear rate at the cylinder wall. The chemical species were flowed into a cylindrical geometry of radius 2 mm and length 20 mm at varying shear rates (1, 4, 12, 24, 60, 120 s^{-1}), and polyP reacted with the clotting factors as a species either immobilized on the surface of the cylinder or dispersed throughout its volume. For each shear rate, [thrombin] was sampled after the incoming flow had displaced the channel volume 12.5 times.

Task 2 — Conduct in vitro experiments to test recommended threshold conditions with human plasma and whole blood.

The local concentration of activators can profoundly influence their ability to initiate clotting of blood [10]. We hypothesized that short-chain polyP, when spatially localized, may be a more effective activator than previous reports suggest, capable of accelerating clotting of flowing blood. Initiation of blood coagulation is triggered when the local concentration of activators reaches a critical threshold, upon which the proteolytic cascade amplifies its enzymes to form a cross-linked fibrin mesh [11, 12]. The spatial localization of activators to surfaces effectively increases their local concentration, allowing coagulation to be triggered with less total amount of activator [13, 14]. Several activators have displayed this effect of spatial localization in microfluidic models of clotting, including tissue factor, bacteria that activate prothrombin and factor X, and glass [11, 15]. To clot blood flowing at higher shear, greater amounts of activator need to be localized in order to achieve a higher local concentration and/or a larger surface area of activators. High shear continuously strips catalytic surfaces of clotting factors being produced, impending and preventing clot initiation [16, 17]. Conversely, clotting can occur by lower local concentrations of activators in regions of low shear, where active enzymes can reach the threshold before transporting away [18]. Here we evaluated if spatially localizing polyP would enhance its ability to accelerate clotting. Short, polyP macromers near their limit of solubility were tested either in solution, or localized to surfaces or in nanoparticle formulations. Long polyP (>1000mer), which is less soluble as macromers in aqueous solution containing physiologic calcium concentrations [19], was also tested, comparing dispersed nanoparticles to surface-immobilized macromers. Acceleration of clotting was measured under flow, at various shear rates, using microfluidic channels.

We tested if surface-patterned polyP initiates clotting of both stagnant and flowing blood plasma. To determine if surface-immobilized polyP (SI-polyP) is able to clot flowing blood plasma, $polyP_{1000}$ was immobilized onto the walls of microfluidic channels (Fig. 2A). Half of each chamber was patterned with biotinylated lipids followed by an excess of streptavidin (Fig. 2B). Biotinylated-$polyP_{>1000}$ was then flowed through the channel, becoming immobilized onto streptavidin. The surface concentration of polyP was varied by diluting biotinylated-$polyP_{>1000}$ in a solution of biotinylated-polyethylene glycol (PEG) before coating the channel. The concentration of polyP was determined by staining it with DAPI. Fluorescence intensities from known concentrations of DAPI-stained soluble, dispersed polyP (D-polyP) were used to generate a standard curve, which was used to calculate the surface concentration of SI-polyP (Fig. 2C). The surface concentration of polyP was 300 $nmol/m^2$, and could be decreased to 60 $nmol/m^2$ by diluting with biotinylated-PEG. To test the ability of patterned polyP to initiate clotting, platelet-poor human plasma was flowed through the chambers. The plasma clotted selectively on areas with immobilized polyP (300 $nmol/m^2$) in 50-70 min at a shear rate of 1 s^{-1}. No clotting was observed over 5 hrs in channels without polyP (Fig. 2D,E).

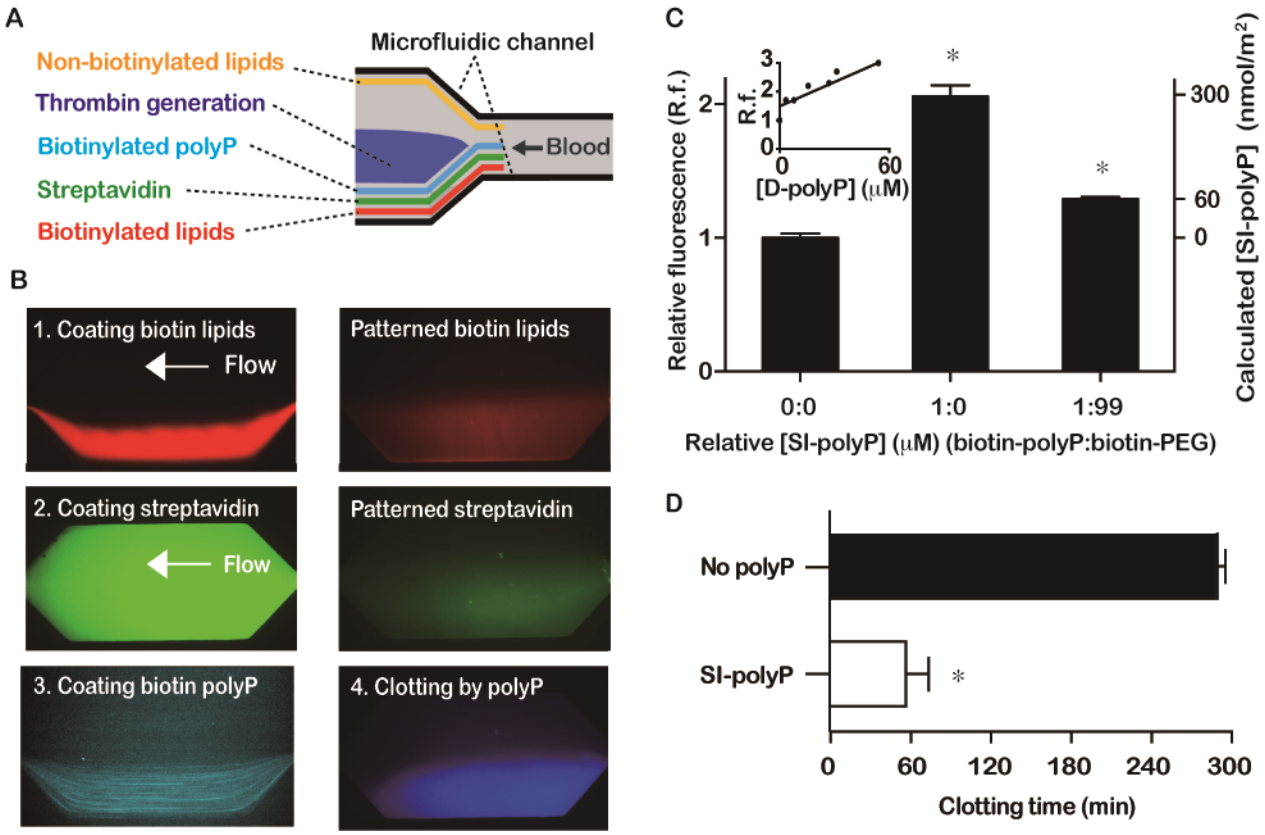

Figure 2. PolyP initiates clotting of flowing blood plasma when localized on a surface. (A) Schematic of biotinylated polyP (cyan) patterned onto the surface of half of a microfluidic channel, which initiates production of thrombin and clotting (blue) of flowing blood plasma (grey). (B) Images of fluorescent-labeled agents flowing and patterned along one side of a microfluidic channel. Biotinylated lipids (tagged red) self-assembled on the channel wall. Non-biotinylated lipids (not tagged in these images) were simultaneously flowed and patterned on the other side of chamber. Then, streptavidin (tagged green) was flowed through and bound to the biotinylated lipids, followed by flowing biotinylated polyP labeled with DAPI (cyan), which bound streptavidin. A substrate (blue) for thrombin was activated, indicating initiation of clotting, selectively on patterned $polyP_{>1000}$ (300 nmol/m^2). (C) Quantifying of the amount of surface immobilized polyP (SI-polyP) by measuring the fluorescence of DAPI bound to it. Channels with SI-polyP were compared to channels without polyP and to channels treated with polyP diluted with biotinylated PEG. Inset is a standard curve of known concentrations of solubilized polyP dispersed throughout the solution (D-polyP), which was used to calculate the surface concentration of SI-polyP in coated channels. (D) The clotting times of normal human plasma flowing through channels coated with $polyP_{>1000}$ at a shear rate of 1 s^{-1}. *p = < 0.01 compared to controls without polyP. Data indicate mean ± SEM, n = 3.

Task 3 — Design and test particles that will function as candidate TSPs.

Development of candidate nanometer- and micron-scale particles suitable for supporting TSPs: Research in the Stucky group focused on polyphosphate (polyP)-functionalized silica nanoparticles (SNP) (polyP-SNP) as a promising TSP candidate for delivering a large enough dose to activate coagulation in internal injuries. As previously discovered, the ideal SNP-polyP candidate uses roughly 70 monomer polyP provided by the Morrissey group to synthesize SNP-P70. The ideal concentration for minimizing clot time was approximately 0.25 mg/ml, though the clot time remains under 2 min for concentrations as low as 0.05 mg/ml SNP-P70. Below 0.05 mg/ml, the concentration was too low to significantly activate coagulation (Figure 3). In vitro blood clotting experiments were conducted on a thromboelastograph (TEG).

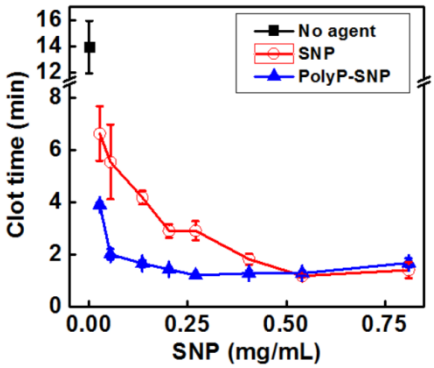

Figure 3 - Approximately 0.25 mg/ml was the ideal SNP-P70 concentration to minimize clot time as determined by in vitro blood clotting experiments using the TEG.

Using the reverse micelle method and the modified Stober method, the Stucky group was able to control the size of SNPs produced based on reagent ratios and synthesis conditions. This controlled synthesis ensured that SNPs post functionalization with polyP were within the desired size regime. In addition, we refined our synthesis protocol to prevent particle aggregation. For instance, smaller SNPs and storing the particles in solution (Figure 4) minimized aggregation. Nanoparticle size was determined by dynamic light scattering (DLS).

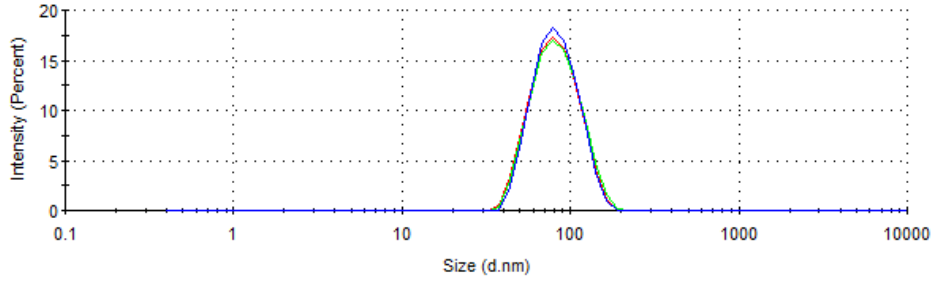

Figure 4 - Size of monodisperse SNPs determined to be 83.73 ± 26.03 nm by DLS with a polydispersity index (PdI) of 0.081. SNPs were synthesized by the modified Stober process in ethanol.

For functionalization with 3-aminopropyltriethoxysilane (APTES), the reaction required ethanol as a solvent. However, for reaction with polyP, peptides and other molecules in the functionalization effort required an aqueous environment. To create suspensions of monodisperse SNP in water, we dialyzed the SNP prepared n ethanol with water. Figure 5 showed that SNPs retained their monodispersity with a slightly smaller nanoparticle size due to the particle's interaction with is environment.

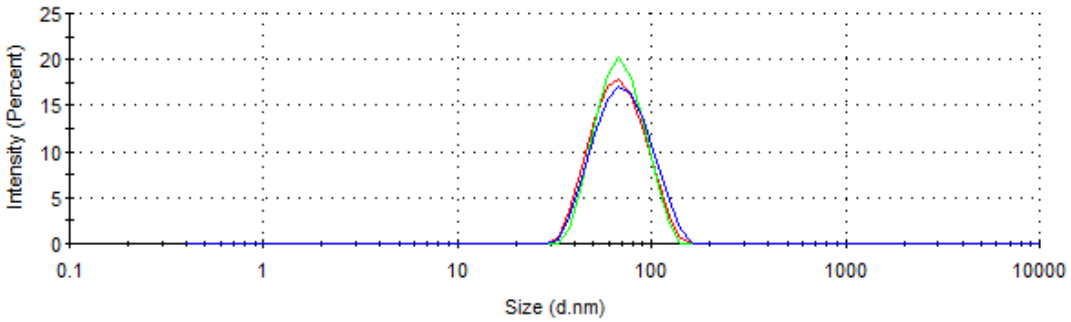

Figure 5 - Solvent exchange from ethanol to water retained the monodispersity of SNPs as determined by DLS. SNP size of 70.20 ± 21.14 nm was smaller in water than in ethanol due to the particle's interaction with its environment.

In addition to silica, the Stucky group looked at other oxide nanoparticle materials as polyP delivery platforms. In particular, we identified iron oxide (Fe_3O_4) nanoparticles as a potential nanoparticle carrier that is complementary to silica for our TSP. In contrast to silica, iron oxide particles are not as strongly procoagulant, which means the particles will not significantly activate the intrinsic pathway. Furthermore, iron oxide can be detected using magnetic resonance imaging (MRI) technology to track particle biodistribution within in the cardiovascular system. The main obstacle in using iron oxide nanoparticles was converting the particles from the organic solvent in which they were synthesized to a more biocompatible solvent, while retaining the small particle size. One method of preparing biocompatible iron oxide was to add poly(acrylic) acid (PAA) to the particles' surface. However, addition of PAA resulted in nanoparticle aggregation (Figure 4). A second method was to synthesize iron oxide in benzyl alcohol followed by solvent exchange to ethanol and then water through dialysis. The sample was then lyophilized. However, aggregation remained an issue. A third method was to synthesize iron oxide in an aqueous solution using hydrophobic micelles as templates, which greatly reduced nanoparticle aggregation (Figure 7). Characterization was conducted via transmission electron microsocopy (TEM) and DLS.

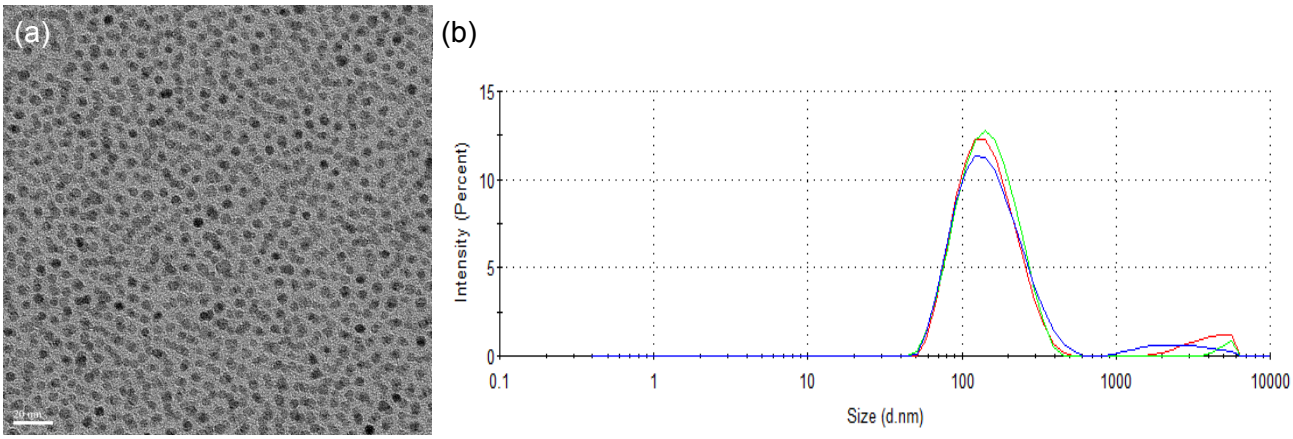

Figure 6 - (a) TEM image and (b) DLS characterization of iron oxide nanoparticles reacted in oleylamine and cyclohexane show nanoparticle aggregation and a size of 153.7 ± 66.53 nm, PdI 0.243.

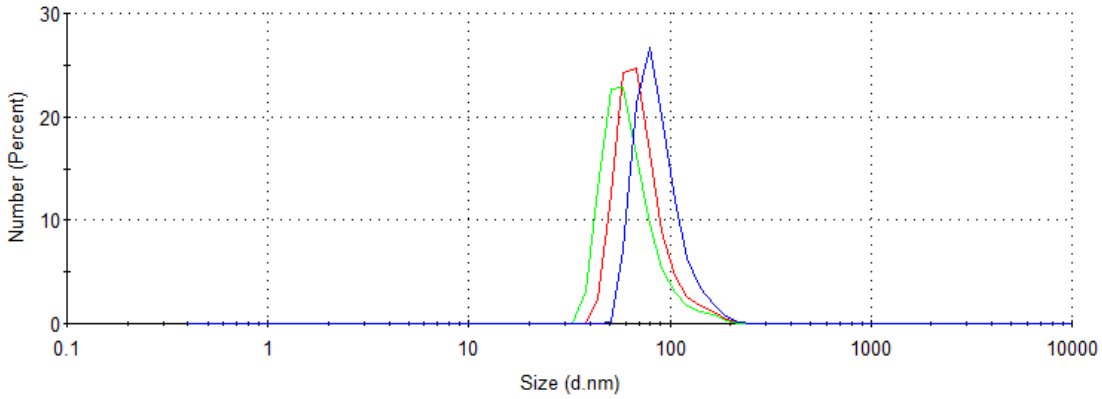

Figure 7 - Iron oxide particles (73.44 ± 24.93 nm, PdI 0.307) suspended in deionized water.

We then leveraged the properties of silica and iron oxide nanoparticles by synthesizing iron oxide nanoparticles of 5-6 nm that served as the core for the formation of a silica shell that surrounded the iron oxide particles. Based on transmission electron microscopy, the resulting iron oxide core-silica shell nanoparticles were 20-30 nm (Figure 8) in diameter. Taking into consideration the nanoparticles' zeta potential of -32.0 ± 1.76 mV (Figure 9), the hydrodynamic size of the nanoparticles in ethanol from DLS was 82.30 ± 6.00 nm and a polydispersity index of 0.122 (Figure 10). This formulation allowed for the benefits of the iron oxide to serve as a contrast agent for real-time tracking via MRI techniques, while allowing for the ease of subsequent functionalization steps that facilitate covalent binding of polyP. In addition, the silica shell maintained the biocompatibility of the TSP.

The iron oxide nanoparticles were synthesized using a standard microwave reaction procedure with reagents consisting of iron (III) acetylacetonate in oleylamine and oleic acid. The synthesized iron oxide nanoparticles were then added to silica nanoparticle precursor reagents for incorporation into the reverse micelle framework prior to the addition of tetraethyl orthosilicate to form the silica shell. This produced nanoparticles that were smaller than desired. We continue to modify the synthesis conditions and reagents to increase the size of the iron oxide core to 10-15 nm to maximize the contrasting properties of the material.

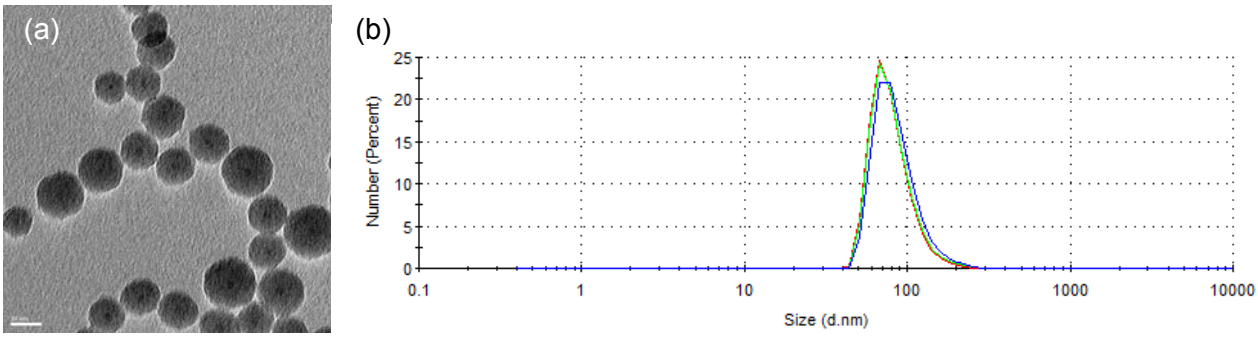

Figure 8 - (a) TEM image of 20-30 nm iron oxide core-silica shell nanoparticles (iron oxide core of 5-6 nm). (b) Size of iron oxide core-silica shell nanoparticles in ethanol characterized by DLS showed nanoparticles on average was 82.30 ± 6.00 nm. DLS results effected by nanoparticle interaction with the solvent and typically gives larger values than microscopy techniques.

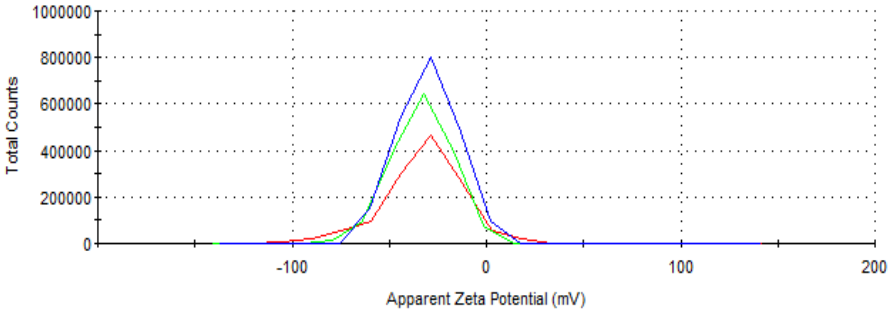

Figure 9 - Zeta potential for iron oxide core-silica shell nanoparticles in ethanol was -32.0 mV.

Development of procedures for chemically (covalently) attaching molecules that can trigger or enhance blood clotting (polyphosphate, tissue factor, etc.) to solid supports: Stucky group research continued using polyphosphate 70mer (P70) produced by the Morrissey group. The P70 was bound to the silica surface via the P-O-Si oxygen bridge. Our latest procedure was to develop a TSP with an SNP core and P70 corona via an APTES bridge and 1-ethyl-3-(3-dimethylaminopropyl) carbodiimide (EDAC) cross-linker by modifying previous Morrissey experiments [20, 21]. Among the potential benefits, use of APTES and EDAC allowed us improved control on the amount and mechanism by which polyP attached to the SNP (Figure 10). The core would be covered with P70 bound to the surface to produce a corona effect. This corona effect was designed to improve the TSP efficacy internally by preventing the SNP surface from initiating coagulation in healthy vessels. Instead, the sole procoagulant agent would be the short chain P70 exposed on the particle surface. As P70 is a clotting accelerator rather than an initiator, clotting would only occur at injury sites. If this design is successful, it would allow us to use exposed P70 in localized, non-compressible injuries as we work to improve a particle for general injection.

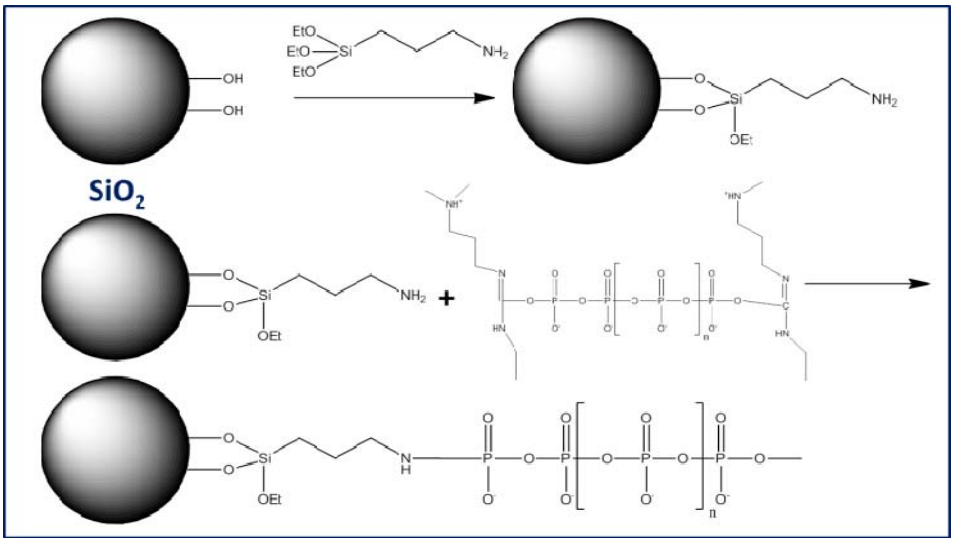

Figure 10 - Schematic of SNP core and P70 corona via an APTES bridge and EDAC cross-linker.

Characterization to confirm successful functionalization of SNP with APTES relied on the presence of the amine functional groups via Fourier Transform infrared spectroscopy (FTIR) and Raman spectroscopy. The modified Stober method was used to synthesis SNPs functionalized with APTES to result in the presence of the amine functional groups for further reaction with polyP. Figure

11 shows an FTIR transmission spectrum of SNP functionalized with APTES. Primary amines typically show two bands from 3400-3300 and 3330-3250 cm^{-1}, a peak from 1650-1580 cm^{-1}, and a peak from 910-665 cm^{-1}. The spectrum in Figure 11 show indications of primary amine bands from 3400-3300 and 3330-3250 cm^{-1} that may be partially eclipsed by the broad silica peak at 3276 cm^{-1}. The signals at 1636 cm^{-1} and 690 cm^{-1} are indications of the presence of primary amines. Follow-up characterization with longer scan times may improve resolution of the spectrum.

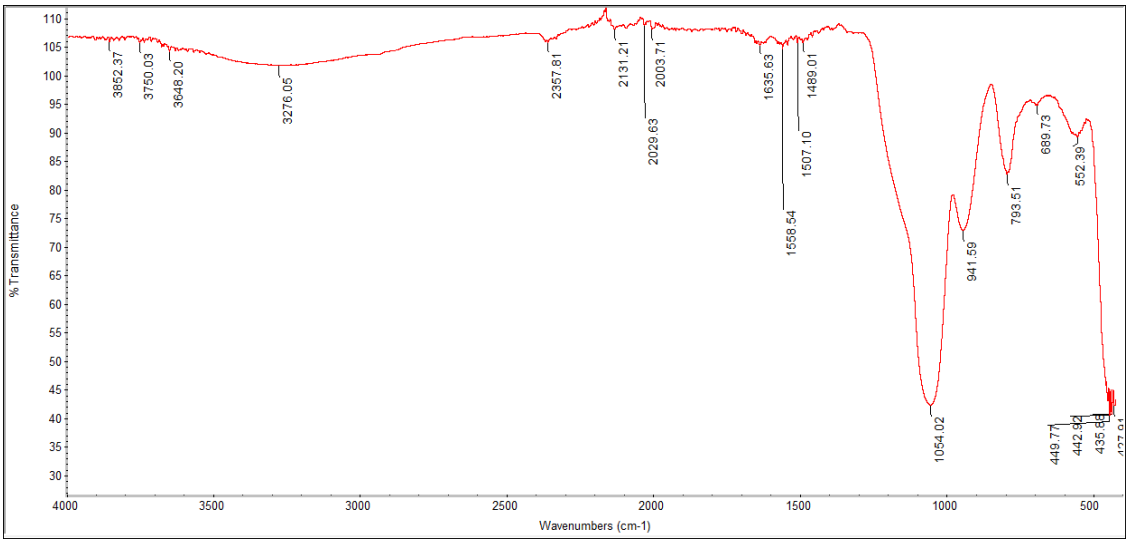

Figure 11. FTIR transmission spectrum of SNP functionalized with APTES resulting in the presence of primary amine signals.

In Raman spectroscopy, primary amines typically show peaks between 700-600 cm^{-1}, 1120-1030 cm^{-1}, 1640-1550 cm^{-1} and 3500-3100 cm^{-1}, indicating the presence of N-H bend and stretch signals, respectively. In our studies we saw peaks peaks within the 700-600 cm^{-1}, 1120-1030 cm^{-1}, 1640-1550 cm^{-1} ranges, and 3500-3100 cm^{-1} (Figure 12). Additional study is required to fully leverage the characterization benefits of Raman spectroscopy in confirming functionalization of SNP with APTES.

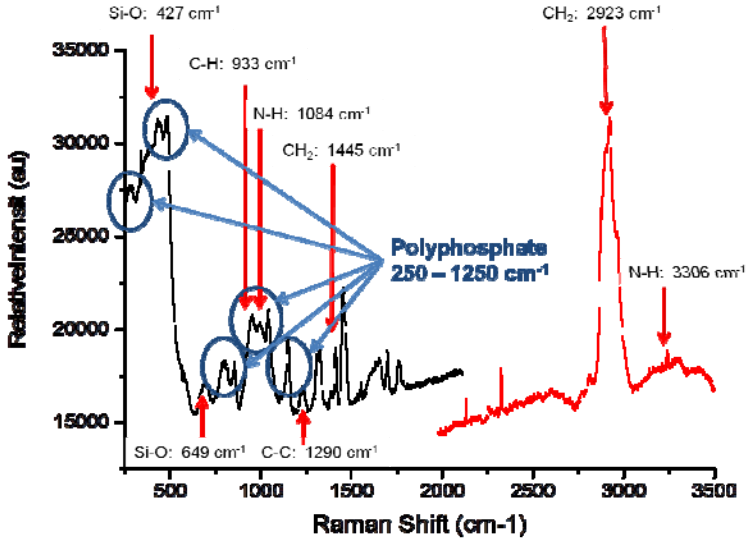

Figure 12 - Raman spectroscopy of SNP-P70 indicating covalent binding of polyP.

Using the Morrissey lab's strategy of esterifying polyP, we attempted a new method to attach polyP to inorganic oxides. In water, the surface oxygen atoms of inorganic oxides react to become OH groups, which readily react with esters. This strategy allowed us to attempt to cover the inorganic surface with a polyP "corona" without the use of the aggregation-inducing linker APTES. The strong negative value of - 36.2 ± 9.59 mV from zeta potential measurements via eletrophoretic light scattering (ELS) indicated the stable and successful incorporation of polyP (Figure 13).

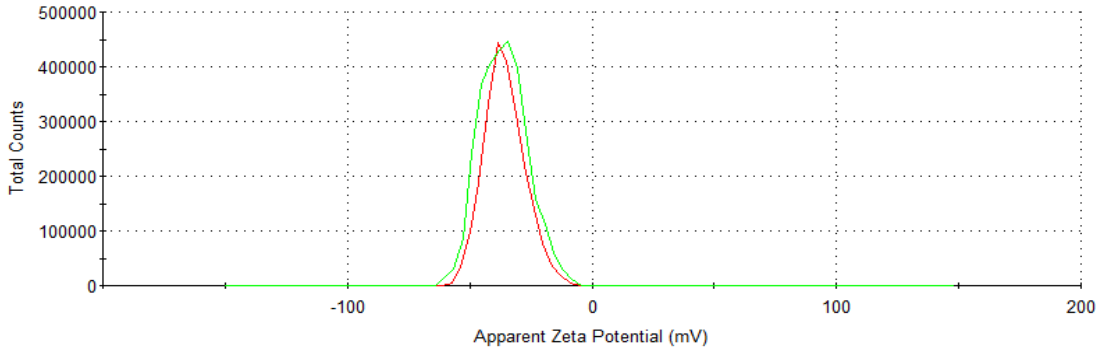

Figure 13 - Zeta potential of SNP-P70 ester particles (-36.2 ± 9.59 mV).

We also saw that iron oxide was amenable to functionalization with polyP using both the traditional Lewis acid mechanism (Figure 14), as well as by esterification. We intend to refine the esterification strategy to produce desired TSPs.

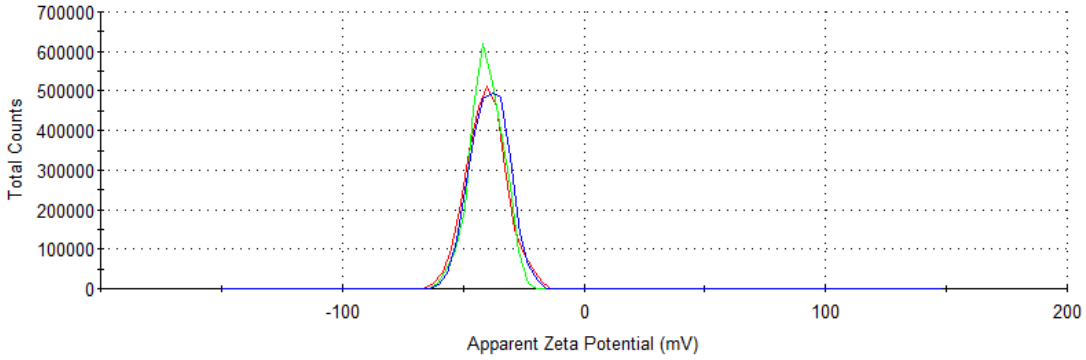

Figure 14 - Zeta potential of iron oxide nanoparticles capped with P70 using the traditional Lewis acid mechanism (-40.3 ± 8.20 mV).

In addition, control of APTES or 3-aminopropyltrimethoxysilane (APTMS) and EDAC allowed for quantitative characterization techniques and calculations that facilitate formulation refinement to develop effective TSPs. For instance, from carbon, hydrogen, and nitrogen analysis, we were able to determine quantitatively the actual ratio of APTMS bound to silica, and by x-ray photoelectron spectroscopy (XPS) (Figure 15), we were able to determine the relative amount of covalently bound nitrogen and phosphorus bound to the silica. Inductively coupled plasma provided us with the concentration of elemental silicon and phosphorus, which can be used to determine the ratio of polyP via phosphorus coverage of the silica nanoparticles. Malachite Green Assay can be used to provide quantitative information on the amount of phosphate present in the sample. All together, the characterization techniques and calculations can be used to corroborate and affirm our findings.

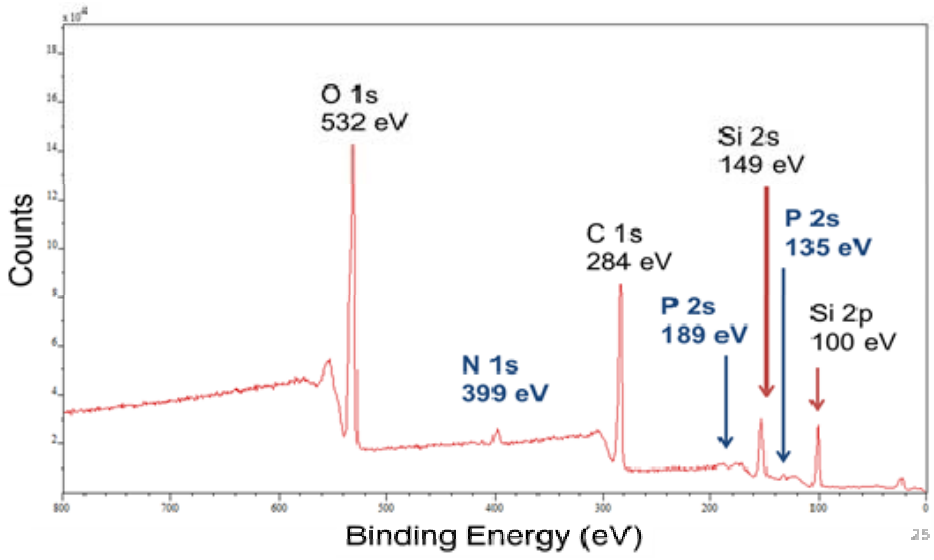

Figure 15 - XPS spectroscopy of an SNP-P70 sample confirming the presence of covalent binding.

Using the Morrissey lab's quantification techniques, we were able to determine the polyP loading on bare silica particles. The particles were digested in 1 M HCl and decanted to remove the silica from the phosphate-rich solution. The phosphate solution was then measured using ^{31}P NMR and inductively coupled plasma atomic emission spectroscopy (ICP-AES). ^{31}P NMR showed the qualitative presence of a phosphorous peak (Figure 16). ICP-AES quantitatively determined the concentration of PO_3 monomers per mg SNP between 20 µmol PO_3/ mg SNP, which corresponded to a range of roughly 100 – 200 polyphosphate molecules attached to each silica particle (Table 1-2).

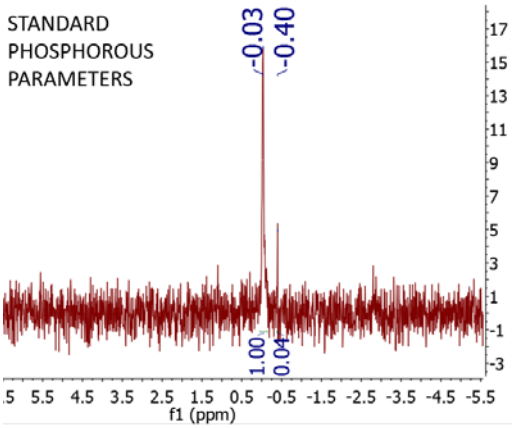

Figure 16 - ^{31}P NMR spectrum of digested polyP-SNPs shows evidence of phosphorous.

Table 1. Concentration of P (20x dilution) in a 170.35 mg polyP-SNP sample digested in 1 M HCl as measured by ICP-AES.

Element	Wavelength (nm)	Units	Avg	Std Dev	RSD
Phosphorous	177.495	ppm	1.574	0.0105	0.6675
Phosphorous	178.284	ppm	1.563	0.0038	0.2463
Phosphorous	178.766	ppm	1.56	0.0054	0.344
Phosphorous	213.618	ppm	1.565	0.0123	0.7855
Phosphorous	214.914	ppm	1.55	0.0066	0.4243
Average		**ppm**	**1.562**		

Table 2. Concentration of P (9x dilution) in a 79.10 mg polyP-SNP sample digested in 1 M HCl as measured by ICP-AES.

Element	Wavelength (nm)	Units	Avg	Std Dev	RSD
Phosphorous	177.495	ppm	11.06	0.0105	0.6675
Phosphorous	178.284	ppm	11.08	0.0038	0.2463
Phosphorous	178.766	ppm	11.08	0.0054	0.344
Phosphorous	213.618	ppm	11.06	0.0123	0.7855
Phosphorous	214.914	ppm	11.04	0.0066	0.4243
Average		**ppm**	**11.06**		

Attachment of clotting triggering/enhancing agents to particles: Previously, we showed that bare silica nanoparticles can be functionalized with a targeting peptide and polyethylene glycol (PEG) to protect the molecule from clotting in healthy vessels (Figure 17-18). We subsequently tested the same strategy with the SNP-P70 system. Aggregation remained the key issue. We used EDAC to bind P70 and APTES to limit aggregation via the cationic amine terminal on APTES and the anionic P70. Keeping the nanoparticle system in solution also resolved the aggregation issue.

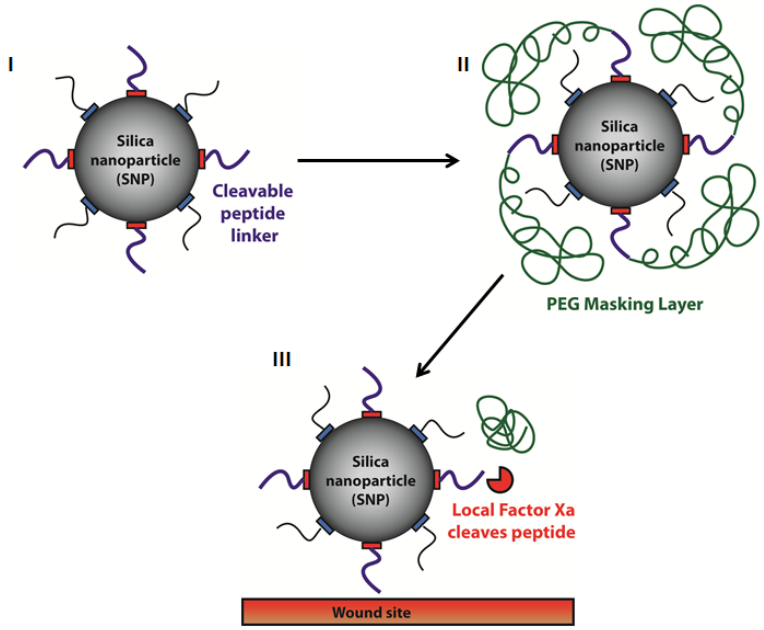

Figure 17 - I) TSP with peptide linker that cleaves at wound site. II) PEG masking layer protects TSP from clotting in healthy vessels. III) At injury site, the peptide is cleaved, PEG layer released and the TSP activates to accelerate clotting.

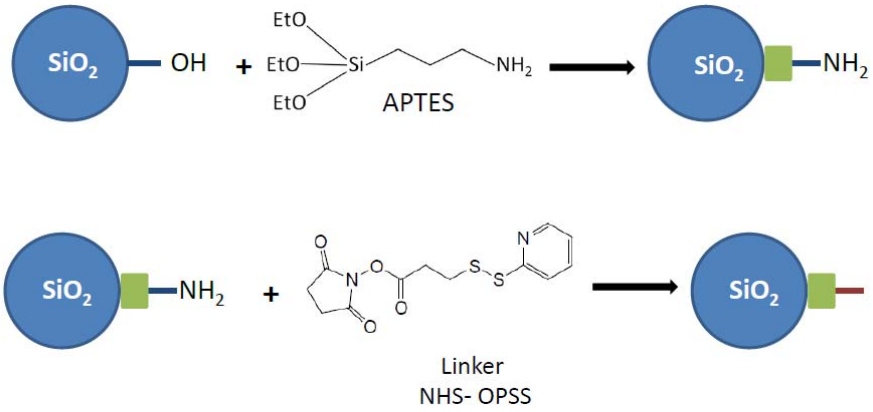

Figure 18 - Functionalization of the TSP with APTES and an NHS- orthopyridyl disulfide (OPSS) cross-linker. The peptide is attached to the TSP via the cross-linker. PEG is attached to the peptide to fully protect the molecule.

Using a SNP particle functionalized with APTES (SNP-APTES) (Figure 19), we were able to further functionalize the TSP to attach a peptide and polyethylene glycol (PEG) (Figure 20). After attaching the cross-linker, peptide and PEG molecules, the average particle size remained below 100 nm. The polydispersity index (PdI) increased slightly above 0.1. Once we are able to fully synthesize a TSP with PdI below 0.1 at all steps, we will add P70 to the TSP system. This allowed us to test the particles' targeting and clotting ability in vitro.

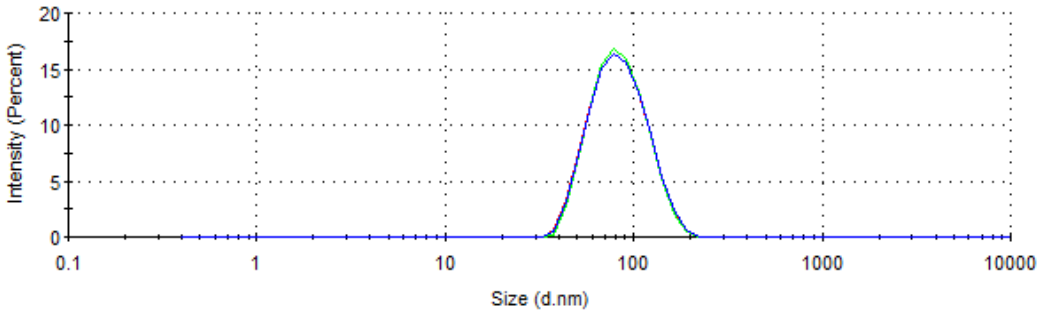

Figure 19 - Attachment of cross-linker to SNP-APTES caused minimal aggregation (86.21 ± 28.83 nm, PdI 0.133).

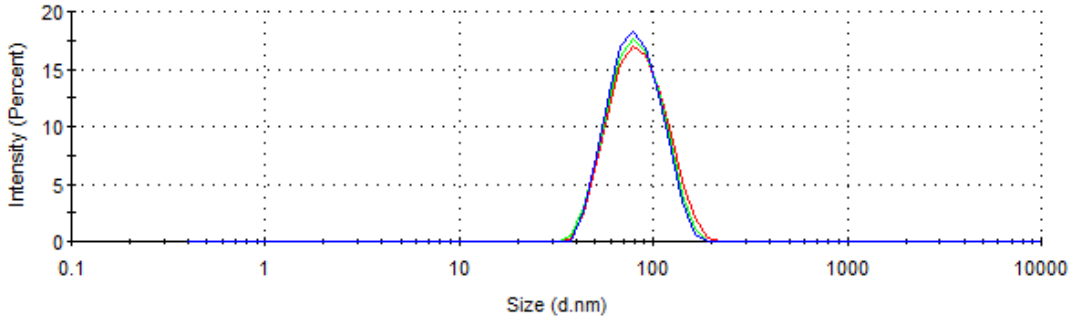

Figure 20 - Upon PEGylation, the fully-functionalized TSP remained approximately the same size (86.99 ± 27.85 nm, PdI 0.093).

In addition, based on the work of Ruoslahti and co-workers, we identified a new targeting strategy (Figure 20). Rather than placing the linker inside the PEG coating, we used a peptide that targets the physical clot to deliver the particles to the injury site. Ruoslahti and co-workers used the peptide Cys-Arg-Glu-Lys-Ala (CREKA) to bind iron oxide nanoparticles to fibrin in tumors. Using the same strategy, we can attach TSPs to the forming clot at the wound site and safely deliver polyP to more quickly seal the wound with stronger clots. Having attached CREKA to iron oxide, produced a strong positive charge, which allows it to bind to fibrin (Figure 22).

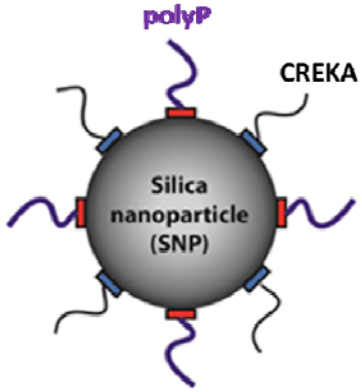

Figure 21 - Scheme for targeting internal injuries. CREKA is attached to the surface of the nanoparticle and targets fibrin to attach the particle to the physical clot. Once attached, polyP accelerates clotting activity at the wound site.

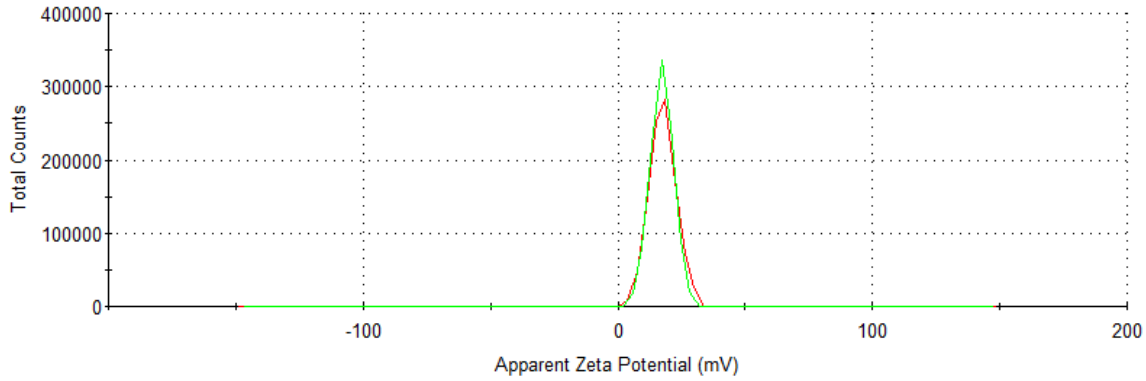

Figure 22 – Zeta potential (17.6 ± 5.21 mV) of iron oxide particles functionalized with CREKA.

Designing and testing of particles that can function as candidate TSPs: We showed that particles retain their clotting function even after months of storage at room temperature and pressure (Figure 22). The TSP is an improvement over polyphosphate, which must be frozen to remain effective.

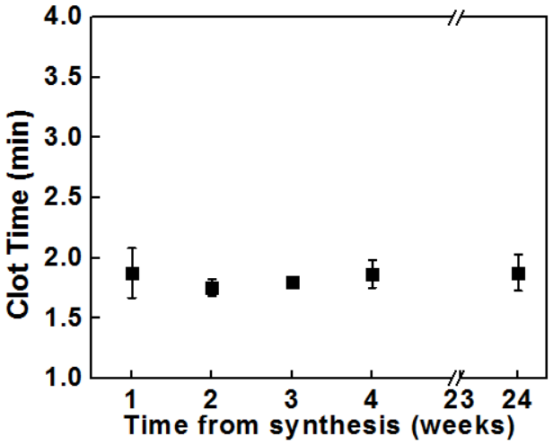

Figure 23 - SNP-P70 retained its procoagulant properties after months of storage at room temperature and pressure.

We tested the esterified SNP to determine their clotting activity in healthy and injured conditions. Particles suspended in water were considered healthy, while a phospholipid solution (PL) was used to mimic an in-progress clotting site. Ideally, the particles suspended purely in water would be within the recalcified range of 12-16 minutes, while the clot time would be lowered significantly in PL. In our initial tests, we found that the esterified particles in water clotted in approximately 9 min, while the clot time decreased to approximately 3 min in PL (Figure 24). This suggested that we have a potential TSP that minimally induces coagulation in healthy sites, while still accelerating coagulation at injury sites. We will continue to test the particles to increase the range between healthy (non-PL) and injured (PL) conditions to maximize safety.

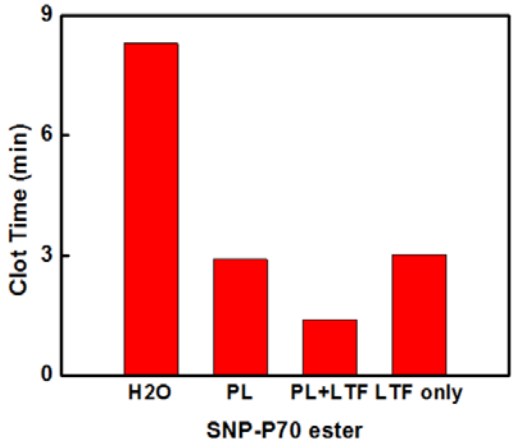

Figure 24 - SNP-P70 ester nanoparticles in water, in PL, in PL with tissue factor and tissue factor only with no nanoparticles.

The Stucky lab also conducted thrombin-generation assays using a pelleted version of SNP-P70 under static conditions (Figure 25-27). These experiments showed a slightly lower clotting time compared to that of SNP-P70 in solution. The results favored nanoparticles in solution when run

under static conditions. When attached to the well instead of in solution, the 100ul sample of plasma had less surface area to activate on a pelleted SNP-P70 than SNP-P70 in solution. This was the reason for the slightly lengthened thrombin generation times. We are working to test the pelleted nanoparticles under flow to better estimate their clotting activity. Under flow, the clustering simulated by pelleting the SNP-P70 particles should reach the threshold faster than particles in solution, which may never aggregate in a sufficient concentration to achieve coagulation. Only under flow conditions can we closely mimic *in vivo* conditions.

After testing the pellet concentrations at above coagulation-threshold concentrations, we moved to sub-threshold concentrations. In the dye tests, we verified that sub-threshold concentrations of SNP-P70 in solution did not lead to increased thrombin production. Using pellets, thrombin generation times were elongated but not as long as the same conditions in solution. The plate reader measured the average thrombin generation over a 100 ul sample.

To better identify local clotting, we attempted to recreate previous Ismagilov experiments on a fluorescence microscope. Using microscopy, we were able to identify local sources of thrombin generation within a plasma drop. At sub-threshold pellet concentrations, bright spots signify local sources of increased thrombin production and clot formation. Using the same analytical technique as the microfluidic experiments, we collected time-course images to generate thrombin curves. We found the threshold of SNP-P70 performance in solution to be close to 0.125mg/ml. We showed that clustered SNP-P70 at subthreshold (0.1mg/mL) concentrations outperformed 0.125mg/mL SNP-P70 solution.

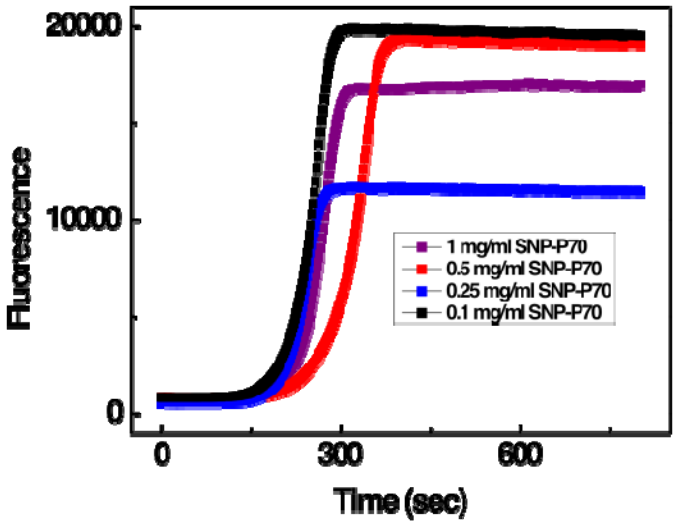

Figure 25 - Clotting assay of pelleted SNP-P70. SNP-P70 was dissolved in ethanol and evaporated overnight to attach to the well surface prior to experiment.

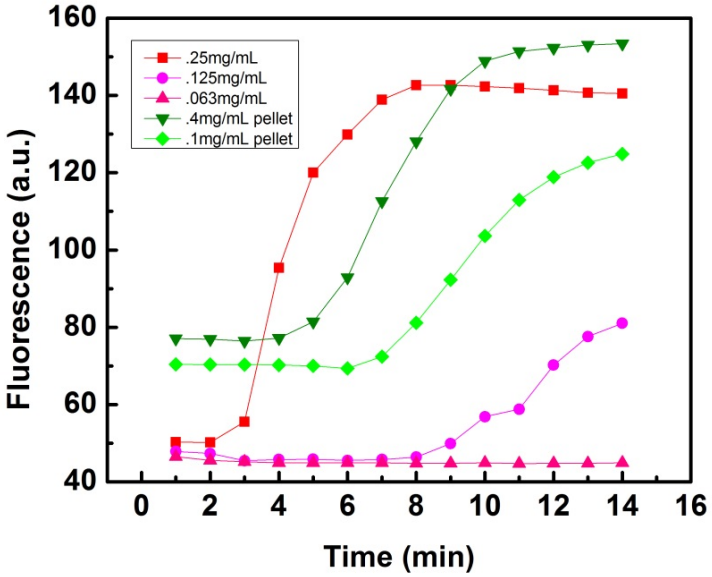

Figure 26 - Clotting assay of pelleted SNP-P70 by microscopy. SNP-P70 was patched onto a microscope slide via a 1 mm diameter by 250 µm height template prior to experiment.

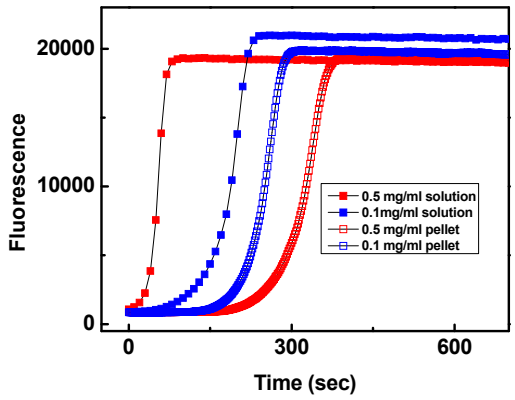

Figure 27 - SNP-P70 in solution generates thrombin faster than SNP-P70 pellets. The time difference decreases with decreasing concentration.

We also tested the iron oxide nanoparticles using TEG to determine their clot times. Iron oxide functionalized with CREKA at a concentration around 0.25 mg/ml minimized clot times (Figure 28). Iron oxide functionalized with polyP needed a much higher concentration around 1 mg/ml to minimize clot time (Figure 29). Our goal is to combine these strategies in the future to produce a particle capable of both accelerating coagulation and at the same time improving the strength of the physical clot that forms.

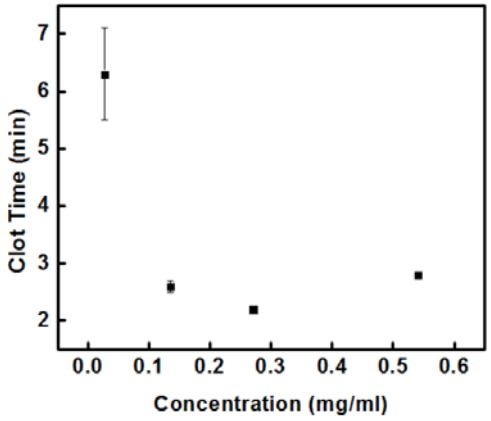

Figure 28 – Clotting Times of iron oxide particles functionalized with CREKA peptide. The ideal concentration is around 0.25 mg/ml

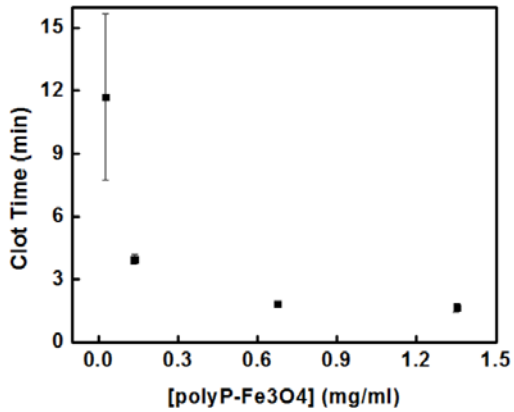

Figure 29 – Clotting Times of iron oxide particles functionalized with polyphosphate peptide. The concentration required to minimize clotting is higher than iron oxide functionalized with CREKA.

Systematic data collection allowed for determining trends and to conduct comparisons between the effectiveness of different functionalized types of inorganic nanoparticle carriers, such as silica and iron oxide; and to confirm that iron oxide core-silica nanoparticles exhibit the same clotting properties as silica nanoparticles. We also considered size and charge of the nanoparticles as a function of blood clotting ability in refining and determining the best nanoparticle system for TSPs. Table 3 provides blood clotting data for covalently bound SNP-P70 as a function of concentration. Clotting time decreased with an increase in concentration. The data is promising for use in determining the ideal concentration for this particular SNP-P70 nanoparticle system using ~ 50 nm SNPs. In determining the ideal TSP nanoparticle composition, we need to consider size and charge, as well as other properties unique to each formulation and type of inorganic nanoparticle.

Conc (mg/mL)	SP(min)	R(min)	K(min)	Angle(deg)	MA(mm)
10.4	7.0	7.7	2.0	62.5	26.4
10.4	8.1	9.2	3.6	46.4	27.7
20.8	6.7	7.2	1.8	65.3	28.8
20.8	6.2	6.9	1.8	63.7	26.4

Table 3 - TEG data showing blood clotting performance of covalently bound SNP-P70 nanoparticle composition.

We also began tested the clotting activity of iron oxide nanoparticles. Iron oxide particles do not induce clotting as well as silica and with only a minor initiation of clotting. Functionalizing iron oxide with PAA increased clotting times compared to no PAA (Figure 30). Upon addition of iron oxide-P70, the clotting time decreased at higher concentrations (Figure 31).

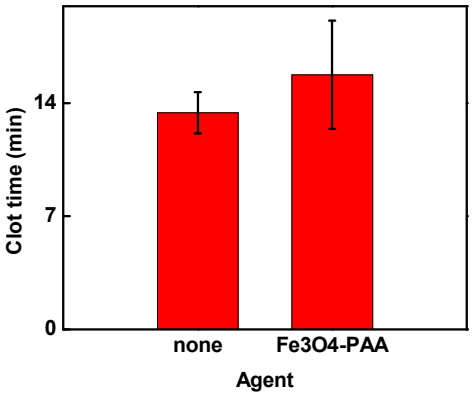

Figure 30 - Iron oxide particles functionalized with PAA increased clotting time compared to no PAA.

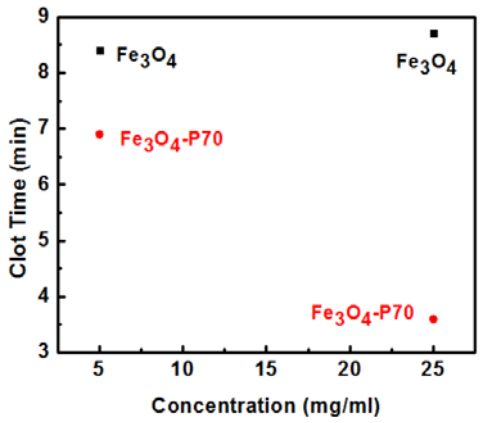

Figure 31 - Clotting activity of iron oxide nanoparticles and polyP iron oxide particles.

Preparation of "Artificial Dense Granules": PolyP is stored intracellularly almost without exception in condensed, spherical granules surrounded by a phospholipid bilayer measuring approximately 250 nm across [22]. Maintained within the organelle membrane are protein transporters, like Ca^{2+} and H^+ ATPases and Ca^{2+}/H^+ and Na^+/H^+ exchangers, whose sole function is to maintain a mildly acidic environment and sequester alkali and alkali earth metals within the granule, especially Ca^{2+}, Mg^{2+}, Na^+, and Zn^{2+}, at concentrations many times higher than that encountered in the cytosol or in the extracellular medium [23]. Docampo and colleagues were the first to extensively characterize these electron-dense phosphate bodies in trypanosome protozoans, including human pathogens [23]. These calcium-sequestering subcellular compartments, or *acidocalcisomes [23]*, were soon demonstrated to be ubiquitous in both prokaryotic and eukaryotic organisms alike [22]. Ruiz et al. established that the acidocalcisome has been largely evolutionarily conserved even in complex mammals, taking the shape of the human platelet dense granule [24].

The striking ubiquity of this granular organelle is no coincidence as we have established that the self-assembly of PolyP granules is thermodynamically spontaneous in aqueous media containing biological concentrations of divalent and polyvalent metal ions [25] such as Ca^{2+} and Mg^{2+}. Moreover, the granular PolyP nanoparticles (NPs) retain the powerful procoagulant effects of their molecularly dissolved counterparts, as they maintain their colloidal integrity both in aqueous buffer and albumin suspension for hours, time scales more than sufficient to induce clotting. **Scheme 1** shows that the nanoprecipitation is a thermodynamically reversible process.

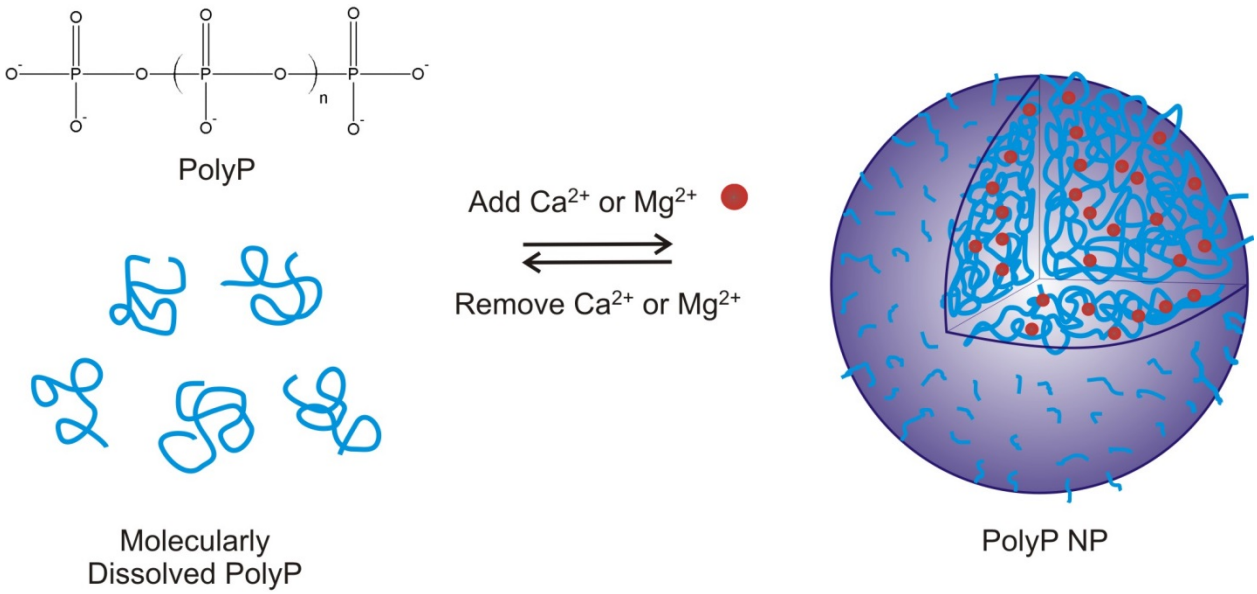

***Scheme 1**. Molecularly dissolved polyP spontaneously precipitates into granular nanoparticles upon addition of calcium or magnesium ions. The precipitation of polyP could be conceived as an equilibrium process with the binding affinities of the metal ions to monoP governing the polymer's precipitation.*

The solubility of polyP under different precipitative conditions and as a function of polymer chain length was invesitgated in the Liu lab using dynamic light scattering (DLS). Similar to calculating the critical micelle concentration (CMC) of surfactants, phospholipids, copolymers, and other amphililic moieities, the scattering intensity begins to increase when polyP self-assembles into nanoparticles (NPs). **Figure 32A** shows the scattering intensity of polyP1000+, commonly found in bacteria, in the presence of biologically relevant concentrations of mono- and divalent metal ions. At 1.2 mM $CaCl_2$, equivalent to the free ionic calcium concentration in human blood plasma, polyP1000+ begins to precipitate at ~23 μM polyP (with the polyP concentration given in terms of the

concentration of phosphate monomer). Increasing the calcium concentration to 5 mM, typical of levels used in *in vitro* cogulation assays, reduces the polyP solubilty to 4.3 μM. Physiological amounts of ionic magnesium have a synergistic effect on polyP nanoprecipitation, with its solubility decreasing by ~60% when combined with 1.2 mM $CaCl_2$. Biologically relevant amounts of monovalent ions like Na^+ and K^+ exert negligible precipitative effects. **Figure 32B** shows the scattering intensity of polyP in 5 mM $CaCl_2$ as a function of polymer length. Bacterial polyP (polyP1000+) precipitates most robustly, while platelet-sized polyP (polyP80) remains molecularly dissolved at much higher monophosphate (monoP) concentrations, precipitating at 78 μM. Intermediate length polyP (polyP250) starts to precipitate at roughly double the solubility concentration of polyP1000+. **Figure 32C** shows the solubilities of three polyP chain lengths (80, 250, 1000+) at different precipitative conditions calculated by finding the intersection of the two regimes representing: (1) molecularly dissolved polyP; and (2) polyP NPs.

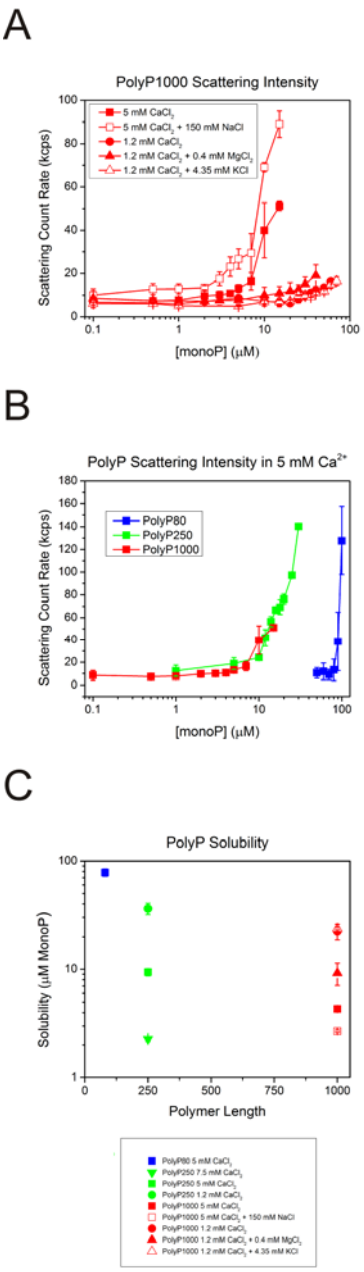

Figure 32. Solubility of polyP as revealed by DLS. *A*: **The precipitative effects of different metal cations on very long chain polyP**. Divalent metal cations such as Ca^{2+} and Mg^{2+} cause polyP1000+ to robustly nanoprecipitate at physiological concentrations, as evidenced by the steep rise in the scattering intensity count rate, whereas monovalent cations such as Na^+ and K^+ at biologically relevant concentrations exert negligible effects on the polymer's solubility. *B*: **5 mM $CaCl_2$ wields divergent precipitative effects on polyP depending on the polymer length.** polyP1000+ precipitates most robustly with a steep rise in scattering intensity at 4.3 μM monoP concentration. PolyP250 is more soluble than polyP1000+, with the count rate increasing near 9.4 μM. Platelet-size polyP (polyP80) is more soluble than both very long- and intermediate-chain length polyP, with the scattering intensity markedly increasing at a monoP concentration almost a magnitude higher than polyP250. *C*: **Solubility of polyP of different polymer lengths.** PolyP's solubility in various aqueous salt solutions buffered with 8 mM Tris·HCl, pH 7.4 plotted against polymer length in monoP units. There is a strongly non-linear relationship, with very long chains (i.e. polyP1000+) being much more readily precipitated than shorter polymers, e.g. polyP80. Divalent metal cations like Ca^{2+} and Mg^{2+}, which are known to chelate strongly to phosphate-containing compounds, exert precipitative effects at biologically relevant concentrations, while monovalent ions such as Na^+ and K^+ induce little or no significant effects on polyP's solubility.

PolyP nanoprecipitation was further explored using other divalent and polyvalent precipitative ions. **Figure 33** shows a representative, intensity-weighted particle size distribution of 125 μM polyP1000+ NPs precipitated in 5 mM $MgCl_2$, pH 7.4. The precipitation yields a monodisperse particle population with an average effective diameter of 180 nm, roughly equivalent to 5 mM $CaCl_2$. Precipitation as a function of cation valency was subsequently investigated using iron salts. 50 μM polyP1000+ was precipitated in 5 mM $FeCl_2$ and 5 mM $FeCl_3$ (**Figure 34**). Both precipitating conditions yielded bimodal particle populations. However, increasing cation valency led to bigger precipitates.

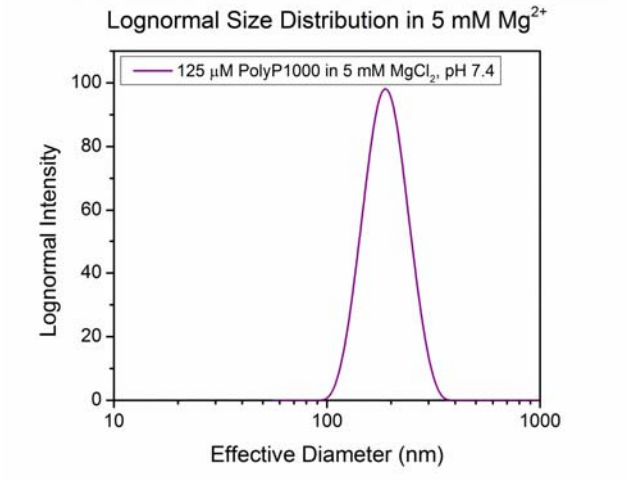

Figure 31. **Lognormal particle size distribution of polyP1000+ in 5 mM Mg^{2+} only**. 125 μM polyP1000+ was precipitated in 5 mM $MgCl_2$, 8 mM Tris·HCl, pH 7.4 in the absence of ionic calcium, yielding monodisperse nanoparticles approximately 180 nm in diameter, comparable to polyP precipitates synthesized in 5 mM $CaCl_2$ alone. Interestingly, polyP305 and polyP80 could not be precipitated at equivalent monoP and Mg^{2+} concentrations, implying that ionic magnesium's influence on polyP precipitation is an even more highly nonlinear function of polymer size in relation to calcium's exerted effects (data not shown). Moreover, polyP1000+ could not be precipitated at 0.4 mM $MgCl_2$, pH 7.4 (ionic [Mg^{2+}] in blood) (data also not shown).

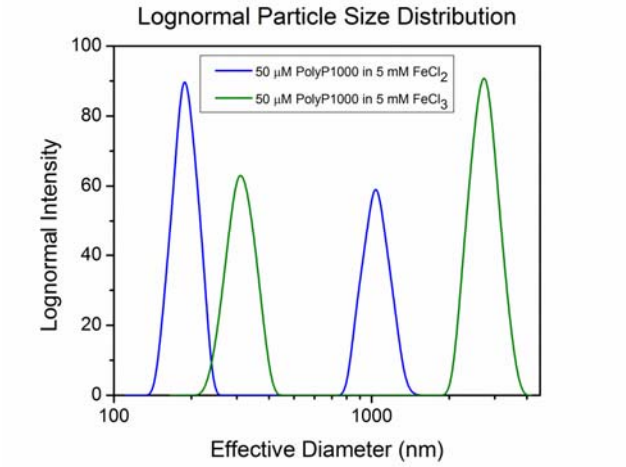

Figure 34. **Particle size distribution of polyP1000+ precipitates in Fe^{2+}/Fe^{3+}**. 50 μM polyP1000+ was precipitated in DI H_2O, pH 5.4 with either 5 mM $FeCl_2$ or 5 mM $FeCl_3$. Both conditions lead to bimodal particle populations. In the case of Fe^{2+}, there are particles approximately 180 nm in diameter, with a smaller population approximately one micron in diameter. Fe^{3+} produces particles that are several hundred to several thousand nanometers in size, suggesting that increasing cation valency leads to bigger precipitates.

PolyP is stored across all phylogenetic taxa under mildly acidic conditions in condensed form [22]. In order to investigate this phenomenon, the solubility of platelet-sized polyP was determined using DLS at pH 7.4 (resembling blood plasma) and pH 5.4 (resembling the environment in human platelet dense granules). Suprisingly, the scattering intensity profiles were nearly identical for both cases (**Figure 35**). Organisms must therfore store polyP at acidic pH for reasons that have not yet been fully elucidated. **Table 4** shows the calculated solubilty of polyP as a function of chain length and pH at 5 mM $CaCl_2$.

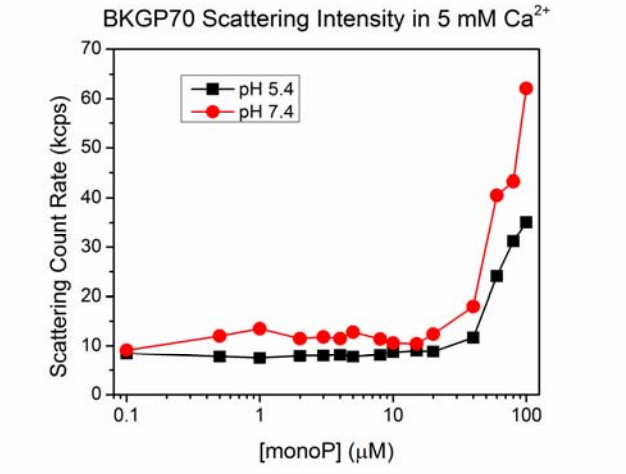

Figure 35. Scattering intensity of heterodisperse, platelet-sized polyP ("BKGP70," range 20-125 phosphate units) in 5 mM $CaCl_2$ at pH 5.4 and 7.4. The scattering intensity begins to rise at roughly the same concentration, even though the overall scattering count rate is slightly higher at pH 7.4.

Table 4. Solubilities of polyP in 5 mM $CaCl_2$ (aq) based on pH and polymer length.

PolyP Polymer Length (Range)	Solubility (μM) in 5 mM CaCl2, pH 7.4 ±S.D.	Solubility (μM) in 5 mM $CaCl_2$, pH 5.4
PolyP80 (76-84)	78±6	--
BKGP70 (20-125)	34.5	33.8
PolyP250 (100-390)	9.4±0.7	--
PolyP1000+ (>1000)	4.3±0.1	--

The stability, particle size distribution, and scattering intensity were therefore investigated at the two pH conditions in order to determine the basis for why organisms store condensed polyP under mildly acidic conditions. 125 μM polyP1000+ was precipitated in 5 mM $CaCl_2$ at pH 5.4 and 7.4 (buffered with 8 mM Tris·HCl). The stability of the granular NPs was monitored by DLS for 1 hr. The polyP NPs manifest the same Ostwald ripening growth kinetics (**Figure 36A**), with the NPs at physiologic pH being slightly bigger (possibly due to the pK_a of polyP). However, the scattering intensity decreases significantly at pH 7.4, while at acidic pH it is stable (**Figure 36B**). The scattering intensity is a means to approximate the number of particles in a colloidal dispersion, as nanoparticles scatter light as a nonlinear function of their radius. A drop in the scattering count rate implies that particles have sedimented to the bottom or redissolved. Therefore, it appears that organisms store condensed polyP under acidic conditions because the colloid (or perhaps the polymer itself) is more stable. **Figure 37C** shows the polydispersity index (PDI) of the polyP1000+ NPs. The PDI is extremely low against any rigorous standard, comparable to, or better than, commercial colloidal standards.

A

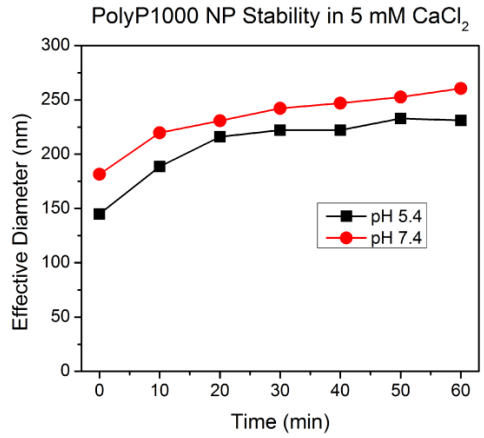

B

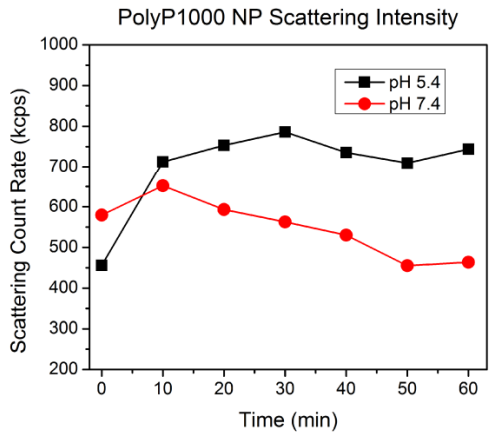

C

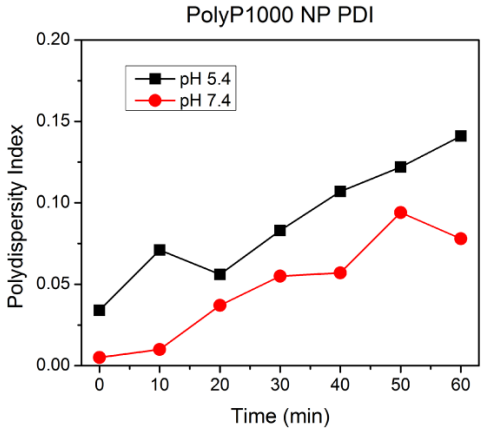

Figure 36. *A:* **Stability of polyP1000+ NPs in acidic and basic conditions.** 125 μM polyP1000+ was precipitated in 5 mM $CaCl_2$ in DI H_2O, pH 5.4 or 8 mM Tris·HCl, pH 7.4. Both precipitating conditions lead to initial particle diameters of 150-200 nm and manifest typical power law growth kinetics. The initial difference in size may be due to polyP's pKa. *B*: **Scattering count rates at pH 5.4 and 7.4**. The scattering count rate increases in the first 10 min then stabilizes at acidic pH, while at blood's pH the count rate marginally decreases. *C*: **Polydispersity index of polyP1000+ NPs at pH 5.4 and 7.4**. The polydispersity index (PDI) in 8 mM Tris·HCl, pH 7.4 is exceedingly low, comparable to colloidal standards, remaining less than 0.10 after 1 hr. The particles are slightly more polydisperse at acidic pH.

PolyP250 was chosen as a model polymer length to investigate the colloidal stability of granular polyP NPs in conditions approximately the environment in human blood plasma. 125 μM polyP250 was precipitated in 8 mM Tris·HCl, pH 7.4 containing 1.2 mM and 5 mM $CaCl_2$, respectively. The stability of the granular NPs was then monitored every 5 minutes for 1 hr using DLS (**Figure 37A**). The initial effective diameters of the polyP NPs are approximately 50 nm and 160 nm for 1.2 mM and 5 mM $CaCl_2$, respectively. The aggregation behavior of both are characterized by power law growth kinetics typical of metastable polymeric nanoparticles. In order to more closely resemble the physiological environment, the stability of polyP NPs was studied in the presence of bovine serum albumin (BSA), the most abundant protein in blood plasma, possessing critical regulatory and homeostatic functions including the buffering of blood pH and the chelation of divalent metal ions including Ca^{2+}. 125 μM polyP250 was again precipitated in 5 mM $CaCl_2$, 8 mM Tris·HCl, pH 7.4 and mixed 1:1 (v:v) with 70 mg/ml BSA with and without calcium saturation (**Figure 37B**). The final ionic calcium and serum albumin concentrations were therefore identical to those in human blood plasma. In both instances, the effective diameter drops from approximately 160-170 nm to 100 nm immediately. This rapid change in the effective diameter is not due to multiple scattering effects or changes in dispersion viscosity. In the case in which BSA is not saturated with $CaCl_2$, the effective diameter of the polyP NPs continues to drop, being approximately 50 nm after 3 hrs. However, if the BSA is first saturated with 2.5 mM $CaCl_2$ for 24 hrs beforehand, the polyP NPs only change negligibly in size, being about 80 nm after 3 hr. **Figure 37C** shows the intensity-weighted particle size distributions for polyP NPs in BSA with and without calcium pre-equilibration. The two small peaks are the BSA monomer and multimer, while the large peak must be the polyP NPs. The two small peaks increase in size after polyP addition, suggesting that a polyP-BSA complex has formed. A possible explanation for this phenomena, characterized first by a rapid shrinkage upon addition to the BSA suspension, followed by a gradual decrease in the effective diameter, is centered on BSA interacting directly with the polyP NPs, via direct electrostatic binding to the protein's cationic residues or competitive Ca^{2+} chelation, with BSA's dissociation constant for calcium possibly being lower than polyP's K_D. However, much more work needs to be done to corroborate these findings.

A

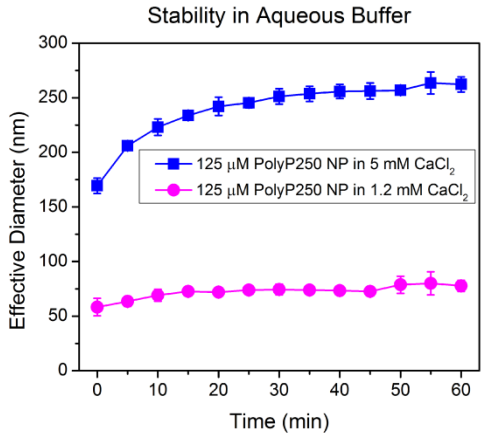

B

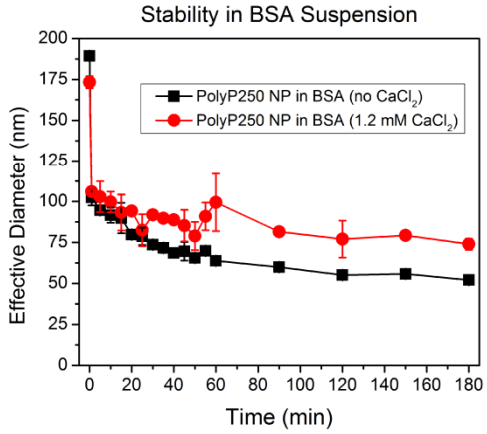

C

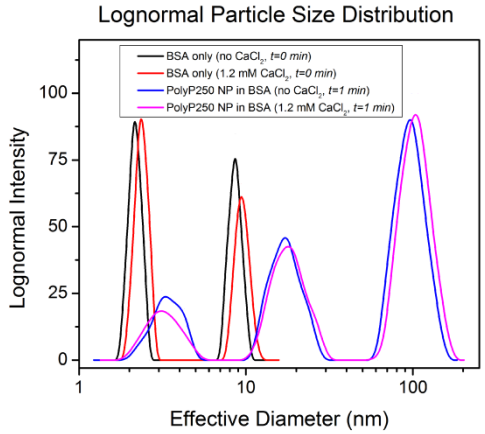

Figure 37. **PolyP nanoparticle stability.** *A*: **polyP250 nanoparticle stability in aqueous buffer.** 125 μM polyP250 was nanoprecipitated in 8 mM Tris·HCl, pH 7.4 containing 1.2 mM or 5 mM $CaCl_2$. Average effective diameter was assessed every five minutes for one hour, a typical timescale for a bleeding event. At 5 mM $CaCl_2$, the initial particle diameter was 169 nm and slowly grew to be approximately 260 nm after one hour. At 1.2 mM $CaCl_2$ the particles were initially 58 nm and steadily increased to ca. 80 nm. The growth behavior of both suspensions appears to follow power-law kinetics typical of many metastable colloidal dispersions. *B:* **PolyP250 nanoparticle stability in suspensions containing BSA.** 125 μM polyP250 was precipitated in aqueous buffer containing 5 mM $CaCl_2$ as described previously and then mixed 1:1 (v:v) with 70 mg/ml BSA suspension buffered to pH 7.4 with or without 1.2 mM $CaCl_2$. Final BSA and $CaCl_2$ concentrations were 35 mg/ml and 1.2 mM, respectively. In both cases, the polyP250 NPs shrank from approximately 170-180 nm before mixing with the BSA solution, to 100 nm immediately after mixing with the BSA solution. This was not due to changes in dispersion viscosity or multiple scattering effects. After 3 hours, the polyP NPs in BSA without $CaCl_2$ equilibration shrank to approximately 50 nm in diameter, while the NPs in the BSA equilibrated with 1.2 mM $CaCl_2$ were roughly the same size (ca. 80 nm). It is hypothesized that BSA may be initially forming a complex with polyP (the rapid shrinkage upon addition to the suspension) and then competitively binding Ca^{2+}, unless it has been pre-equilibrated. *C*: **Lognormal size distributions for (1) BSA suspension without Ca^{2+} pretreatment; (2) BSA suspension with 1.2 mM $CaCl_2$; (3) immediate addition of polyP 250 NPs in 35 mg/ml BSA without $CaCl_2$ pre-equilibration; and (4) immediate addition of polyP 250 NPs in 35 mg/ml BSA with 1.2 mM $CaCl_2$.**

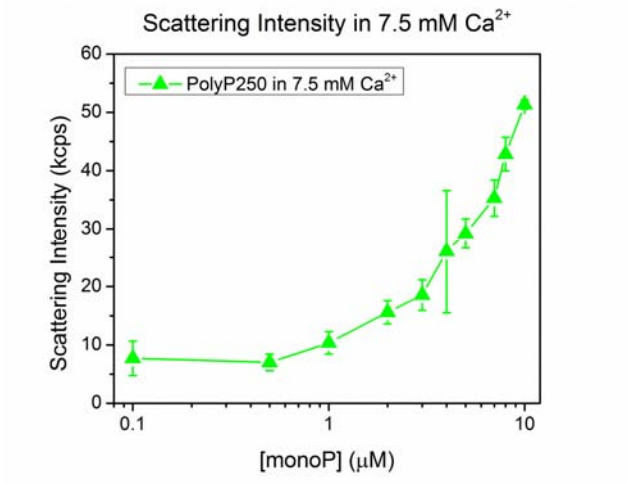

Figure 38. **Scattering intensity vs. monoP concentration for Poly250 in 7.5 mM $CaCl_2$, 8 mM Tris·HCl, pH 7.4.** The solubility was calculated to be 2.27±0.12 μM.

Table 5. **Absence of multiple scattering effects in BSA suspensions containing polyP**. The effective diameter of 125 μM polyP250 NPs in 5 mM $CaCl_2$, 8 mM Tris·HCl, pH 7.4 before and after addition to suspensions of Tris-buffered 35 mg/mL BSA suspensions. To verify that multiple scattering was not occurring, the BSA+polyP250 NP samples were serially diluted up to 8 times with 5 mM $CaCl_2$, 8 mM Tris·HCl, pH 7.4. As is evident above, the polyP NPs shrink in size by approximately 40% after addition to the BSA suspensions independent of the dispersion viscosity or scattering intensity count rate.

Sample	PolyP250 NP Effective Diameter (nm)	Dispersion viscosity η* (centipoise)	BSA volume fraction (φ)
125 μM polyP250 NP in 5 mM $CaCl_2$ buffer	165.3	0.89	0.00
PolyP250 NP in BSA (1X = 35 mg/mL)	100.4	1.02	0.0531
PolyP250 NP in BSA (2X diluted)	83.5	0.953	0.0266
PolyP250 NP in BSA (4x diluted)	88.0	0.921	0.0133
PolyP250 NP in BSA (8X diluted)	86.7	0.905	0.00664

*$\eta = \eta_S(1 + 2.5\varphi + 6.2\varphi^2)$ for dilute BSA suspensions.

Table 6. PolyP250 NP effective diameter is hysteretic. 125 μM polyP250 was precipitated in 5 mM $CaCl_2$, 8 mM Tris·HCl, pH 7.4 and immediately diluted 2X, 5X, and 10X. The effective diameter does not appreciably change above the solubility for polyP250 (9.4 μM).

Sample	Effective Diameter (nm)	Dilution Factor
125 μM polyP250	158	1
62.5 μM polyP250	146	2
25 μM polyP250	161	5
12.5 μM polyP250	147	10

After determining the solubility of polyP as a function of polymer length and precipitative condition and exploring the stability in aqueous buffer and BSA suspension, NP formation was systematically investigated as a function of monoP supersaturation ratio. Again, polyP250 was used as a paradigmatic chain length. PolyP250 was precipitated at 1.2, 5, and 7.5 mM $CaCl_2$, and the effective diameter was measured using DLS as a function of the monomer concentration. **Figure 38A** shows that there is a clear relationship between [Ca^{2+}] and polyP NP diameter, with higher amounts of calcium leading to bigger particles. When the monoP concentration is divided by the solubility of polyP250 at each respective precipitative condition (cf. **Figure 38**), giving the dimensionless supersaturation ratio, a clear trend emerges: The polyP NP diameter is only a function of the [Ca^{2+}], with no dependence on the monoP concentration across a wide supersaturation ratio range (~1-50) (**Figure 38B**). In order to not saturate the laser detector, polyP NPs prepared at higher supersaturation had to be diluted with more 5 mM $CaCl_2$, 8 mM Tris·HCl, pH 7.4. However, the NP effective diameter is hysteric upon dilution. The polyP NPs also manifest solubility-dependent hysteresis. A supersaturated polyP250 NP dispersion was serially diluted with more 5 mM $CaCl_2$, 8 mM Tris·HCl, pH 7.4, keeping constant [Ca^{2+}] while decreasing the [monoP], and the scattering intensity was monitored by DLS (**Figure 38C**). Upon dilution, the scattering intensity remains elevated, even approaching the thermodynamic solubility limit. This hysteretic behavior could have profound *in vivo* ramifications, as condensed polyP secreted from platelets could maintain its particle format after being transported away from the site of vascular injury.

A

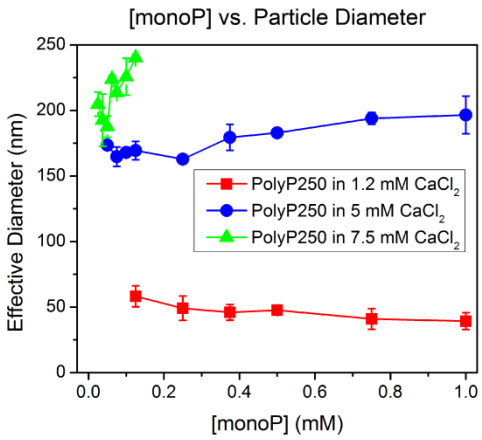

B

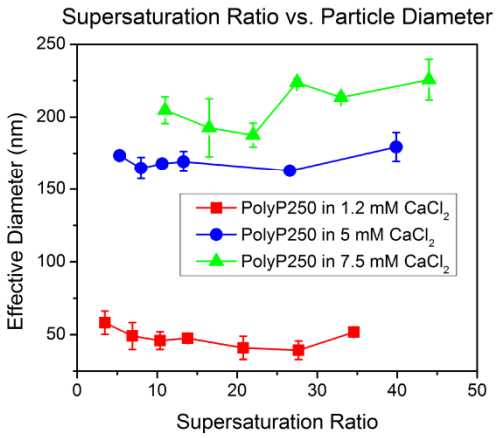

C

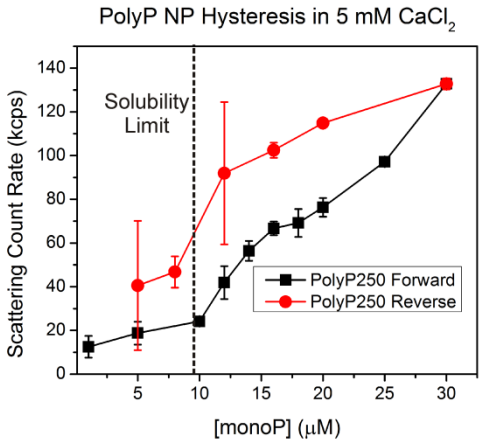

Figure 39. **PolyP NP effective diameter as a function of supersaturation ratio**. *A:* **polyP250 NP initial effective diameter versus monoP and Ca^{2+} concentrations**. Initial polyP250 NP sizes were measured with up to 1 mM monoP concentration at three different calcium concentrations: 1.2, 5, and 7.5 mM Ca^{2+}. No trends are manifest except for a dependence on calcium concentration. *B:* **PolyP250 NP initial effective diameter as a function of supersaturation ratios and Ca^{2+} concentrations**. When the monoP concentrations are divided by the solubility of polyP250 at the respective calcium concentrations, it appears that at moderate supersauration ratios (~1-50), the polyP particle diameter is only a function of the calcium concentration. *C*: **PolyP NP solubility hysteresis**. 30 μM polyP250 was nanoprecipitated in 5 mM $CaCl_2$, generating a supersaturated colloidal dispersion of polyP250 NPs. The suspension was then serially diluted with 5 mM $CaCl_2$, 8 mM Tris·HCl, pH 7.4 in order to decrease monoP concentration, while maintaining constant [Ca^{2+}]. As is evident from the reverse solubility curve (shown in red above), the scattering intensity remains elevated, even approaching polyP250's solubility (9.4 μM) in 5 mM $CaCl_2$ despite a thermodynamic driving force for resolubilization. This suggests that polyP colloidal dispersions manifest hysteresis, a characteristic that may have profound ramifications for potential downstream therapeutic usage of polyP NPs as clotting agents.

PolyP250 NP structure, morphology, and composition were examined utilizing transmission electron microscopy (TEM). 125 μM polyP250 was precipitated in 5 mM $CaCl_2$, 8 mM Tris·HCl, pH 7.4. The polyP NPs are mondisperse with some larger agggregates (**Figure 40A**). However, the polyP NP effective diameter is a function of [Ca^{2+}]. Undoubtedly, some of the polyP NPs aggregated during the drying process. **Figure 40B** shows a pair of granular polyP NPs at higher magnification, revealing that they are spherical in shape. Extended exposure to the electron beam bleaches the uniformly electron dense particles, causing the granules to appear like round sponges or soccer balls. **Figure 40C** demonstrates that the polyP NP is approximately the same size as an individual platelet dense granule. **Figure 40D** is an X-Ray microspectrum of the granule in *C*. Its elemental composition is quasi-identical to a human platelet dense granule, with a P:Ca ratio of 67:32. C, Cu, and Si are from the grid. Ruiz et al. reported similar findings in 2004, with a P:Ca ratio of 1.76 [24]. However, the synthetic polyP NPs were synthesized at neutral pH, while the enivironment in platelet dense granules is slightly acidic, possibly yielding a different P:Ca ratio.

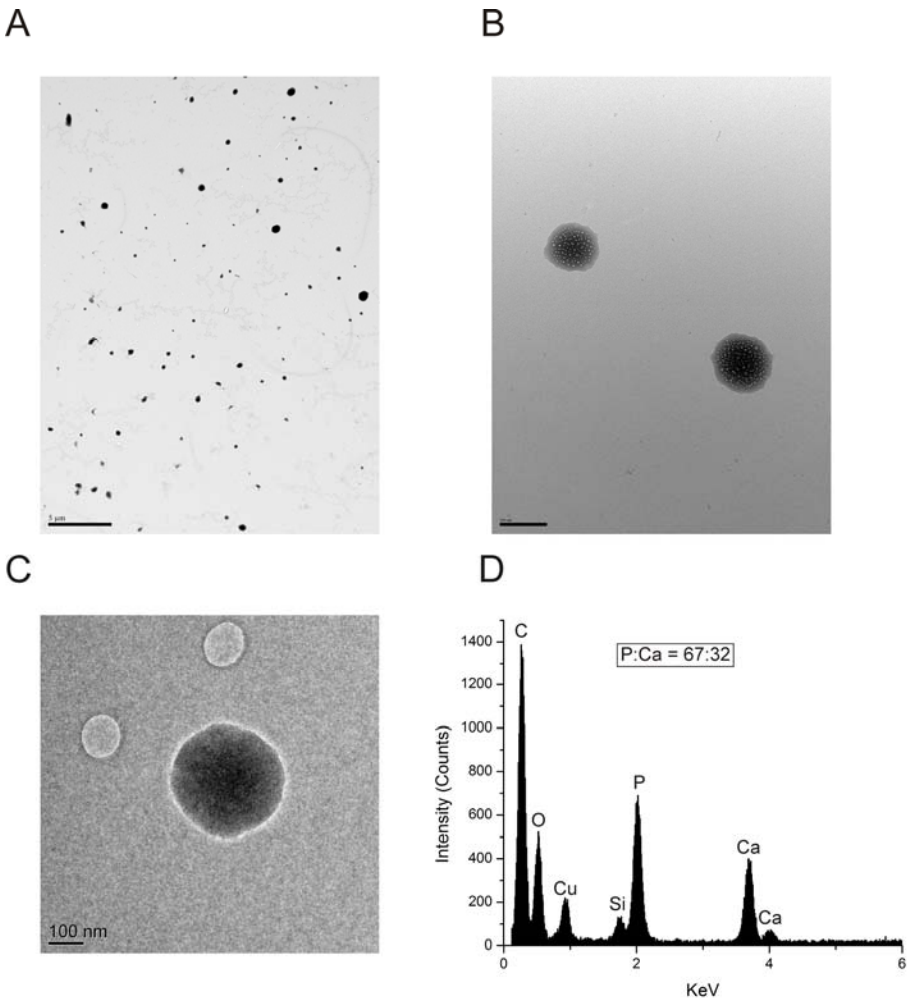

Figure 40. PolyP NP morphology, structure & elemental composition. *A*: **PolyP forms monodisperse particles in solution.** 125 μM polyP250 was precipitated in 5 mM $CaCl_2$, 8 mM Tris·HCl, pH 7.4. PolyP250 forms monodisperse particle populations in the presence of 5 mM $CaCl_2$. Scale bar: 5 μm. *B*: **PolyP NPs appear spongy after prolonged electron beam exposure just like acidocalcisomes and platelet dense granules**. Even though polyP250 NPs are uniformly electron dense, after sustained exposure to the electron beam, white spots begin to appear so that the particles appear like round sponges or porous balls. This same phenomenon was also observed in Ruiz *et al*.'s investigation of polyP-containing dense granules in platelets. *C*: **A granular polyP250 nanoparticle**. A single polyP 250 NP is shown at higher magnification revealing that the granule is

roughly spherical and approximately 200-250 nm in diameter, in good agreement with DLS data. Scale bar: 100 nm. *D*: **Elemental composition of the synthetic polyP250 NPs.** Copper, carbon, and silicon are from the grid. The ratio of the phosphorous to the calcium peak is 67:32. Ruiz *et al*. performed the equivalent analysis with human platelet dense granules, and their resulting X-Ray microspectrum is quasi-identical, except for the presence of a small K peak. However, potassium was not used here for polyP nanoprecipitation.

Smith *et al.* demonstrated that polyP is a potent activator of the contact pathway of coagulation, and its activity is related nonlinearly with its polymer length [8], with long polymers being more robust activators than shorter chains, which exert their effects at different points in the cascade such as via acceleration of FV activation and alteration of fibrin clot architecture and morphology. **Figure 41B** shows a schematic representation of the intrinsic pathway of coagulation and the points in which polyP exerts its effects. It is well accepted in the literature that anionic "surfaces" such as collagen, glass or kaolin are required to form the primary complex consisting of FXII (Hageman Factor) and its activation partners, plasma prekallikrein and high molecular weight kininogen (HMWK) [26]. However, countless other soluble substances serve as scaffolds for the (auto)activation of FXII. Examples include ellagic acid, lipopolysaccharides, dextran sulfate, and phospholipids [27]. It has been reported previously that there exists a threshold molecular weight for activation of the intrinsic pathway for polystyrene polymers and dextran derivatives, with contact activity for both polymer types rising sharply ~25,000 Da [28]. Others have communicated that the threshold molecular weight for dextran sulfate is as low as 10,000 Da [29]. Nonetheless, the mechanism by which polyP acts on FXII has yet to be clearly elucidated.

Previous studies assaying the procoagulant effects of polyP were performed under conditions where the polymer would presumably exist in its molecularly dissolved state. Typically, polyP was incubated together with pooled normal plasma (PNP) for 3-5 minutes prior to recalcification. Since the plasma is citrated, there would be very little ionic calcium available to chelate polyP, and thus no calcium-dependent precipitation would take place. The activation of contact enzymes and the generation of FXIIa are calcium-independent; therefore prior studies investigating polyP's contact activity are confined to an examination of the polymer in the absence of calcium-dependent precipitation. Moreover, plasma contains countless proteins and peptides such as serum albumin which may prevent or hinder its precipitation after recalcification. Due to polyP's role in the early stages of natural selection, pre-dating the arrival of polypeptides and quite possibly serving as the precursor to deoxyribonucleic and ribonucleic acid, it is only natural that polyP would serve as the paradigmatic anionic scaffold for serum and cytosolic proteins, emerging as a favored binding partner for peptides with cationic amino acid residues.

Figure 42 shows the clotting time of polyP molecules or nanoparticles when assaying for contact activity using citrated PNP. The polyphosphates (polyP80, polyP305, and polyP1000+) were first added to 5 mM $CaCl_2$, 8 mM Tris·HCl, pH 7.4 at three times the final assay concentration and characterized by DLS (data not shown). Once the polyP was incubated with the calcium solution, it was added to the PNP and immediately recalcified to initiate coagulation. Platelet-size polyP (polyP80) weakly shortened time to clot formation, saturating near 10-50 μM monoP. PolyP305 and polyP1000+, on the other hand, were robust contact activators, drastically reducing clotting times even at sub-micromolar concentrations. Interestingly, the clotting activities of the two longer polymer sizes are quasi-identical (the error bars overlap for every concentration except one).

These data suggest that platelet polyP only weakly promotes the activation of FXII, with the reduction in clotting time deriving mostly from effects on the final common pathway of clotting. On the other hand, the longer polymer sizes are large enough to serve as scaffolds for primary complex formation after treatment with calcium. One possibility is that there is a threshold polymer length (molecular weight) (as was previously reported for polystyrene and dextran sulfate) needed to exert the conformation change on the FXII zymogen (or to recruit a sufficiently high local surface density of FXII and its activators) as shown in **Figure 41A**. Interestingly, polyP305's molecular weight is approximately 24 kDa, corroborating past results on threshold contact activation measured using polystyrene and dextran sulfate polymers. The fact that the concentration dependence is identical for polyP305 and polyP1000+ also suggests that the nanoparticle solubility is not the threshold condition

for contact pathway activation for polymers over the threshold size, as polyP1000+'s solubility is approximately two-fold lower in 5 mM $CaCl_2$. If the solubility were the limiting condition, then polyP1000+'s clotting time would drop at ~4 μM, whereas polyP305's would drop at ~ 9 μM. However, there are several important caveats that limit the completeness of this analysis: (1) PolyP NPs have been shown to exhibit dilution-dependent hysteresis; (2) the solubility of polyP in plasma or serum with its diversity of proteins and peptides and additional polyvalent cations such as Mg^{2+}, Cu^{2+}, Zn^{2+}, Mn^{2+}, and Fe^{2+}/Fe^{3+} could be vastly different than in aqueous buffer containing only calcium; and (3) the effect of citrate and other calcium chelators such as EDTA on polyP nanoparticle stability has yet to be investigated.

The zeta potential of the polyP NPs was determined to be between -15 and -20 mV independent of particle diameter and polymer length (see **Tables 7** & **8**). The negative surface charge of polyP precipitates could therefore conceivably support autoactivation of Factor XII or recruitment of its activators, plasma prekallikrein and high molecular weight kininogen independent of polymer molecular weight, discounting other factors that would influence polyP NP stability in human plasma mentioned above.

Regardless of the physical interpretation, the fact remains that polyP precipitation under aqueous conditions at physiologic salt concentrations is a facile means to synthesize large amounts of condensed polyP granules similar in structure to human platelet dense granules for potential downstream uses such as a biocompatible procoagulant agent.

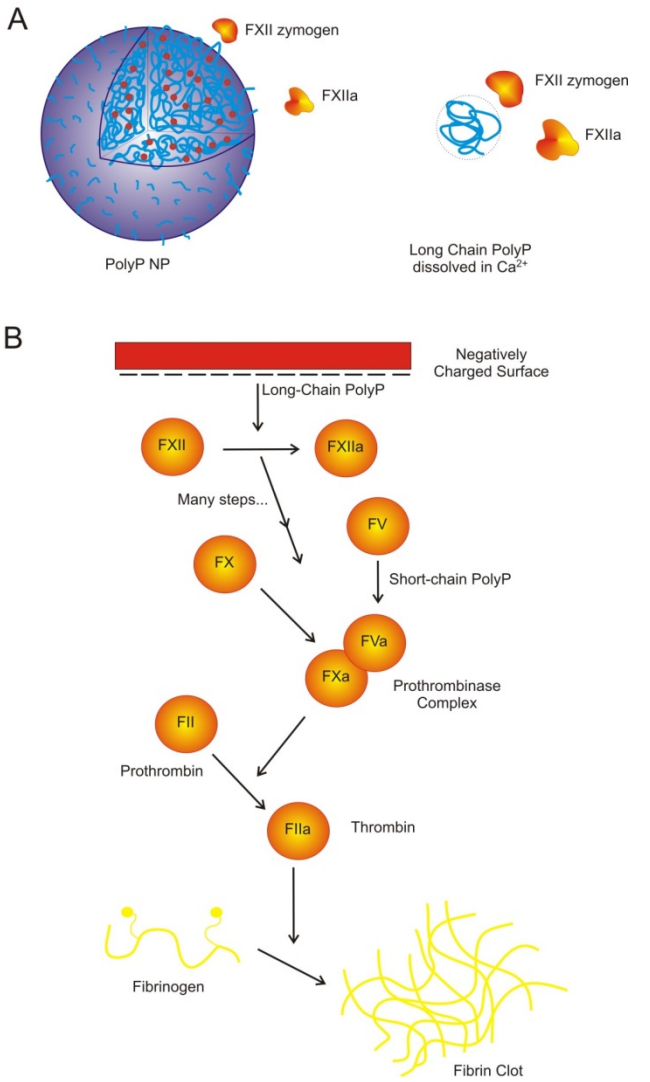

Figure 41. **PolyP NPs as contact activators.** *A*. **Possible mechanisms by which polyP exerts its contact pathway activity**. PolyP could serve as a surface for FXII activation as a colloidal particle like kaolin (left) or as a soluble anionic polymer like dextran sulfate (right) with a threshold molecular weight needed to elicit a conformational change in the FXII zymogen. *B*: **Schematic of the intrinsic pathway of blood coagulation**. A negatively charged surface serves as the site for assembly of the primary complex consisting of FXII, kallikrein, and high molecular weight kininogen. Long-chain polyP is able to support activation of the contact pathway, while shorter polymer lengths (like those in human platelets) are weak contact activators. polyP also exhibits procoagulant effects further downstream in the final common pathway of blood clotting.

Table 7. Average zeta potential and effective diameter of polyP NPs precipitated at 125 μM monoP in 5 mM $CaCl_2$, 8 mM Tris·HCl, pH 7.4. The zeta potential is approximately -15 to -20 mV irrespective of polymer length. The average initial effective diameter is approximately 160 nm regardless of the polymer molecular weight, being only a function of the calcium concentration.

Polymer Length (range, phosphate units)	Mean Zeta Potential in mV ±S.E.	Mean Particle Effective Diameter in nm ±S.D.
BKGP70 (20-125)	-16.53±3.83	159.55±3.32
PolyP250 (100-390)	-17.89±3.69	169.40±6.97
PolyP1000+ (>1000)	-15.41±0.53	162.50±11.46

Table 8. Average zeta potential and effective diameter of 125 μM polyP1000+ NPs synthesized at various precipitating conditions. The mean zeta potential is again in the range of -15 to -20 mV. The potential does not change substantially as a function of $[Ca^{2+}]$, with the surface charge at physiologic calcium being comparable to 5 mM $CaCl_2$.

Precipitating Condition	Mean Zeta Potential in mV ±S.E.	Mean Particle Effective Diameter in nm ±S.D.
5 mM $CaCl_2$, 10 mM NaCl, pH 5.4	-14.94±1.54	170.20±2.55
5 mM $CaCl_2$, 10 mM NaCl, 8 mM Tris·HCl, pH 7.4	-19.28±1.15	177.30±4.38
1.2 mM $CaCl_2$, 10 mM NaCl, 8 mM Tris·HCl, pH 7.4	-15.72±0.65	47.80±4.81

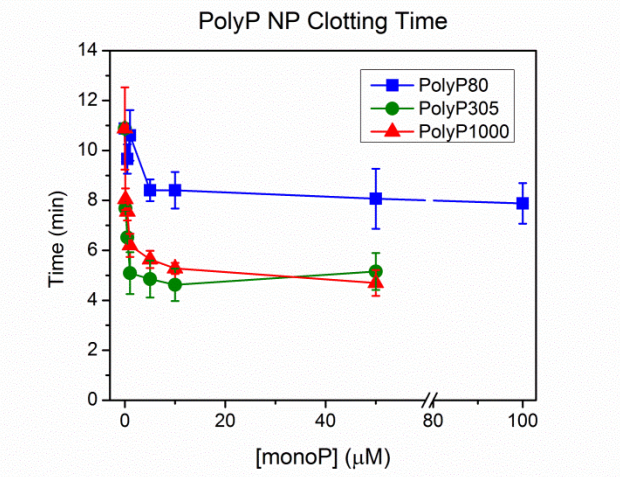

Figure 42. Initiation of the contact pathway by polyP based on polymer length and concentration. Clotting time of polyP is plotted as a function of monoP concentration from 0-100 μM. PolyP was added to 5 mM $CaCl_2$, 8 mM Tris·HCl, pH 7.4 at concentrations above and below its solubility. The presence of precipitated polyP was monitored by DLS before addition to plasma. Intermediate- and very long-chain length polyP (polyP305 and polyP1000+) are clearly more robust contact activators than platelet-sized polyP (polyP80). The concentration dependence on clotting time for polyP305 and polyP1000+ are identical, suggesting that a "saturating condition" has been established.

Encapsulation of small molecules and colloidal particles into phospholipid vesicles [30], polymersomes [31, 32], micelles [33], viral or viral-mimetic capsids [34, 35], and other supramolecular assemblies is an established stratagem in drug delivery to mitigate harmful side effects, prolong therapeutic efficacy, and diminish immune response (e.g. minimize complement pathway activation). Doxil is a liposomal formulation of the chemotherapeutic agent doxorubicin, and has been FDA-approved to treat Kaposi's sarcoma since 1993 [36]. Liangfang Zhang and colleagues have

successfully camouflaged PLGA nanoparticles by encapsulating the NPs in erythrocyte (red blood cell, RBC) membranes [37]. Naturally, liposomally encapsulated, granular polyP NPs—*Artificial Dense Granules*—would be the logical choice to treat catastrophic vascular injury by simply imitating the body's intrinsic hemostatic mechanisms, while simultaneously sequestering the polyP cargo.

After a complete characterization of polyP nanoprecipitation, we employed a facile, biomimetic approach for assembling Artificial Dense Granules by encapsulating granular polyP NPs in sterically stabilized liposomes at high efficiency (**Scheme 2**). TEM demonstrates that the Artificial Dense Granules (ADGs) are virtually indistinguishable from real dense granules isolated from human platelets in terms of morphology and structure. Moreover, digestion with secretory phospholipase A_2 ($sPLA_2$), a Ca^{2+}-dependent enzyme released by activated platelets during thrombotic or inflammatory events [38, 39], or solubilization of the lipid envelope with the non-ionic detergent Tween 20, exposes the condensed polyP, allowing it to activate Factor XII *in vitro*.

Although several nanoparticle hemostats have been developed in recent years that imitate platelet morphology and procoagulant response adjacent to the bleeding site, they fail to completely encapsulate the body's totality of threshold-switchable behavior to maintain hemostasis. Anselmo and Mitragotri approach true mimicry with their platelet-like nanoparticles (PLNs), synthesized by alternatively depositing the polyelectrolytes bovine serum albumin (BSA) and poly(allylamine) hydrochloride on a polystyrene (PS) core nanoparticle [40, 41]. Further functionalization of the PLN with binding peptides for fibrinogen, von Willebrand Factor (VWF), and collagen confer PLNs with the ability to marginate at the bleeding site, bind with activated platelets, and rapidly induce clotting in a directed manner, as evidenced by *in vitro* and *in vivo* methods [40]. However, the current approach is arguably more feasible as the synthetic scheme is simple, reproducible, and rapid. Moreover, polyP is already biologically ubiquitous, intrinsically procoagulant, and relatively inexpensive. Artificial Dense Granules are a potentially promising hemostatic agent to mitigate the deleterious effects of catastrophic bleeding scenarios.

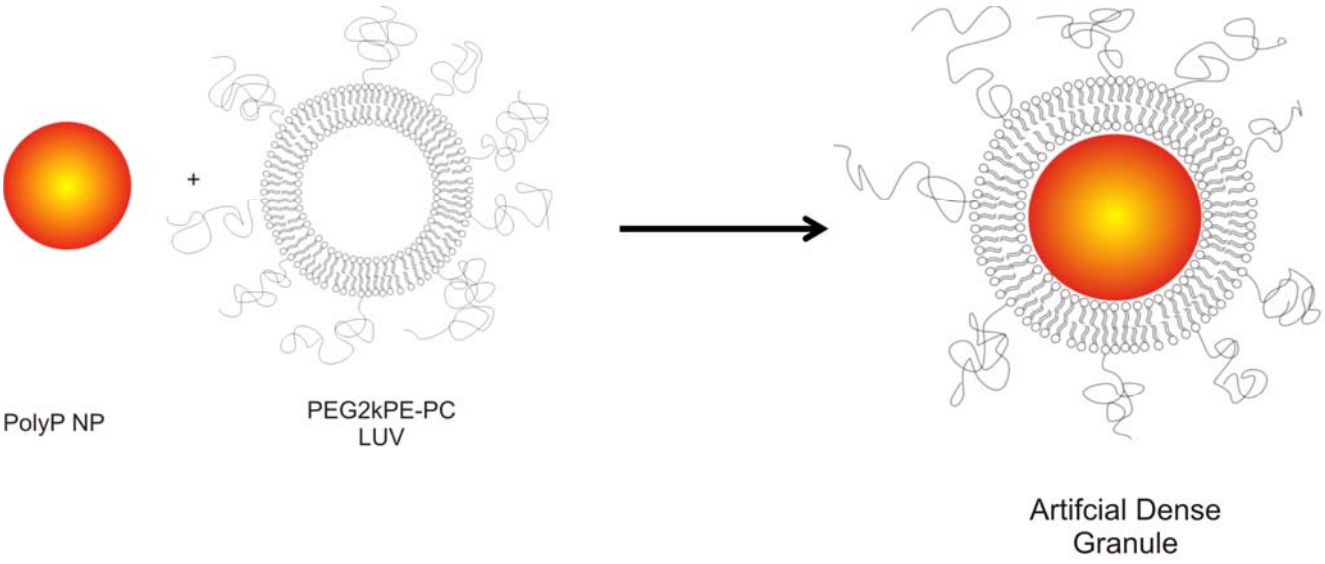

Scheme 2. Synthesis of Artificial Dense Granules. *Platelet-sized polyP is first precipitated in 5 mM $CaCl_2$(aq), pH 5.4, closely resembling the conditions inside human platelet dense granules. A stoichiometric excess of PEGylated phospholipid vesicles is subsequently added to the polyP NP dispersion, and the polyP precipitates are encapsulated inside the lipid envelope by sonication*.

Platelet-sized polyP (BKGP70, range 20-125 phosphate units) was precipitated at high supersaturation in acidic 5 mM $CaCl_2$. Brief vortexing of the mixture yielded monodisperse granular NPs approximately 160 nm in diameter with PDI ≤0.1. A stoichiometric excess of PEGylated

unilamellar phospholipid vesicles (PEG_{2k}PE-PC LUV) was subsequently added to the NP dispersion, and the granular polyP was encapsulated via bath sonication. The stability of the Artificial Dense Granules was monitored by DLS for 1 hr at RT. **Figure 43A** demonstrates that the phospholipid envelope tightly wraps around the bare polyP NP, as evidenced by the negligible change in effective diameter after vesicular encapsulation. Moreover, the vesicular integrity was maintained and the encapsulation appears to be nearly complete, as the Artificial Dense Granules did not ripen like the bare polyP NPs.

In order to gain a semi-quantitative measure of the degree of encapsulation, the calcium concentration was modulated and a non-ionic detergent, Tween 20, which does not affect polyP nanoprecipitation (data not shown), was added to the Artificial Dense Granules in order to exploit the dependence of polyP NP diameter on [Ca^{2+}]. The Artificial Dense Granules were first synthesized at 5 mM Ca^{2+} and the effective diameter was monitored by DLS for 30 minutes, at which point the [Ca^{2+}] was increased to 7.5 mM and 0.5% (v:v) Tween-20 was added (**Figure 43B**). In the absence of detergent, the Artificial Dense Granules do not significantly increase in size, as the polyP NPs are shielded from the increased calcium by the phospholipid envelope. However, in the presence of Tween 20, the growth kinetics is similar to the bare polyP NPs due to the vesicle solubilization by the detergent. In light of this behavior, one can conclude that the encapsulation efficiency is very high.

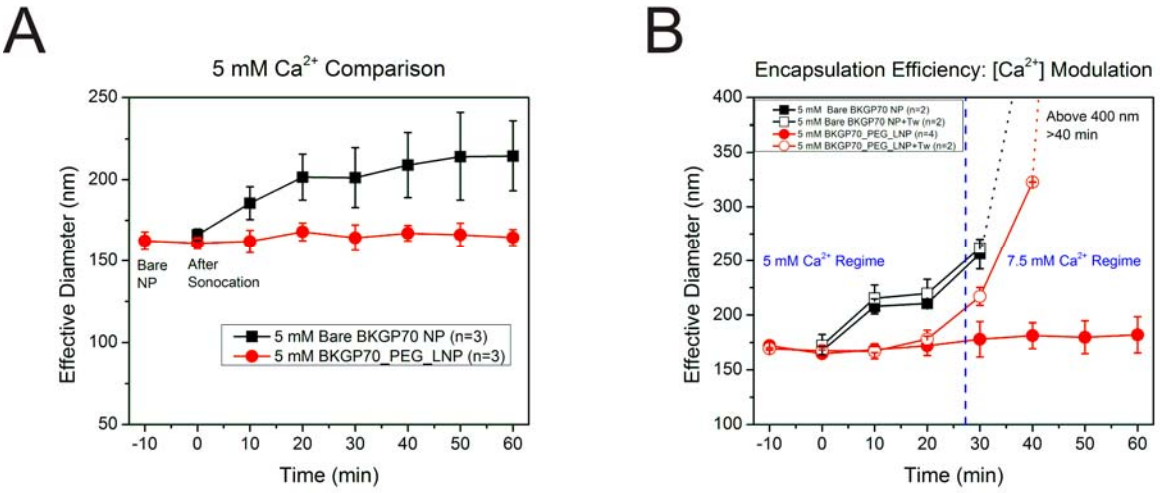

Figure 43. Stability & encapsulation efficiency. (A) Stability of ADGs and bare polyP NPs at 5 mM $CaCl_2$, pH 5.4 (B) Encapsulation efficiency using [Ca^{2+}] and non-ionic detergents for lipid solubilization.

The Artificial Dense Granules were subsequently physically characterized by transmission electron microscopy (TEM). The Artificial Dense Granules were prepared as above and stained with 2% uranyl acetate in order to enhance contrast. Low magnification images reveal that the liposomally encapsulated polyP is very monodisperse with hardly any aggregates, corroborating DLS measurements (**Figure 44A**). The granules at high magnification are nearly identical in appearance to isolated human platelet dense granules. An electron-dense core that bleaches with the electron beam, manifesting as a round sponge, is surrounded by a corrugated corona, which is most likely the PEGylated lipid bilayer. The presence of divalent metal ions (5 mM Ca^{2+}) likely alters the morphology of the bilayer, making it asymmetric with grooves and invaginations (**Figure 44B**). The Artificial Dense Granules are also comparable in size to human platelet dense granules, being approximately 200 nm in diameter.

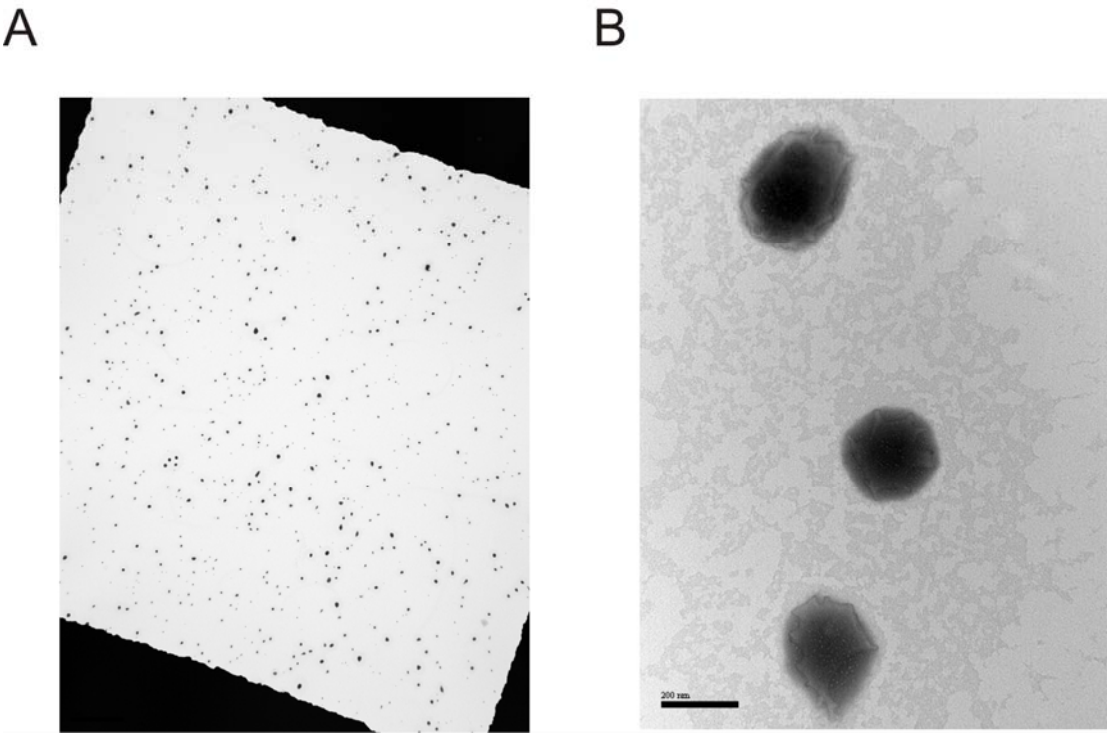

Figure 44. ADG Structure & Morphology. *A*: **Encapsulation of polyP NPs yields monodisperse ADGs** *B*: **Exposure of ADGs to the electron beam leads to bleaching just like human platelet dense granules.**

Secretory phospholipase A_2 ($sPLA_2$) is a known inflammatory marker, with concentrations of the enzyme being substantially elevated in cancer, rheumatism, and other inflammatory diseases [42]. The enzyme is also released during bleeding events by activated platelets [39], perhaps reaching local concentrations orders of magnitude higher than baseline levels. As such, $sPLA_2$ is a potential targeting mechanism for delivery of procoagulants for treatment of incompressible hemorrhage. Artificial Dense Granules were synthesized at RT following the same scheme as delineated above. The stability of the granules was monitored for 30 minutes, at which point the granules were transferred to a buffered enzyme solution at 37°C containing 10 μg/ml $sPLA_2$, 7.5 mM $CaCl_2$, 25 mM Tris·HCl, 100 mM NaCl, pH 7.4. **Figure 45A** demonstrates that in the presence of enzyme, the scattering intensity rapidly drops at the time of enzyme addition (t=30 min), and approaches 0 thirty minutes later. This indicates that the enzyme is able to unwrap the polyP NP by hydrolyzing the ester linkages between the acyl chain and phosphate head group of the phospholipid, exposing the NP to higher Ca^{2+}, allowing it to aggregate and sediment out of the dispersion, as in the encapsulation efficiency experiments. In the absence of $sPLA_2$, the scattering intensity marginally drops after a change in temperature and ionic strength. However**, Figure 45B** indicates that no vesicular fusion takes place. The effective diameter remains constant and vesicular integrity is maintained. **Figure 45C & D** show representative lognormal particle size distributions (intensity-weighted) for the Artificial Dense Granules with 10 μg/ml $sPLA_2$. Two peaks are clearly evident as the polyP NPs are aggregating in the increased calcium environment.

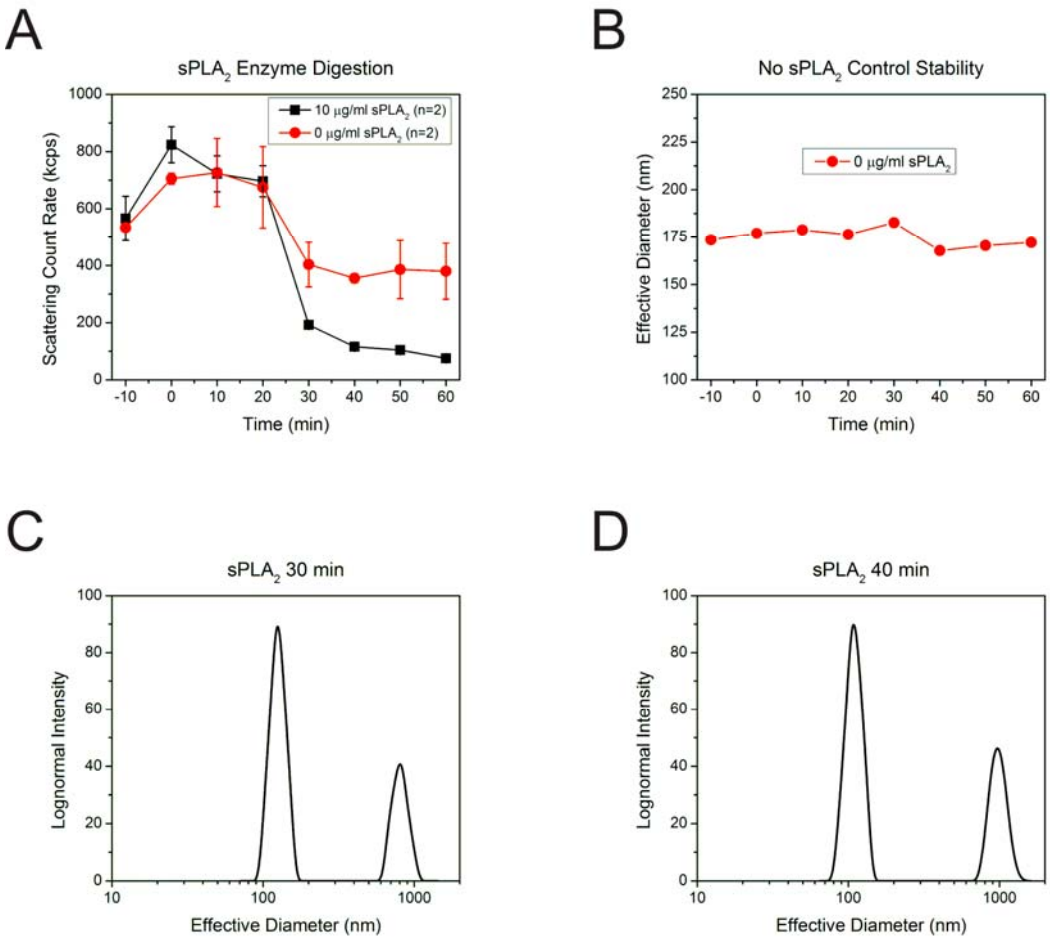

Figure 45. $sPLA_2$ Digestion of the ADG lipid envelope. (A) Scattering intensity of ADGs incubated with (i) no $sPLA_2$ and (ii) 10 μg/ml $sPLA_2$. (B) Effective diameter of ADGs not treated with enzyme. (C) Representative intensity-weighted particle size distribution of ADGs treated with 10 μg/ml $sPLA_2$ at t=30 min (immediately after enzyme addition). (D) Representative intensity-weighted particle size distribution of ADGs treated with 10 μg/ml $sPLA_2$ at t=40 min, (10 min after enzyme addition).

Mutch and colleagues have recently demonstrated that platelet polyP is able to autoactivate FXII in an *in vitro* coagulation model, arguing that low molecular weight polyP can serve as a contact surface for initiation of the intrinsic pathway of coagulation [43]. Our aim was to show that our Artificial Dense Granules manifest similar contact pathway activity. The ability of 500 μM Artificial Dense Granules with and without the presence of Tween-20 was assayed using the same technique. Artificial Dense Granules without detergent showed minimal activation of the Factor XII zymogen, while Artificial Dense Granules incubated with Tween 20 were able to robustly activate FXII in a similar manner to bare polyP NPs at equivalent concentration (**Figure 46**). Taken together, these results suggest that the synthetic scheme developed here for making Artificial Dense Granules provides a novel route for treatment of incompressible hemorrhage in a directed manner.

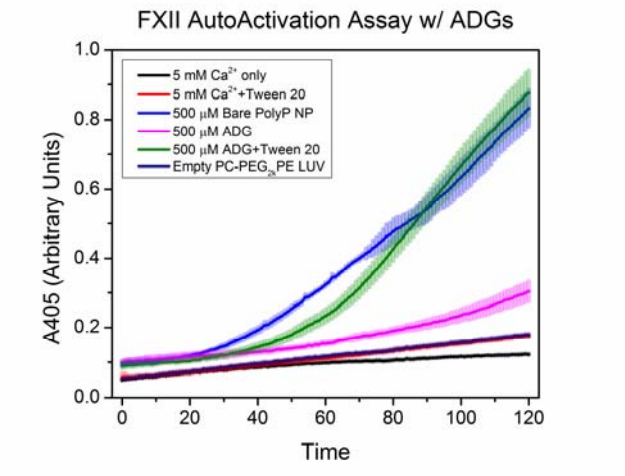

Figure 46. Figure XII Autoactivation by Artificial Dense Granules (ADGs).

Mutch and colleagues showed that physiological concentrations of ionic zinc (10-20 μM) enhanced the autoactivation of FXII by platelet-sized polyP [43]. As Zn^{2+} is a divalent metal cation, it may be able to nanoprecipitate polyP. Therefore, 1 mM platelet-sized polyP (BKGP70) was precipitated under the same conditions as the FXII assay (~1.5 mM $CaCl_2$, 10 μM $ZnCl_2$) at pH 5.4 and 7.4. At neutral pH, the NPs are about 200nm (**Figure 47**), much larger than expected with solely 1.5 mM $CaCl_2$. However, the scattering intensity rapidly decreases (**Figure 48**), likely due to Zn^{2+}-catalyzed hydrolysis of polyP. However at acidic pH, the NPs are approximately the same size and are colloidally stable (**Figure 47 and 48**, respectively). The scattering intensity remains constant, and the particles do not grow over time. At mildly acidic pH, there is no metal-catalyzed hydrolysis and no Ostwalt ripening is occurring, possibly due to changes in the zeta potential or solvent dielectric constant.

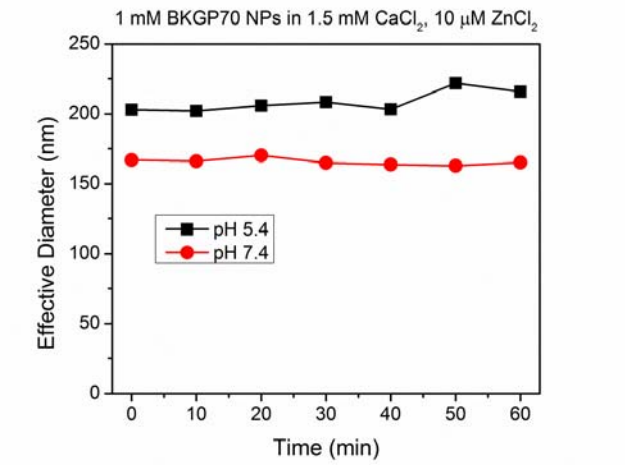

Figure 47.1 mM polyP NP Stability in 1.5 mM $CaCl_2$ + 10 μM $ZnCl_2$ at pH 5.4 and 7.4.

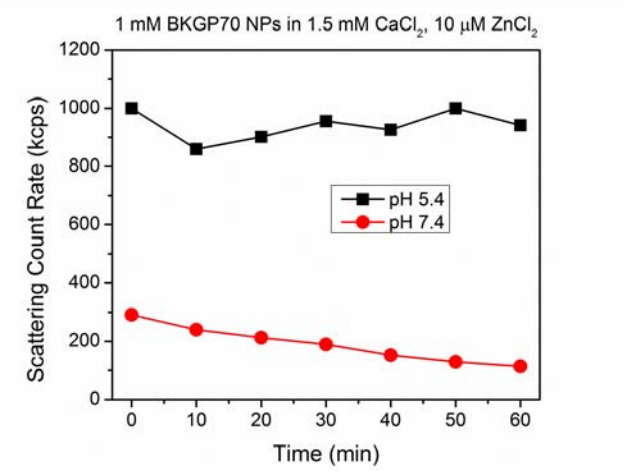

Figure 48. Scattering intensity of 1 mM polyP NP in 1.5 mM $CaCl_2$ + 10 µM $ZnCl_2$ at pH 5.4 and 7.4.

Rapid, accurate sizing of polyP polymers: Given our need to prepare and characterize polyP with well-defined polymer lengths, we worked to develop a new method to allow more rapid, cost-effective, and precise sizing of polyP using polyacrylamide gel electrophoresis and commercially-available DNA-based molecular weight markers. We used narrowly sized polyP fractions whose polymer lengths were definitively determined using a very laborious NMR technique to determine the relationship between the migration of polyP polymers and that of DNA bands from commercially available DNA ladders (Figure 49). The model that was developed can be utilized for sizing of polyP regardless of the polyacrylamide content in the gels, and applies across a wide range of polymer sizes. Inter-assay coefficients of variation were <0.01 for this approach (Figure 50).

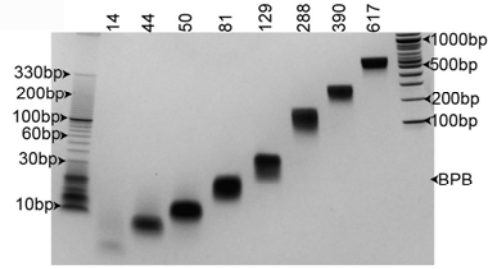

Figure 49. Example of a 4-20% polyacrylamide gel demonstrated comigration of polyP and DNA. The sizes of the polyp polymers are defined at the top of each lane. The sizes of the DNA ladder bands are as indicated on the side margins.BPB: bromphenol blue

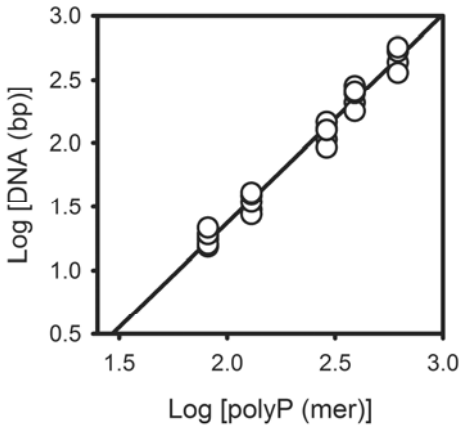

Figure 50. Description of the model describing the relationship between migration of polyP and DNA. The model was developed using polyP polymers of 81, 129, 288, 390, and 617 units in length.

Extending the covalent coupling chemistry for polyP beyond phosphoramidate linkages: Studies in the Morrissey lab focused on extending the coupling chemistry available for covalently attaching polyP to nanoparticles. We had previously identified facile conditions under which to generate phosphoramidate linkages between primary amines and the terminal phosphates of polyP

[20]. However, while phosphoramidate linkages are stable under neutral mildly alkaline conditions, they are acid-labile. We therefore sought to identify conditions that would allow us to generate phosphoester linkages between the terminal phosphates of polyP and alcohols. This would substantially expand the coupling chemistry available for production of polyP-bearing nanoparticles, and would have the additional advantage that phosphoester linkages are far more acid-stable than are phosphoramidate linkages [44]. As proof of principle, and to identify reaction conditions more readily, we examined EDAC-mediated esterification of polyP with methanol (see **Scheme 3**).

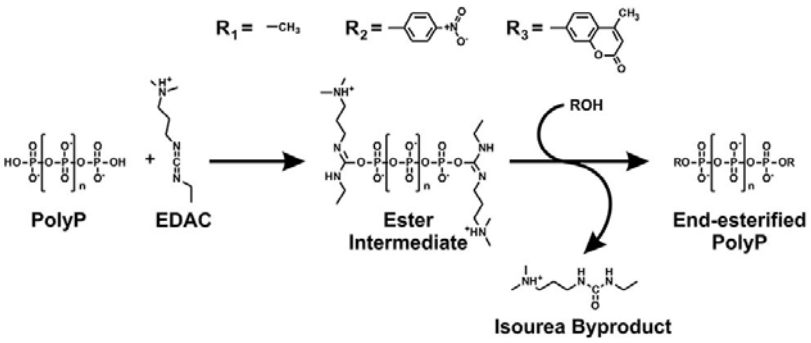

Scheme 3*. EDAC-mediated esterification of the terminal phosphates of polyP. R_1 = methanol; R_2 = NOL; R_3 = MU.*

The reaction of polyP with EDAC and methanol resulted in a product that was protected from digestion by exopolyphosphatase (calf intestine alkaline phosphatase, CIAP) to an extent comparable to polyP that had been end-labeled with spermidine via phosphoramidate linkages (Table 9). We confirmed the presence of methyl groups on the terminal phosphates of polyP treated with EDAC + methanol using NMR (not shown).

Table 9. Resistance of PolyP Derivatives to Digestion with Alkaline Phosphatase (CIAP)

polyP end-labeled with:	hydrolysis (%)
nothing (underivatized polyP)	96.0 ± 16.7
spermidine	20.8 ± 2.1
methanol	19.8 ± 2.0
NOL	27.0 ± 2.0
MU	3.9 ± 1.6

We also were able to covalently couple two dyes, 4-nitrophenol (NOL) and 4-methylumbelliferone (MU) to the terminal phosphates of polyP using EDAC-mediated coupling, resulting in polyP covalently labeled on the ends with these alcohols (as shown by resistance to CIAP digestion; Table 9). This has allowed us to create chromogenic and fluorogenic substrates for detecting polyphosphatases and quantifying their enzyme activities. NOL does not absorb visible light when coupled covalently to polyP, but complete digestion of end-labeled polyP releases free NOL dye, which then absorbs light at 405 nm, allowing us to quantify polyphosphatase activity spectrophotometrically in high-throughput, multiwall format. Similarly, MU is non-fluorescent when covalently coupled to polyP, but when free MU is released from polyP-MU after polyphosphatase digestion, the free dye is highly fluorescent. This allows us to follow polyphosphatase activity using high-

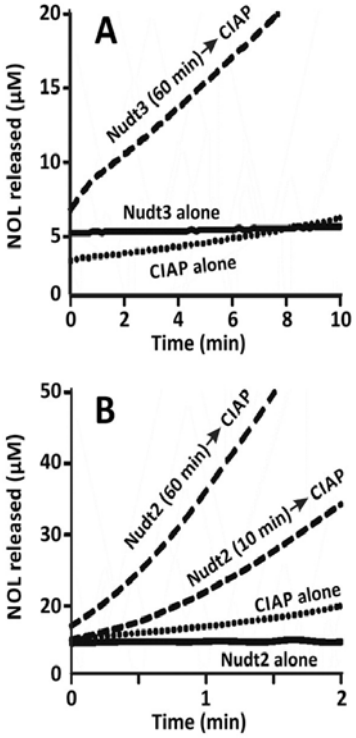

Figure 51. Sequential digestion of doubly end-labeled polyP-NOL with endo- and exopolyphosphatases. In both panels, doubly end-labeled polyP-NOL was first incubated with or without endopolyphosphatase (Nudt2 or Nudt3) for 10 or 60 min at 37°C. Exopolyphosphatase (120 U/mL CIAP) was then added to the indicated samples and NOL release was quantified over time. (A) Treatment with 850 nM Nudt3. (B) Treatment with 250 nM Nudt2.

sensitivity fluorescent polyP substrates. We are now able to use these polyP derivatives to detect the action of endo- and exopolyphosphatases, depending on assay configuration. An example of such an assay is depicted in **Figure 51**, using polyP that was completely labeled on both ends with NOL, which causes it to be protected against exopolyphosphatase (CIAP) digestion. We employed two endopolyphosphatases (Nudt2 and Nudt3) in this experiment and showed that digestion with endo- or exopolyphosphatase alone released negligible amounts of NOL dye, while predigestion of polyP with endopolyphosphatase clearly allowed robust exopolyphosphatase digestion. These studies also demonstrate conditions under which we can readily generate phosphoester linkages between alcohols and the terminal phosphates of polyP, which substantially expands the coupling chemistry now available to us for nanoparticle fabrication using polyP as the procoagulant payload, and the other labs within this collaborative study have productively applied this coupling chemistry in generating candidate TSPs. This coupling chemistry was recently published [21] and a reprint is included in the appendix.

Task 4 — Design and utilize microfluidic devices that reproduce shear flow and surface chemistries relevant to internal hemorrhage.

Measuring clot times simultaneously at various shear rates: A microfluidic system was used to measure clot times of blood plasma flowing at different shear rates. The device contained six regions with varying shear rates of 1-128 s^{-1} (Fig. 54A). Physiologic shear rates are typically in the range of 50 s^{-1} to 100 s^{-1} [17]. Clotting was monitored by visualizing the movement of fluorescent tracer beads, which stopped flowing in clotted regions, and by a fluorogenic substrate, which fluoresced when cleaved by thrombin during clotting (Fig. 54B). Clotting under flow, as it was measured in this device, is expected to occur within many minutes or hours, as it occurs inside vessels *in vivo*, rather than within seconds or minutes, which occurs during external bleeding or in standard, static clotting assays [45]. To validate the system and determine the range of clot times of flowing blood plasma in it, coagulation factor VIIa (FVIIa) was mixed with plasma inside the device (Fig. 54C). FVIIa is administered during severe hemorrhage to aid in hemostasis at doses of 90 to 270 μg/kg, which roughly corresponds to approximately 1 to 4 μg/mL in plasma [46, 47]. In the device, plasma containing 4 μg/mL of FVIIa clotted in approximately 1 hr, whereas 4 ng/mL, which is the approximate concentration found in normal human plasma, did not clot within 6 hr [48]. In addition, with an intermediate concentration of 400 ng/mL and 40 ng/mL, clot times depended on shear rate, ranging from 1 and 2 hr respectively at a shear rate of 1 s^{-1}, to over 4 hr at 128 s^{-1}. This shear-dependence of clotting in the microfluidic system is consistent with the normal behavior of clotting *in vivo* [49].

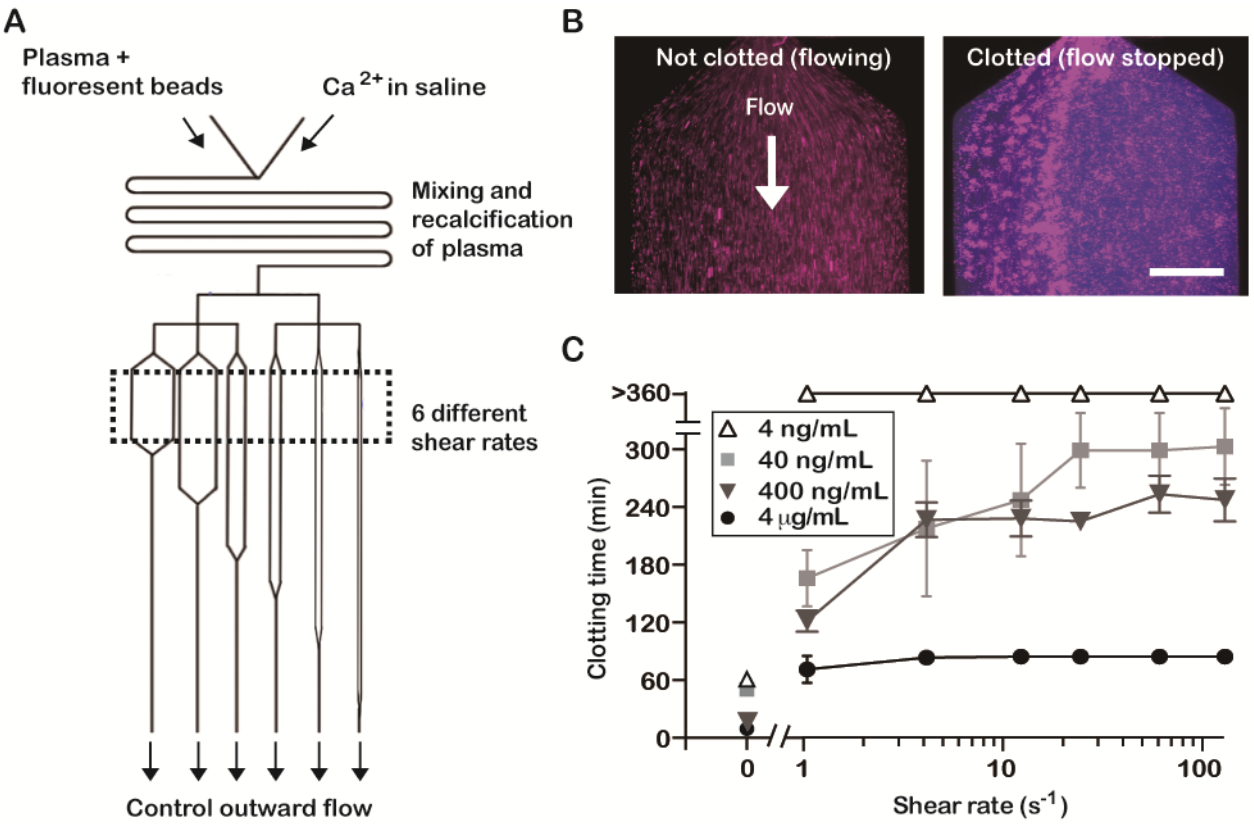

Figure 52. The microfluidic system used to measure clotting over a range of shear rates. (A) Schematic of the microfluidic system. Box (dashed lines) indicates the region where shear rates were varied and clot times were measured. (B) Fluorescence images showing that clotting was detected by the cessation of flow of tracer beads (pink) and by the cleavage of a substrate for thrombin (blue). Scale bar is 250 µm. (C) Assessing the range of clot times in this flow system by adding various concentrations of FVIIa to the plasma. Data indicate mean ± SEM, *n* = 3.

PolyP initiates clotting faster when spatially-localized than when dispersed in solution: PolyP$_{>1000}$ naturally self-assembles, localizing into nanoparticles of 150 ± 30 nm in diameter in solutions containing Ca^{2+} at millimolar concentrations. It is a known activator of clotting under static conditions, without flow, when dispersed throughout plasma [19]. To test if localizing polyP$_{>1000}$ onto surfaces would further enhance its ability to initiate clotting, biotin-polyP$_{>1000}$ was immobilized onto microfluidic channels and clotting of flowing plasma in the channel was measured (Fig. 53A). At a low shear rate of 1 s^{-1}, 7 µM and 1 µM of dispersed polyP$_{>1000}$ nanoparticles (NP-polyP) initiated clotting slowly, at ~4 hr and over 6 hr, respectively. In contrast, the same amounts of SI-polyP initiated clotting much faster, at ~60 and ~140 min, respectively. Surface concentrations of polyP$_{>1000}$ of 300 and 60 nmol/m^2 correspond to volumetric concentrations of 7 µM and 1 µM in a channel with a cross-section of 1000 X 100 $µm^2$. At higher shear rates, above 4 s^{-1}, the difference between dispersed and surface-immobilized polyP was even more pronounced, with NP-polyP$_{>1000}$ not clotting within 6 hr, but SI-polyP initiating between ~70-180 min.

These final concentrations of polyP$_{>1000}$ in plasma were close to the solubility limit. For example, the solubility of polyP$_{>1000}$ in aqueous 5 mM Ca^{2+} is ~4 µM [19]. However, the NP-polyP were initially formed under supersaturated conditions, and NP-polyP, once formed, remain as NPs even when diluted to below their solubility point. To compare the abilities of SI-polyP and soluble polyP to initiate clotting, polyP$_{160}$ was tested next. The solubility of short-chained polyP is less than long-chained polyP, and polyP$_{160}$, can be formulated to be soluble or to form NP-polyP by varying the concentration of polyP and Ca^{2+} [19]. We used concentrations of polyP$_{160}$ near its limit of solubility. To use soluble polyP$_{160}$, it was dissolved into water first and then diluted into plasma. When dissolved in

citrated plasma soluble polyP will likely remain dissolved, as there are no free divalent cations to facilitate NP formation [19]. PolyP binds to a myriad of coagulation and serum proteins such as Factor XI, thrombin, kallekrein, and serum albumin [19]. Once recalcified, PolyP likely remains protein-bound even in the presence of millimolar amounts of ionic calcium, at least for the 35 sec that it is present in the microfluidic devices. To form NP-polyP, $polyP_{160}$ was precipitated in 5 mM Ca^{2+}, forming nanoparticles that were stable for over 6 hr, as measured by dynamic light scattering. NP-polyP was diluted in the calcium-saline solution that mixed with blood plasma inside the microfluidic devices.

$PolyP_{160}$ was not previously believed to be a strong initiator of clotting, but we examined the hypothesis that spatially localizing $polyP_{160}$ would enhance its ability to initiate clotting. Plasma was either mixed with soluble $polyP_{160}$ or NP-$polyP_{160}$ or flowed over SI-$polyP_{160}$, and the resulting clot times were measured (Fig. 53B). Soluble $polyP_{160}$ activated clotting slowly, at 250 min or more at all shear rates. Clotting occurred faster when polyP was localized as nanoparticles (250 nm dia.), in approximately 170 min and 200 min at a shear rate of 1 s^{-1} and 24 s^{-1} respectively with 1 Mm polyP. When a similar amount of $polyP_{160}$ was localized onto the channel surface, clotting occurred in approximately 70 min and 100 min at a shear rate of 1 s^{-1} and 24 s^{-1} respectively. Overall, clotting occurred faster with SI-$polyP_{160}$ than soluble $polyP_{160}$ or NP- $polyP_{160}$, even with 6-43 fold less SI-$polyP_{160}$ in the channels.

Together, these data show that the spatial localization of polyP greatly affects its ability to activate clotting (Fig. 53C). Soluble polyP only clotted stagnant blood (near-zero shear) in our experiments, and clotting did not occur within a span of hours at low shear rates. Localization of polyP onto the surface of channels showed the greatest activity overall. Interestingly, $polyP_{160}$ localized onto surfaces clotted flowing blood in a manner very similar to $polyP_{>1000}$, but appeared to clot faster with similar amounts of phosphate. One might expect polyP to activate clotting factors at a similar rate regardless of their chain length, assuming they have the same negative surface charge. However, when the concentration of phosphate monomer was kept constant, short-chain polyP was more active. This is likely because shorter chains had higher surface coverage of the channel wall, localizing at high surface density compared to longer-chain polyP that had lower surface coverage at identical concentrations of phosphate monomer. That is, clot initiation occurred more quickly with increasing surface concentration or surface density of phosphate.

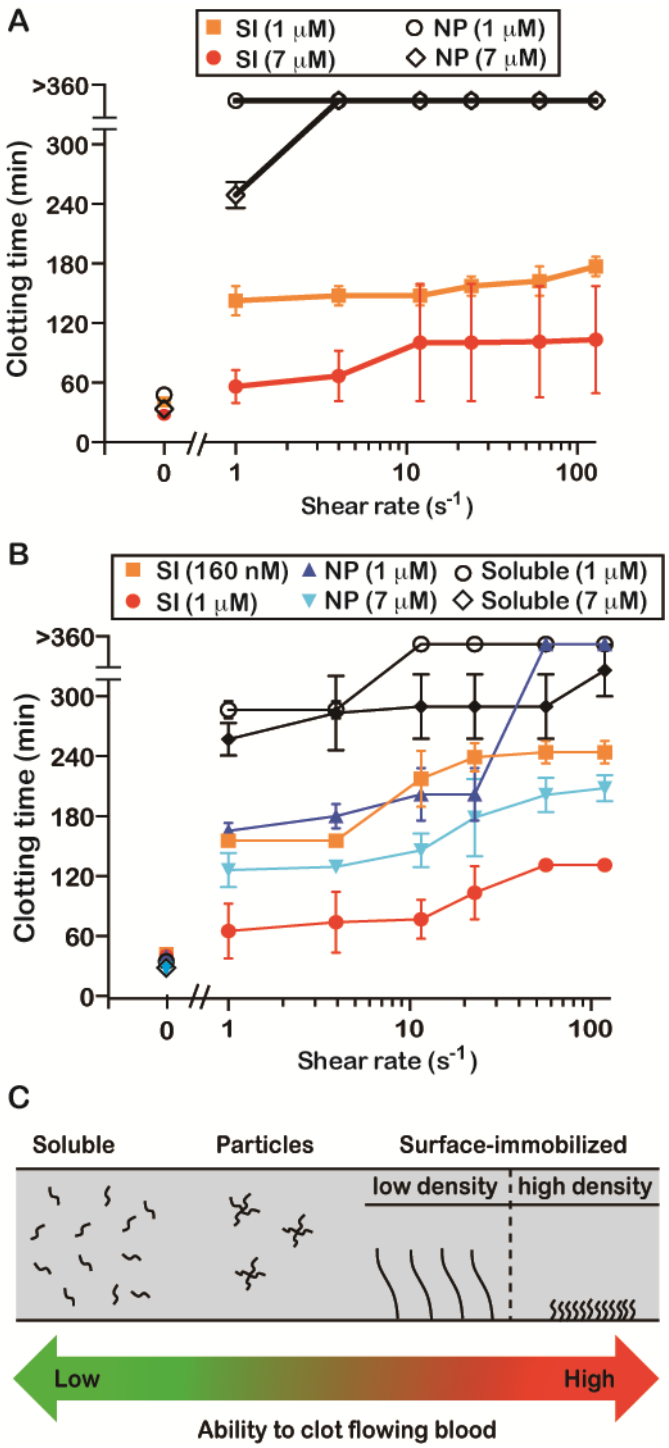

Figure 53. PolyP initiates clotting faster when surface-immobilized than when dispersed, at physiological shear rates. (A) SI-polyP$_{1000}$ activates clotting of flowing plasma faster than polyP dispersed in solution as self-assembled nanoparticles (NP), even at a 7-fold lower concentration (B) PolyP$_{160}$ initiates clotting faster when spatially-localized in either nanoparticles or when surface-immobilized than when solubilized. At physiological shear rates, only SI-PolyP$_{160}$ significantly accelerates clotting. (C) Schematic summarizing the relationship between spatial distribution of polyP and the initiation of clotting in the above experiments. Data indicate mean ± SEM, n = 3-4.

PolyP with chain-lengths similar to platelet polyP can initiate clotting when surface-localized: To test whether polyP of lengths similar to those found in human platelets can clot flowing blood, $polyP_{70}$ was tested (Fig. 54). Soluble $polyP_{70}$ was not able to initiate clotting of flowing blood plasma at the shear rates test at 400 nM. In contrast, SI-$polyP_{70}$ rapidly clotted plasma, in approximately 70 min and 160 min at shear rates of 1 s^{-1} and 128 s^{-1} respectively. The amount of SI-$polyP_{70}$ used corresponded to surface concentration of 21 nmol/m^2 and a total concentration of around 400 nM in the volume of the channel. This is within the range of amounts of polyP released into plasma following platelet activation (up to 1-3 μM) [50, 51]. This suggests that if polyP can surface-localize onto cells or is initially localized between aggregated platelets, such as within a platelet plug, it may help activate clotting following platelet activation.

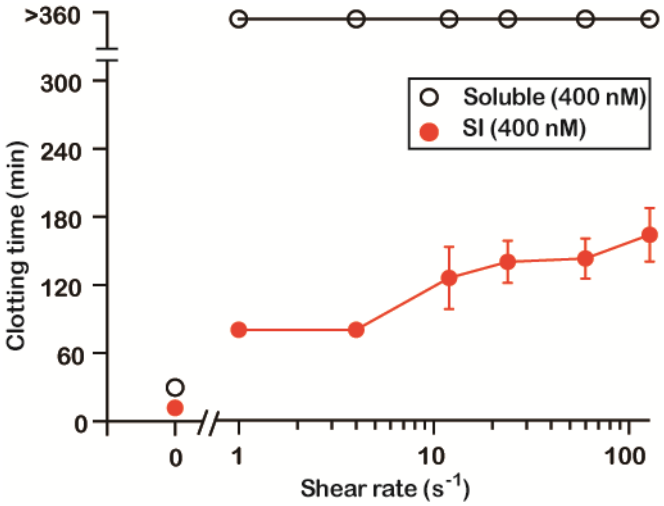

Figure 54. Platelet-length polyP initiates clotting when localized. $PolyP_{70}$ accelerates clotting of flowing plasma at all shear rates tested when surface-immobilized, but not when soluble and dispersed throughout the solution. Data indicate mean ± SEM, n = 3.

PolyP nanoparticles initiate clotting in a shear-dependent manner: In the experiments described above we observed that dispersed polyP nanoparticles initiated clotting in a shear-dependent manner. An agent that initiates clotting at low, sub-physiological, shear in a robust and specific manner could potentially be used to help manage internal hemorrhage. Low shear is characteristic of regions of internal hemorrhage where blood is pooling. To understand if this effect of NP-polyP on clotting is robust, we tested a range of concentrations of NP-$polyP_{>1000}$. We also tested a second formulation of polyP nanoparticles, where $polyP_{70}$ was coated on silica nanoparticles. The clot times using NP-$PolyP_{>1000}$ showed shear- and concentration-dependence at 2000, 200, and 20 MM (200, 20, 2 μg/mL) (Fig. 55A). NP-$PolyP_{>1000}$ was most potent at 2000 μM, initiating clotting at 60 min at 1 and 4 s^{-1}, but had slow clot times at 8 s^{-1} and above. At physiological shear rates, the propensity of NP-$PolyP_{>1000}$ to initiate clotting was much less than surface-immobilized polyP, even when its concentration was 285-fold higher (7 MM SI-$PolyP_{>1000}$ -vs 2000 μM NP-$PolyP_{>1000}$). Lower concentrations of particles also accelerated clotting selectively at lower shear, with 20 μM initiating at 2 hr, but at high shear it took over 6 hr. Silica nanoparticles coated with $polyP_{70}$ (SNP-$polyP_{70}$) were tested in a similar manner and they also showed strong dependence on shear and concentration (Fig. 55B). SNP-$polyP_{70}$ were prepared by previously described methods. At 200 μg/mL SNP-$polyP_{70}$, clot times ranged from 50 min at low shear (1 s^{-1}) to 170 min at high shear (120 s^{-1}). At 20 μg/mL SNP-$polyP_{70}$, clot times were slower, but showed increased shear dependence, with clot times ranging from 80 min at low shear to over 6 hr at high shear.

These results with nanoparticles of polyP reaffirm that polyP can be used as an activator of clotting when localized into particles. Moreover, nanoparticles of polyP have the ability to initiate

clotting selectively at low shear, and not at the higher shear rates typical of physiological blood flow. This shear-dependent behavior may potentially be useful for treating particular types of bleeding. During internal hemorrhage the volume of blood can be relatively large compared to the amount of procoagulant surfaces it is in contact with, and amount of activator is not enough to clot a suitably large area of blood to seal the damage. Administering a traditional activator to trigger clotting in the wound is challenging because of the high potential of clotting in other areas of the vasculature. The shear-dependent behavior of NP-polyP, or future particles like it, may help make clotting more selective for the wound. Although the flow rate of blood during hemorrhage is high, the flow velocities and shear rate are much lower in portions of the wound than in circulation. The shear-dependent behavior of NP-polyP may arise from the increased propensity of polyP to initiate clotting when localized and the ability of activated clotting factors to be rapidly transported off the small particles at higher shear. Thus, there may be potential for developing NP-polyP further toward an intravenous treatment for incompressible hemorrhage, where current external interventions fail to stop bleeding. The results here indicate a good future approach for developing polyP into a hemostatic agent would be to design polyP to localize into particles or onto surfaces in wounds. PolyP has advantages; it is naturally found in blood, can be degraded and cleared from blood by hydrolysis to phosphate monomers [19], and it is a low-cost, inorganic material.

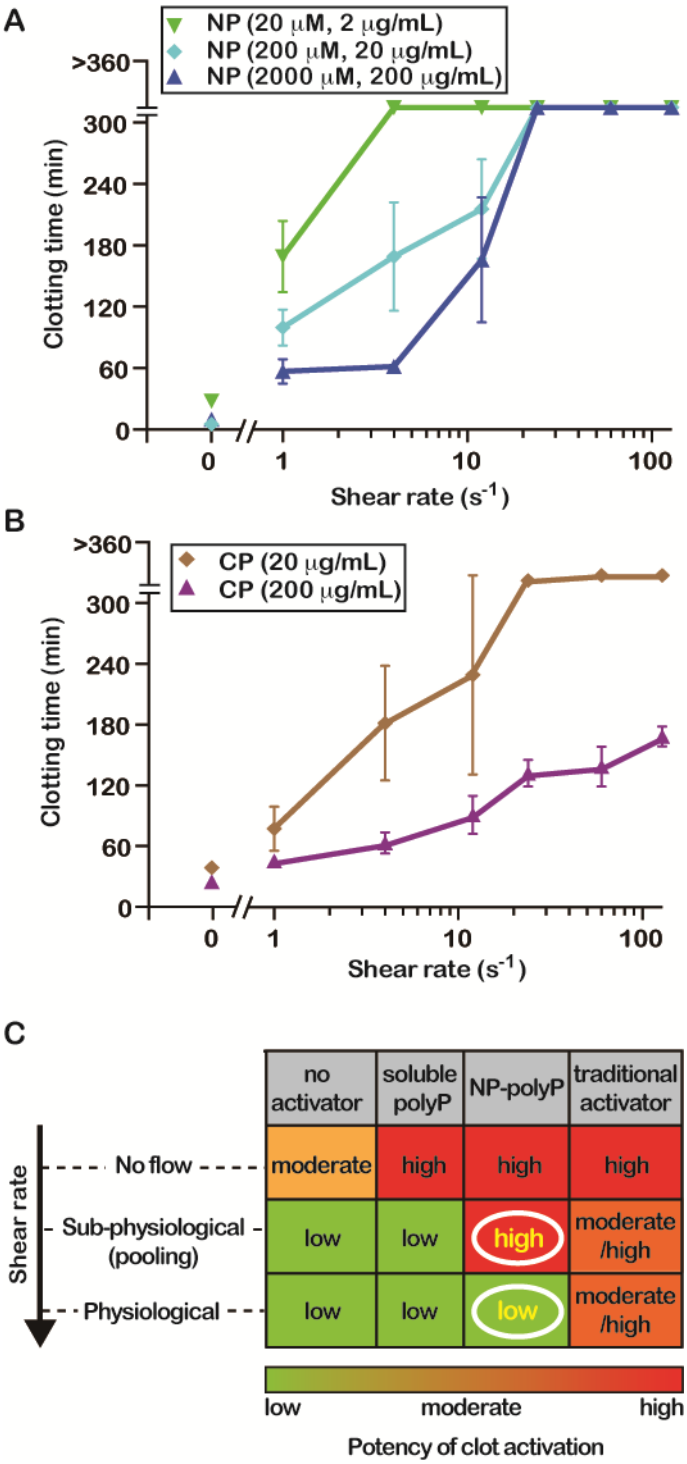

Figure 55. Dispersed polyP nanoparticles can selectively clot blood at sub-physiological shear rate. (A) NP-PolyP$_{1000}$ nanoparticles accelerate clotting in a shear- and concentration-dependent manner. (B) PolyP-coated silica nanoparticles (CP) also showed shear- and concentration-dependence in accelerating clotting. (C) A summary of the influence of nanoparticles of polyP on clotting at physiological and sub-physiological shear. The ability of dispersed NP-polyP to selectively clot at sub-physiological shear, such as what may occur in blood pooling in wounds outside of the vasculature, is highlighted with white circles.

4. KEY RESEARCH ACCOMPLISHMENTS

Numerical simulations

- Numerical simulations were optimized to include equations that reflect the activity of polyP on clotting.
- Simulations predicted that the localization of polyP increases its coagulability, including when blood is flowing.

Raw materials for conjugation to nanoparticles:

- Synthesized and characterized silica nanoparticles as a carrier for polyP.
- Synthesized and characterized iron oxide nanoparticles for use as a carrier for polyP. Iron oxide is less procoagulant than silica and can be used as a contrast agent for real time imaging.
- Synthesized iron oxide core-silica shell nanoparticles for use as a carrier for polyP. Iron oxide core provides contrast agent properties, while silica improves biocompatibility.

Coupling chemistries for conjugation of polyP to nanoparticles:

- Applied both adsorbed and covalently bound polyP techniques to silica.
- For covalently bound polyP to silica, used APTMS or APTES to form the amide bond followed by EDAC cross-linker.
- An alternative to EDAC as a cross-linker for covalent binding of polyP to silica was through the use of NHS-OPSS.
- A facile, EDAC-mediated coupling chemistry was developed to allow ester linkages between alcohols and the terminal phosphates of polyP.
- Leveraging an aqueous solvent environment, esterification was used to couple polyP to silica.
- Iron oxide-polyP conjugates were prepared using Lewis acid chemistry.
- An alternate technique for conjugating polyP to iron oxide was by esterification.

Microfluidics:

- Devices were developed for measuring clot times simultaneously at various shear rates.
- Found that surface-immobilized polyP initiates clotting of flowing blood plasma.
- Found that polyP with chain-lengths similar to platelet polyP can initiate clotting when surface-localized far more efficiently than when present in bulk solution.

PolyP-based procoagulant nanoparticles:

- Size-controlled nanoprecipitation of polyP in aqueous solutions containing biologically relevant concentrations of divalent metal cations (e.g. Ca^{2+}, Mg^{2+}, Zn^{2+} etc.)
- Synthesis of Artificial Dense Granules as a drug delivery system (DDS) for treating incompressible hemorrhage
- Found that particles of polyP initiate clotting faster than solubilized macromers of polyP.
- Found that polyP nanoparticles initiate clotting in a shear-dependent manner, where they clot plasma at the low shear rates typical of blood that is pooling in wounds.

5. CONCLUSION

This past year, we made significant progress in synthesizing, characterizing, and understanding the properties of iron oxide, silica, and iron oxide core-silica shell nanoparticles with respect to the blood clotting process, and to leverage their properties in developing an effective TSP upon conjugation with polyP. We also expanded the coupling chemistries available for covalently linking various functional groups to the terminal phosphates of polyP, thereby expanding our ability to fabricate pro-hemostatic nanoparticles of varying compositions and properties.

Using systematic methods of synthesis and characterization of SNP functionalized with linkers, such as APTES followed by EDAC, to covalently bind polyP, we enhance our understanding of the chemistry involved in developing procoagulant agents. Synthesis techniques for silica focused on the Stober and reverse micelle method, while iron oxide nanoparticles were synthesized using protocols in organic solvent and later modified to allow for biocompatible solvent. Chemical and morphological characterization methods were expanded to include scanning and transmission electron microscopy; elemental analysis; dynamic and electrophoretic light scattering; and Raman, fourier transform infrared, x-ray photoelectron, energy dispersive x-ray spectroscopy. In vitro studies of nanoparticle-polyP conjugate systems to determine blood clotting time as a function of simulated environmental conditions and nanoparticle-polyP composition continue to be conducted using the thromboelastograph.

Our future plans are to further our study of silica, iron oxide, and iron oxide core-silica nanoparticles to refine size and charge parameters, as well as functionalization techniques with polyP to maximize TSP function. This is followed by comprehensive characterization of the composite TSP for its chemical and in vitro blood clotting properties. Functionalization techniques of the nanocomposite TSP will incorporate protecting groups and targeting peptides. Specifically, we plan to use biotinylated polyP and biotinylated nanoparticles as proof-of-concept targetable particles with immobilized streptavidin as the target. Another pursuit is the use of the CREKA peptide sequence to facilitate targeting and physical binding of the particles to a site of injury where a clot has started to form, which then serves to initiate the TSP and allows the TSP to enhance the blood clotting process by accelerating it.

We also worked toward a goal of creating "Artificial Dense Granules" via the size-controlled synthesis of monodisperse polyP NPs at physiological concentrations of calcium and magnesium. The solubility is related nonlinearly to the polymer length, with very long-chain polyP precipitating much more facilely than platelet-sized polyP. Further, the NP size is only a function of the calcium concentration across a wide supersaturation range. The granules are stable for at least an hour in aqueous buffer solutions, displaying typical power-law growth kinetics, and are stable in BSA suspensions for three hours.

The polyP NPs possess promising procoagulant activity. Given that the polyP particles are stable on the same time scale as a catastrophic bleeding event raises the question that polyP's powerful procoagulant effects on the intrinsic pathway may be related to its precipitation into micron or sub-micron granular particles serving as negatively charged surfaces for FXII activation. The facile, size-controlled synthesis of these particles in the laboratory serves as a foundation for the future development of targeted procoagulant nanotechnologies exploiting polyP precipitation to mitigate the effects of a diversity of bleeding phenomena such as internal hemorrhage and hemophilia in a minimally invasive manner.

Recent efforts in the Liu Group have centered on this objective of developing a targeted hemostatic nanotherapy to treat incompressible hemorrhage in a minimally invasive fashion. Granular polyP NPs have been successfully encapsulated in sterically stabilized vesicles to produce Artificial Dense Granules, mimicking the body's inherent hemostatic mechanisms. We were able to demonstrate that treatment with the non-ionic detergent Tween 20, or digestion with a Ca^{2+}-dependent hydrolytic enzyme, $sPLA_2$, found at high concentrations proximal to bleeding sites, is able to solubilize/unwrap the protective lipid envelope, allowing for the condensed PolyP cargo to activate FXII *in vitro*. All in all, Artificial Dense Granules are a promising therapy for a constellation of

catastrophic bleeding events, as the synthesis is facile and PolyP is natural, inexpensive, and inherently procoagulant.

Future efforts will be focused on introducing integral membrane proteins derived from human platelets, such as integrins, von Willebrand Factor, fibrinogen, and collagen binding protein so that Artificial Dense Granules can marginate at the bleeding site and bind to activated platelets. New liposomal formulations will be investigated, such as adding cholesterol, to increase vesicular integrity of the Artificial Dense Granules at physiological conditions. Once this is satisfactorily complete, *in vivo* studies can commence. We also wish to further explore polyP nanoprecipitation and formation in more detail with other nontoxic divalent metal ions.

In summary, this work shows that spatial localization of polyP increases its propensity to initiate clotting of blood plasma. The concentration required to initiate clotting is markedly reduced when polyP is spatially localized into particles or onto surfaces. This effect is so pronounced that very short polyP, such as $polyP_{70}$ and $polyP_{160}$, previously considered to be weak activators, can substantially accelerate clotting, even under flow at physiological shear rates. These results support the notion that platelet-derived polyP may play a role in coagulation *in vivo*, but further work would be necessary to verify this. The flow system used here obviously does not include many factors that normally regulate hemostasis, such as platelets, red blood cells, immune cells, other soluble factors and endothelium. The presence of these factors would likely decrease clot initiation times and reduce the threshold concentrations of polyP. The result here also suggest that formulations for polyP nanoparticles may be useful therapeutically at selectively clotting regions of pooling blood, flowing at low shear, during severe and incompressible hemorrhage. Appropriate *in vivo* models are necessary as a next step to fully test the shear- and localization- effects of polyP observed here *in vitro* with blood plasma.

6. PUBLICATIONS, ABSTRACTS, AND PRESENTATIONS

Published and In Press in peer-reviewed scientific journals:

(1) Hebbard CF, Wang Y, Baker CJ, and Morrissey JH. Synthesis and evaluation of chromogenic and fluorogenic substrates for high-throughput detection of enzymes that hydrolyze inorganic polyphosphate. *Biomacromolecules*. **2014**, 15(8):3190-3196. DOI: 10.1021/bm500872g

(2) Donovan AJ, Kalkowski J, Smith SA, Morrissey JH, and Liu Y. Size-controlled synthesis of granular polyphosphate nanoparticles at physiologic salt concentrations for blood clotting. *Biomacromolecules*. **2014**, 15(11): 3976-3984. DOI: 10.1021/bm501046t

(3) Kudela D, Smith SA, May-Masnou A, Braun GB, Pallaoro A, Nguyen CK, Chuong TT, Nownes S, Allen R, Parker NR, Rashidi HH, Morrissey JH, and Stucky GD. Clotting activity of polyphosphate functionalized silica nanoparticles. *Angew. Chemie*, In Press.

In preparation (planned for submission to peer-reviewed scientific journals):

(1) M. Szymusiak*, A.J. Donovan*, R. Ransom, H. Shen, S.A. Smith, J.H. Morrissey, and Y. Liu. "Platelet polyphosphate-functionalized gold nanoparticles synthesized by phosphoramidate conjugation chemistry activate the intrinsic pathway of blood coagulation." To be submitted to *Mol Pharmaceutics*.

(2) A.J. Donovan, J. Kalkowski, M. Szymusiak, S.A. Smith, J.H. Morrissey, and Y. Liu. "Artificial platelet dense granules to treat catastrophic bleeding phenomena. To be submitted to *Nano Letters*.

Conference Presentations:

(1) A.J. Donovan, J. Kalkowski, S.A. Smith, J.H. Morrissey, and Y. Liu. "Size-controlled synthesis of granular polyphosphate nanoparticles at physiologic salt concentrations for blood clotting." 15th Annual Midwest Platelet Conference, 8-10th October 2014.

(2) Damien Kudela, Stephanie A. Smith, Ju Hun Yeon, Anna May-Masnou, Gary B. Braun, Alessia Pallaoro, Tracy Chuong, James R. Baylis, Christian J. Kastrup, James H. Morrissey and Galen D. Stucky. "Treating non-compressible hemorrhage with functionalized nanoparticles," Military Health System Research Symposium (MHSRS), Orlando, Florida, 2014.

(3) Damien Kudela, Stephanie A. Smith, Ju Hun Yeon, Anna May-Masnou, Gary B. Braun, Alessia Pallaoro, Tracy Chuong, James R. Baylis, Christian J. Kastrup, James H. Morrissey and Galen D. Stucky. "Treating non-compressible hemorrhage with functionalized nanoparticles," Nanotech, Washington, D.C., 2014.

7. INVENTIONS, PATENTS AND LICENSES

Provisional Utility Patent Applications:

(1) A.J. Donovan and Y. Liu. “Artificial Platelets.” Filing Date: 26 September 2014.

(2) Damien Kudela, Galen D. Stucky, Anna May-Masnou, Gary B. Braun, James H. Morrissey, Stephanie A. Smith. "Polyphosphate-Functionalized Inorganic Nanoparticles as Hemostatic Compositions and Methods of Use." U. S. Patent Application #20140255336, filed March 7, 2014.

Invention Disclosures:

(1) Y. Liu, R. Ransom, M. Szymusiak, and A.J. Donovan. “Colloidal polyphosphate using an organic or inorganic nanoparticle scaffold to treat internal and external bleeding phenomena.”

8. REPORTABLE OUTCOMES

This research has led to the development of a company, Cayuga Biotech, which seeks to commercialize treatments for hemorrhage.

9. OTHER ACHIEVEMENTS

None (the above categories list our progress and outcomes appropriately).

10. REFERENCES

[1] Smith SA, Mutch NJ, Baskar D, Rohloff P, Docampo R, Morrissey JH. Polyphosphate modulates blood coagulation and fibrinolysis. Proc Natl Acad Sci U S A. 2006;103:903-8.

[2] Morrissey JH, Choi SH, Smith SA. Polyphosphate: an ancient molecule that links platelets, coagulation, and inflammation. Blood. 2012;119:5972-9.

[3] Muller F, Mutch NJ, Schenk WA, Smith SA, Esterl L, Spronk HM, et al. Platelet Polyphosphates Are Proinflammatory and Procoagulant Mediators In Vivo. Cell. 2009;139:1143-56.

[4] Shoffstall AJ, Atkins KT, Groynom RE, Varley ME, Everhart LM, Lashof-Sullivan MM, et al. Intravenous hemostatic nanoparticles increase survival following blunt trauma injury. Biomacromolecules. 2012;13:3850-7.

[5] Chatterjee MS, Denney WS, Jing H, Diamond SL. Systems biology of coagulation initiation: kinetics of thrombin generation in resting and activated human blood. PLoS Comput Biol. 2010;6.

[6] Smith SA, Mutch NJ, Baskar D, Rohloff P, Docampo R, Morrissey JH. Polyphosphate modulates blood coagulation and fibrinolysis. Proceedings of the National Academy of Sciences of the United States of America. 2006;103:903-8.

[7] Müller F, Mutch NJ, Schenk WA, Smith SA, Esterl L, Spronk HM, et al. Platelet polyphosphates are proinflammatory and procoagulant mediators in vivo. Cell. 2009;139:1143-56.

[8] Smith SA, Choi SH, Davis-Harrison R, Huyck J, Boettcher J, Rienstra CM, et al. Polyphosphate exerts differential effects on blood clotting, depending on polymer size. Blood. 2010;116:4353-9.

[9] Choi S, SA S, JH M. Polyphosphate is a cofactor for the activation of factor XI by thrombin. Blood. 2011;118:6963-70.

[10] Kastrup CJ, Runyon MK, Lucchetta EM, Price JM, Ismagilov RF. Using chemistry and microfluidics to understand the spatial dynamics of complex biological networks. Acc Chem Res. 2008;41:549-58.

[11] Okorie UM, Denney WS, Chatterjee MS, Neeves KB, Diamond SL. Determination of surface tissue factor thresholds that trigger coagulation at venous and arterial shear rates: amplification of 100 fM circulating tissue factor requires flow. Blood. 2008;111:3507-13.

[12] Balandina AN, Shibeko AM, Kireev DA, Novikova AA, Shmirev II, Panteleev MA, et al. Positive feedback loops for factor V and factor VII activation supply sensitivity to local surface tissue factor density during blood coagulation. Biophys J. 2011;101:1816-24.

[13] Kastrup CJ, Runyon MK, Shen F, Ismagilov RF. Modular chemical mechanism predicts spatiotemporal dynamics of initiation in the complex network of hemostasis. Proc Natl Acad Sci USA. 2006;103:15747-52.

[14] Kastrup CJ, Boedicker JQ, Pomerantsev AP, Moayeri M, Bian Y, Pompano RR, et al. Spatial localization of bacteria controls coagulation of human blood by 'quorum acting'. Nat Chem Biol. 2008;4:742-50.

[15] Chatterjee MS, Denney WS, Jing H, Diamond SL. Systems biology of coagulation initiation: kinetics of thrombin generation in resting and activated human blood. PLoS Comput Biol. 2010;6:e1000950.

[16] Fogelson Aaron L, Hussain Yasmeen H, Leiderman K. Blood clot formation under flow: the importance of factor XI depends strongly on platelet count. Biophys J. 2012;102:10-8.

[17] Haynes LM, Dubief YC, Orfeo T, Mann KG. Dilutional control of prothrombin activation at physiologically relevant shear rates. Biophys J.100:765-73.

[18] Runyon MK, Kastrup CJ, Johnson-Kerner BL, Van Ha TG, Ismagilov RF. Effects of Shear Rate on Propagation of Blood Clotting Determined Using Microfluidics and Numerical Simulations. J Am Chem Soc. 2008;130:3458-64.

[19] Donovan AJ, Kalkowski J, Smith SA, Morrissey JHL, Ying. Size-controlled synthesis of granular polyphosphate nanoparticles at physiologic salt concentrations for blood clotting. Biomacromolecules. 2014;15:3976-84.

[20] Choi SH, Collins JN, Smith SA, Davis-Harrison RL, Rienstra CM, Morrissey JH. Phosphoramidate end labeling of inorganic polyphosphates: facile manipulation of polyphosphate for investigating and modulating its biological activities. Biochemistry. 2010;49:9935-41.

[21] Hebbard CF, Wang Y, Baker CJ, Morrissey JH. Synthesis and evaluation of chromogenic and fluorogenic substrates for high-throughput detection of enzymes that hydrolyze inorganic polyphosphate. Biomacromolecules. 2014;15:3190-6.

[22] Docampo R, de Souza W, Miranda K, Rohloff P, Moreno SN. Acidocalcisomes - conserved from bacteria to man. Nature reviews Microbiology. 2005;3:251-61.

[23] Docampo R, Moreno SNJ. Acidocalcisome: A novel Ca2+ storage compartment in trypanosomatids and apicomplexan parasites. Parasitol Today. 1999;15:443-8.

[24] Ruiz FA, Lea CR, Oldfield E, Docampo R. Human platelet dense granules contain polyphosphate and are similar to acidocalcisomes of bacteria and unicellular eukaryotes. J Biol Chem. 2004;279:44250-7.

[25] Donovan AJ, Kalkowski J, Smith SA, Morrissey JH, Liu Y. Size-Controlled Synthesis of Granular Polyphosphate Nanoparticles at Physiologic Salt Concentrations for Blood Clotting. Biomacromolecules. 2014;15:3976-84.

[26] Renné T, Schmaier AH, Nickel KF, Blomback M, Maas C. In vivo roles of factor XII. Blood. 2012;120:4296-303.

[27] Samuel M, Pixley RA, Villanueva MA, Colman RW, Villanueva GB. Human Factor-Xii (Hageman-Factor) Autoactivation by Dextran Sulfate - Circular-Dichroism, Fluorescence, and Ultraviolet Difference Spectroscopic Studies. J Biol Chem. 1992;267:19691-7.

[28] Corretge E, Nigretto JM. Molecular Weight-Dependent Contact Activation of Plasma Induced by Soluble Polystyrene and Dextran Derivatives. Thromb Res. 1990;59:463-73.

[29] Silverberg M, Diehl SV. The Autoactivation of Factor-Xii (Hageman-Factor) Induced by Low-Mr Heparin and Dextran Sulfate - the Effect of the Mr of the Activating Polyanion. Biochem J. 1987;248:715-20.

[30] Torchilin VP. Recent advances with liposomes as pharmaceutical carriers. Nat Rev Drug Discov. 2005;4:145-60.

[31] Meng F, Zhong Z, Feijen J. Stimuli-responsive polymersomes for programmed drug delivery. Biomacromolecules. 2009;10:197-209.

[32] Discher DE, Ahmed F. Polymersomes. Annual review of biomedical engineering. 2006;8:323-41.

[33] Huh KM, Lee SC, Cho YW, Lee J, Jeong JH, Park K. Hydrotropic polymer micelle system for delivery of paclitaxel. Journal of controlled release : official journal of the Controlled Release Society. 2005;101:59-68.

[34] Kovacs EW, Hooker JM, Romanini DW, Holder PG, Berry KE, Francis MB. Dual-surface-modified bacteriophage MS2 as an ideal scaffold for a viral capsid-based drug delivery system. Bioconjugate chemistry. 2007;18:1140-7.

[35] Bellomo EG, Wyrsta MD, Pakstis L, Pochan DJ, Deming TJ. Stimuli-responsive polypeptide vesicles by conformation-specific assembly. Nature materials. 2004;3:244-8.

[36] James ND, Coker RJ, Tomlinson D, Harris JR, Gompels M, Pinching AJ, et al. Liposomal doxorubicin (Doxil): an effective new treatment for Kaposi's sarcoma in AIDS. Clinical oncology. 1994;6:294-6.

[37] Hu CM, Zhang L, Aryal S, Cheung C, Fang RH, Zhang L. Erythrocyte membrane-camouflaged polymeric nanoparticles as a biomimetic delivery platform. Proceedings of the National Academy of Sciences of the United States of America. 2011;108:10980-5.

[38] Mounier C, Faili A, Vargaftig BB, Bon C, Hatmi M. Secretory phospholipase A2 is not required for arachidonic acid liberation during platelet activation. European journal of biochemistry / FEBS. 1993;216:169-75.

[39] Emadi S, Mirshahi M, Elalamy I, Nicolas C, Vargaftig BB, Hatmi M. Cellular source of human platelet secretory phospholipase A2. British journal of haematology. 1998;100:365-73.

[40] Anselmo AC, Modery-Pawlowski CL, Menegatti S, Kumar S, Vogus DR, Tian LL, et al. Platelet-like Nanoparticles: Mimicking Shape, Flexibility, and Surface Biology of Platelets To Target Vascular Injuries. ACS nano. 2014;8:11243-53.

[41] Zhou Z, Anselmo AC, Mitragotri S. Synthesis of protein-based, rod-shaped particles from spherical templates using layer-by-layer assembly. Advanced materials. 2013;25:2723-7.

[42] Touqui L, Alaoui-El-Azher M. Mammalian secreted phospholipases A2 and their pathophysiological significance in inflammatory diseases. Current molecular medicine. 2001;1:739-54.

[43] Engel R, Brain CM, Paget J, Lionikiene AS, Mutch NJ. Single-chain factor XII exhibits activity when complexed to polyphosphate. Journal of thrombosis and haemostasis : JTH. 2014;12:1513-22.

[44] Duclos B, Marcandier S, Cozzone AJ. Chemical properties and separation of phosphoamino acids by thin-layer chromatography and/or electrophoresis. Methods Enzymol. 1991;201:10-21.

[45] Mosimann PJ, Sirimarco G, Meseguer E, Serfaty J-M, Laissy J-P, Labreuche J, et al. Is intracerebral hemorrhage a tiime-dependent phenomenon after successful combined intravenous and intra-arterial therapy? Stroke. 2013;44:806-8.

[46] Riddell A, Abdul-Kadir R, Pollard D, Tuddenham E, Gomez K. Monitoring low dose recombinant factor VIIa therapy in patients with severe factor XI deficiency undergoing surgery. Thromb Haemost. 2011;106:521-7.

[47] Herman GDH, Joost MAAvdM, Joost de W, Tjalling WW, Maarten JHS, Jan van der M. An effective treatment of severe intractable bleeding after valve repair by one single dose of activated recombinant factor VII. Anesth Analg. 2001;93:287-.

[48] Morrissey JH, Macik BG, Neuenschwander PF, Comp PC. Quantitation of activated factor VII levels in plasma using a tissue factor mutant selectively deficient in promoting factor VII activation. Blood. 1993;81:734-44.

[49] Mackman N. New insights into the mechanisms of venous thrombosis. J Clin Invest. 2012;122:2331-6.

[50] Smith SA, Choi SH, Collins JNR, Travers RJ, Cooley BC, Morrissey JH. Inhibition of polyphosphate as a novel strategy for preventing thrombosis and inflammation. Blood. 2012;120:5103-10.

[51] Ruiz FA, Lea CR, Oldfield E, Docampo R. Human platelet dense granules contain polyphosphate and are similar to acidocalcisomes of bacteria and unicellular eukaryotes. J Biol Chem. 2004;279:44250-7.

11. APPENDIX

PDF "reprints" of the following three papers resulting from this project are attached as an appendix:

(1) Hebbard CF, Wang Y, Baker CJ, and Morrissey JH. Synthesis and evaluation of chromogenic and fluorogenic substrates for high-throughput detection of enzymes that hydrolyze inorganic polyphosphate. *Biomacromolecules*. **2014**, 15(8):3190-3196. DOI: 10.1021/bm500872g

(2) Donovan AJ, Kalkowski J, Smith SA, Morrissey JH, and Liu Y. Size-controlled synthesis of granular polyphosphate nanoparticles at physiologic salt concentrations for blood clotting. *Biomacromolecules*. **2014**, 15(11): 3976-3984. DOI: 10.1021/bm501046t

(3) Kudela D, Smith SA, May-Masnou A, Braun GB, Pallaoro A, Nguyen CK, Chuong TT, Nownes S, Allen R, Parker NR, Rashidi HH, Morrissey JH, and Stucky GD. Clotting activity of polyphosphate functionalized silica nanoparticles. *Angew. Chemie*, In Press.

Article

pubs.acs.org/Biomac

Open Access on 07/07/2015

Synthesis and Evaluation of Chromogenic and Fluorogenic Substrates for High-Throughput Detection of Enzymes That Hydrolyze Inorganic Polyphosphate

Carleigh F. F. Hebbard,[†,§] Yan Wang,[†] Catherine J. Baker,[†] and James H. Morrissey*[,†]

[†]Department of Biochemistry and [§]College of Medicine, University of Illinois at Urbana−Champaign, Urbana, Illinois 61801, United States

ABSTRACT: Inorganic polyphosphates, linear polymers of orthophosphate, occur naturally throughout biology and have many industrial applications. Their biodegradable nature makes them attractive for a multitude of uses, and it would be important to understand how polyphosphates are turned over enzymatically. Studies of inorganic polyphosphatases are, however, hampered by the lack of high-throughput methods for detecting and quantifying rates of polyphosphate degradation. We now report chromogenic and fluorogenic polyphosphate substrates that permit spectrophotometric monitoring of polyphosphate hydrolysis and allow for high-throughput analyses of both endopolyphosphatase and exopolyphosphatase activities, depending on assay configuration. These substrates contain 4-nitrophenol or 4-methylumbelliferone moieties that are covalently attached to the terminal phosphates of polyphosphate via phosphoester linkages formed during reactions mediated by EDAC (1-ethyl-3-(3-(dimethylamino)propyl)carbodiimide). This report identifies Nudt2 as an inorganic polyphosphatase and also adds to the known coupling chemistry for polyphosphates, permitting facile covalent linkage of alcohols with the terminal phosphates of inorganic polyphosphate.

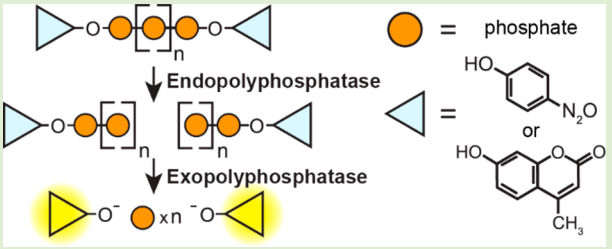

INTRODUCTION

Inorganic polyphosphates (polyP) are linear polymers of orthophosphate joined by high-energy phosphoanhydride bonds and can range in length from tens to thousands of phosphates. PolyP is widespread throughout biology and implicated in a multitude of physiologic processes in organisms from bacteria to man,[1−4] although many of its biological functions likely remain to be discovered and characterized. PolyP is also an industrial chemical with applications in areas such as water treatment, food processing, fertilizers, and flame retardants.[3] The biodegradable and versatile nature of polyP makes it an attractive material with many uses, and it would be desirable to understand how polyP is turned over. Known polyP-digesting enzymes include exopolyphosphatases which sequentially remove terminal phosphates from polyP, and endopolyphosphatases which hydrolyze internal phosphoanhydride bonds.[1] Although some of the enzymes responsible for degrading polyP have been identified in unicellular organisms, they remain relatively poorly studied in higher eukaryotes, with a few notable exceptions.[1,5] Two examples are mammalian alkaline phosphatase,[6] a highly potent exopolyphosphatase, and the human protein, h-prune, a short-chain exopolyphosphatase implicated as a regulator of metastasis.[7] Recent work has shown that polyP is secreted from activated human platelets[8] and mast cells[9] and that it is an important regulator of blood clotting[4] and complement.[10] PolyP is degraded in human plasma with a half-life of about 90 min,[11] which is no doubt important in controlling polyP's biological action, yet the mechanism of its degradation in vivo is currently unknown.

An impediment to identifying and studying the properties of polyP-degrading enzymes is the dearth of high-throughput means for detecting inorganic polyphosphatases and quantifying their activities. Many of the existing methods for quantifying enzymatic polyP degradation are cumbersome, of low sensitivity, or require the use of specialized equipment. The methods also typically rely on multiple steps including chromatography, gel electrophoresis, laborious physical extraction protocols coupled with chemical detection of liberated inorganic orthophosphate, or the use of radiolabeled polyP.[1] On the other hand, recently reported, more facile methods for detecting exopolyphosphatase activity include the continuous recording of released inorganic monophosphate, which was successfully employed to determine the kinetic parameters of the exopolyphosphatase, h-prune.[7] Detecting and quantifying the action of endopolyphosphatases remains substantially more time-consuming, however, as it typically involves resolving the digested polyP products using gel electrophoresis.[12] We therefore sought to develop chromogenic and fluorogenic polyP substrates that would allow polyP degradation to be followed spectrophotometrically and, in particular, a method that would allow high-throughput detection of endopolyphos-

Received: June 13, 2014
Revised: July 2, 2014

   dx.doi.org/10.1021/bm500872g | *Biomacromolecules* XXXX, XXX, XXX−XXX

phatase activity. Ideally, we would covalently attach chromogenic or fluorogenic dyes to the terminal phosphates of polyP. Chromogenic and fluorogenic substrates are available for a number of hydrolases and are readily adaptable to high-throughput assays in multiwell formats. We previously showed that primary amines can be covalently coupled via phosphoramidate linkages to the terminal phosphates of polyP in a reaction promoted by the zero-length cross-linking reagent, 1-ethyl-3-(3-(dimethylamino)propyl)carbodiimide (EDAC).[13] In the present study, we now show that EDAC can also be used to promote the efficient formation of phosphoester linkages with the terminal phosphates of polyP, and we apply this chemistry to create chromogenic or fluorogenic polyphosphatase substrates in which polyP is end-labeled with either 4-nitrophenol (NOL) or 4-methylumbelliferone (MU). We also show that these polyP derivatives can be used to detect the action of endo- and exopolyphosphatases, depending on assay configuration.

EXPERIMENTAL SECTION

Materials. Specified reagents were purchased from Sigma-Aldrich (St. Louis, MO) unless otherwise noted. NOL was recrystallized using hot water and ethanol. All experiments in this report used a polyP preparation (Natriumpolyphosphat P70) that was a kind gift from BK Giulini GmbH (Ludwigshafen, Germany). The polymer lengths of this preparation ranged from about 20 to 100 phosphates, with a mean length of approximately 45 to 50. PolyP concentrations were quantified using malachite green after acid hydrolysis[14] and are reported here in terms of phosphate monomer (monomer formula: $NaPO_3$). PolyP was end-labeled with spermidine via phosphoramidate linkages as described.[13]

Methods. *EDAC-Mediated End-Labeling of PolyP by Esterification with Methanol.* A mixture of 5.9 mM polyP, 150 mM freshly dissolved EDAC, and 6.4 M methanol in 100 mM MES buffer pH 6.5 was incubated for either 5 h at 37 °C or 1 h at 65 °C, after which the reaction mixtures were cooled on ice. Reaction volumes varied from 0.35 to 6.5 mL. PolyP-methanol was purified by acetone precipitation; briefly, NaCl was added to the reaction mixture (to 535 mM) followed by two reaction volumes of acetone, with mixing after each addition. The mixture was then centrifuged at 11,000 × *g* for 7 min at room temperature, after which the supernatant was discarded. The polyP pellet was washed twice by adding acetone to the tube followed by centrifugation. Pellets were then dried and redissolved in water.

Prior to NMR analyses, polyP-methanol was further purified by adsorption to a suspension of silica particles ("glass milk"). Glass milk was produced by a modification of the method of Vogelstein and Gillespie,[15] in which 250 mL silica (325 mesh) was stirred in 400 mL water for 1 h, then allowed to settle for 1 h to remove large particles. The supernatant was then centrifuged for 4000 × *g* for 15 min after which the pellet was collected and resuspended in 200 mL 50% nitric acid. This was then stirred and heated to close to boiling, after which it was cooled to room temperature. The silica fines were then collected by centrifugation and washed five times with water by resuspension and centrifugation. The final pellet of washed silica fines was resuspended as a 50% slurry by volume (glass milk). PolyP was purified by binding to, and elution from, glass milk as described,[14] except that the solutions were kept chilled throughout, and the polyP was eluted with 95 °C water instead of buffer.

EDAC-Mediated End-Labeling of PolyP by Esterification with NOL. A mixture of 5.9 mM polyP, 150 mM freshly dissolved EDAC, and 200 to 525 mM NOL was incubated for 1 h at 65 °C. Reaction volumes varied from 0.35 to 40 mL, and mixtures were agitated throughout, since the NOL concentrations exceeded solubility limits even in hot water. Completed reactions were cooled on ice and polyP was isolated by acetone precipitation. Because some free NOL coprecipitated with polyP in the first acetone precipitation, three full cycles of acetone precipitation were employed in which the collected polyP pellets were completely resuspended in water and reprecipitated by addition of NaCl and acetone followed by centrifugation. PolyP-NOL was then further purified using Bio-Gel P-6 desalting columns (Bio-Rad; Hercules, CA). The polyP-containing column fractions were identified by toluidine blue staining,[16] pooled, and lyophilized.

EDAC-Mediated End-Labeling of PolyP by Esterification with MU. A mixture of 5.5 mM polyP, 150 mM freshly dissolved EDAC, and 280 mM MU in a reaction volume of 1 mL was incubated for 1 h at 65 °C with agitation because the concentrations of MU used exceeded solubility limits. The reactions were then cooled on ice and polyP-MU was isolated using acetone precipitation as described above for the preparation of polyP-NOL.

NMR Analyses. Purified polyP and polyP derivatives were dissolved in water containing 10% (v/v) D_2O. All solution NMR spectra were collected on a Varian Unity INOVA 600 MHz proton frequency spectrometer with a 5 mm Varian AutoTuneX 1H/X PFG Z probe at 23 °C. 1D ^{31}P and ^{13}C spectra were acquired with a 2 s recycle delay. 1D ^{1}H spectra were acquired with a 1 s recycle delay, and solvent suppression was done by presaturation. 2D $^{1}H-^{13}C$ Heteronuclear Single Quantum Coherence (HSQC) spectra were acquired with 2048 and 160 points in the ^{1}H and ^{13}C dimensions, respectively. ^{1}H and ^{13}C spectra were referenced with external tetramethylsilane at 0 ppm, and ^{31}P spectra were referenced with external phosphoric acid at 0 ppm. 1D spectra were processed with MNOVA (MestreLab Research), and 2D spectra with NMRPipe.[17] polyP: ^{31}P NMR (90% H_2O 10% D_2O, 243 MHz) δ: −7.01 (s), −21.14, −21.65. polyP-methanol: ^{31}P NMR (90% H_2O 10% D_2O, 243 MHz) δ: −9.36 (d, $J_{P,P}$ = 17.8 Hz), −21.67. ^{1}H NMR (90% H_2O 10% D_2O, 600 MHz) δ: 3.51 (d, $J_{H,P}$ = 11.42 Hz). ^{13}C NMR (90% H_2O 10% D_2O, 151 MHz) δ: 53.7. polyP-NOL: ^{31}P NMR (90% H_2O 10% D_2O, 243 MHz) δ: −10.43, −16.81(d, $J_{P,P}$ = 17.7 Hz), −21.43, −21.61.

Gel Electrophoresis of PolyP. PolyP preparations were resolved on urea-containing 15% polyacrylamide gels and visualized using DAPI negative staining as described.[18]

Alkaline Phosphatase Digestion of PolyP. Protection against exopolyphosphatase-mediated degradation was employed to determine the extent to which polyP molecules were doubly end-labeled, as previously described.[13] Such digestions used calf intestinal alkaline phosphatase (CIAP, Promega; Madison, WI), a highly active exopolyphosphatase.[6] Typical reactions included 250 μM polyP and 20 units/mL CIAP; the liberated monophosphate was quantified using malachite green analysis.[14]

PolyP-NOL preparations often varied in the extent to which both ends of polyP were derivatized. To rid these preparations of singly labeled polyP, some were digested to completion with recombinant shrimp alkaline phosphatase (SAP, New England BioLabs; Ipswich, MA) by incubating 50 mM derivatized polyP with 50 U/mL SAP for 2 h at 37 °C in the manufacturer's buffer. SAP then was inactivated by heating at 65 °C (7 min), after which the remaining polyP was repurified by acetone precipitation. These preparations were termed SAP-treated polyP-NOL.

Endopolyphosphatase Digestion of PolyP. Certain nudix hydrolases were examined for endopolyphosphatase activity, typically in a two-stage assay. In the first stage, polyP-MU or SAP-treated polyP-NOL was incubated with endoacting enzyme (Nudt2 or Nudt3, Fitzgerald Industries International; Acton, MA) in the appropriate buffer at 37 °C, after which the reactions were chilled on ice. Buffer conditions were the following: for Nudt2, 8 mM SAP-treated polyP-NOL or 2 mM polyP-MU, 50 mM HEPES pH 7.4, and 5 mM $MgCl_2$; for Nudt3: 5.5 mM SAP-treated polyP-NOL or 2 mM polyP-MU, 25 mM HEPES pH 7.4, 20 mM NaCl, 10 mM $MgCl_2$, and 1 mM dithiothreitol.

For the second stage, a solution of CIAP in 100 mM Tris-HCl pH 8.8, 0.2 mM $ZnCl_2$ was prepared and warmed to 37 °C in 96-well polystyrene plates (Corning; Tewksbury, MA). The second stage was initiated by pipetting 100 μL of the chilled nudix-polyP reaction into prewarmed wells containing 100 μL CIAP solution, after which the rate of dye release was monitored spectrophotometrically at 37 °C. For polyP-NOL substrate, absorbance at 400 nm was measured using a SpectraMax M2 microplate reader (Molecular Devices; Sunnyvale, CA); for polyP-MU substrate, fluorescence was quantified in

dx.doi.org/10.1021/bm500872g | *Biomacromolecules* XXXX, XXX, XXX−XXX

Scheme 1. EDAC-Mediated Esterification of the Terminal Phosphates of PolyP[a]

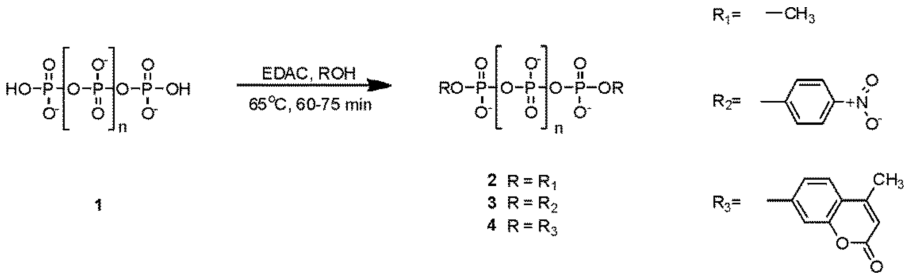

[a]Compounds: **1**, polyP; **2**, polyP-methanol; **3**, polyP-NOL; **4**, polyP-MU.

fluorescence mode using excitation at 360 nm, emission at 450 nm, and a 435 nm cutoff filter.

RESULTS

EDAC-Mediated Esterification of the Terminal Phosphates of PolyP with Methanol. EDAC has been used to promote the formation of ester linkages between alcohols and carboxylates,[19] as well as phosphoester linkages between alcohols and certain organic phosphates.[20] We therefore examined whether EDAC could promote the formation of ester linkages between alcohols and the terminal phosphate groups of inorganic polyP (Scheme 1).

As proof of principle, and to identify reaction conditions more readily, we examined EDAC-mediated esterification of polyP with methanol. The reaction resulted in a product that was protected from exopolyphosphatase (CIAP) digestion to an extent comparable to polyP that had been end-labeled with spermidine via phosphoramidate linkages (Table 1).

Table 1. Resistance of PolyP Derivatives to Hydrolysis by Alkaline Phosphatase (CIAP)

reactant	end label	% hydrolysis		
(none)	–	96.0	±	16.7
spermidine	$NH_2(CH_2)_3NH(CH_2)_4NH$–	20.8	±	2.1
methanol	H_3CO–	19.8	±	2.0
NOL	$O_2NC_6H_4O$–	27.0	±	2.0
MU	$C_{10}H_7O_3$–	3.9	±	1.6

We used solution-state NMR to further verify the product's identity. In the ^{31}P spectra, unmodified polyP displayed a relatively broad alpha (terminal) phosphorus peak at about 7 ppm (Figure 1A); the broadness likely reflects exchange of protonation states of the phosphate group.

Methylated polyP displayed an alpha peak shifted to 9.4 ppm (Figure 1B), which was also much sharper than the alpha peak of underivatized polyP. The methylated polyP alpha peak sharpness likely is caused by attenuation of the exchange broadening. This shifted alpha peak displayed as a doublet (Figure 1C) owing to the ^{31}P–^{31}P *J*-coupling between the alpha- and beta-phosphorus atoms. We next utilized the $^3J_{H-P}$ coupling between the methyl protons and alpha-phosphorus atom to confirm end modification and map connectivity. When proton decoupling was turned off, each peak of the alpha phosphorus doublet signal was split into a quartet pattern (Figure 1D), indicating the presence of three neighboring protons. To assign the chemical shift of the methyl protons, we acquired a 1D ^{1}H spectrum with heteronuclear decoupling irradiation at the alpha phosphorus frequency. The resulting spectrum, when compared to the spectrum without decoupling (compare Figure 1E and F), shows that the peak at around 3.5 ppm is converted from a doublet to a singlet. This transformation is consistent with a proton signal being coupled to a single neighboring phosphorus atom. To identify the carbon signal of the methyl group, we used ^{13}C-enriched (20%) methanol to synthesize methylated polyP. The resulting 1D ^{13}C spectrum (Figure 1H) shows significant enhancement of the carbon peak at ~53.6 ppm, which was almost unobservable in natural abundance methyl-polyP preparation (Figure 1G). To confirm that coupling existed between the carbon peak and the previously identified methyl proton signal, we performed 2D ^{1}H–^{13}C HSQC on the ^{13}C-enriched sample, with clearly observable correlation between the two signals (Figure 1I).

PolyP End-Labeled with NOL or MU. NOL is used often in making chromogenic substrates, as its absorption spectrum shifts dramatically when ester-linked to carboxylates or a single phosphate. MU is also extensively employed in synthesizing fluorogenic substrates because its fluorescence is quenched when ester-linked to carboxylates. Reacting polyP with NOL and EDAC resulted in a polyP preparation that was nearly as resistant to CIAP digestion as was polyP end-labeled with spermidine or methanol (Table 1). Reacting polyP with MU and EDAC resulted in a product with even greater CIAP resistance (Table 1) than that of polyP derivatized with spermidine or methanol. Absorption spectra of polyP-NOL before and after hydrolysis reveal an absorption maximum of 285 nm before hydrolysis (indicating covalent coupling of the NOL dye to phosphate) and 398 nm after hydrolysis (characteristic of free NOL; Figure 2C).

Analyzing polyP-NOL by 1D ^{31}P NMR produced an alpha peak shifted from ~7 ppm in underivatized polyP (Figure 1A) to a doublet at ~17 ppm in polyP-NOL (Figure 3A), consistent with covalent modification of the terminal phosphates. Resolving polyP and polyP-NOL by gel electrophoresis indicated little change in the distribution of polymer lengths after reacting the polyP with NOL and EDAC (Figure 3B).

Exopolyphosphatase (CIAP) Digestion of PolyP-NOL. End-labeling efficiency was calculated after complete acid hydrolysis of polyP-NOL and quantification and comparison of liberated NOL and monophosphate ratios (and assuming a mean polymer length of 50 phosphates). Using a polyP-NOL preparation in which approximately 40% of the polyP molecules were singly end-labeled, we added CIAP and monitored A_{400} versus time at 37 °C (Figure 3C). These results show that singly labeled polyP-NOL can be used to follow the progress of exopolyphosphatase digestion. The curvilinear progress curves probably reflect the fact that the substrate is ~50 phosphates long but the chromophore is

dx.doi.org/10.1021/bm500872g | *Biomacromolecules* XXXX, XXX, XXX–XXX

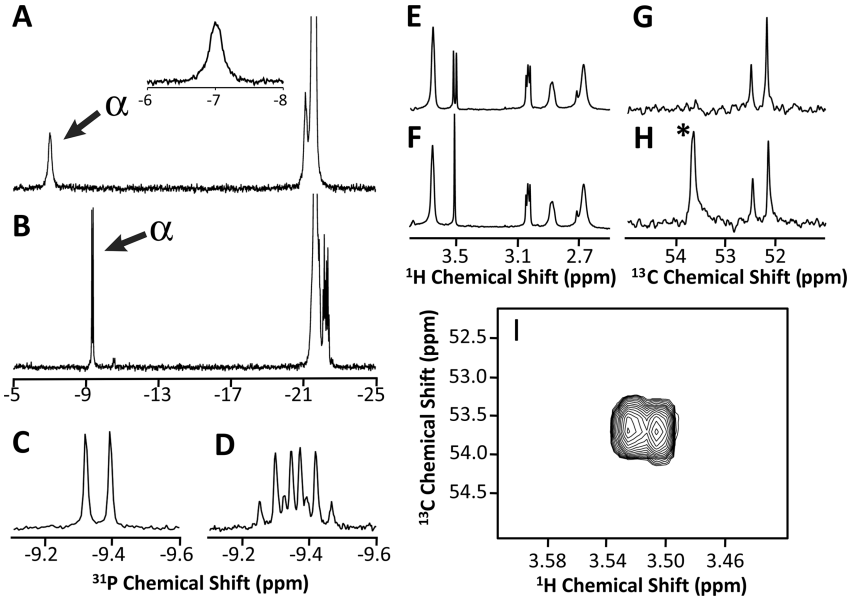

Figure 1. NMR analyses of end-methylated polyP. 1D ^{31}P spectra of (A) unmodified polyP and (B) polyP following reaction with methanol and EDAC. The terminal phosphate (alpha) peaks are indicated by arrows, and the inset in panel A is an expanded view of the alpha peak region of this spectrum. (C) The expanded view shows that the sharp alpha peak in panel B is resolved as a doublet. (D) Without ^{1}H decoupling, the alpha peak from methylated polyP expands into quartets as a result of *J* couplings from methyl protons. (E,F) 1D ^{1}H spectra of methylated polyP with (E) and without (F) applied decoupling irradiation at the alpha-phosphate frequency. The doublet peak at ~3.5 ppm (E) converts into a singlet (F) after irradiation because the proton peak is coupled to a phosphorus atom. (Other peaks in the ^{1}H spectra are from the MES buffer used in product purification and thus not affected by the decoupling.) 1D ^{13}C spectra of methylated polyP prepared with (G) natural abundance methanol or (H) 20% ^{13}C-enriched methanol. Use of ^{13}C-enriched methanol in the reaction greatly enhanced the signal at ~53.7 ppm (asterisk). (Other ^{13}C peaks are from the MES buffer.) (I) 2D HSQC analysis of the 53.7 ppm ^{13}C peak confirmed that the ^{13}C atoms are connected to the methyl protons.

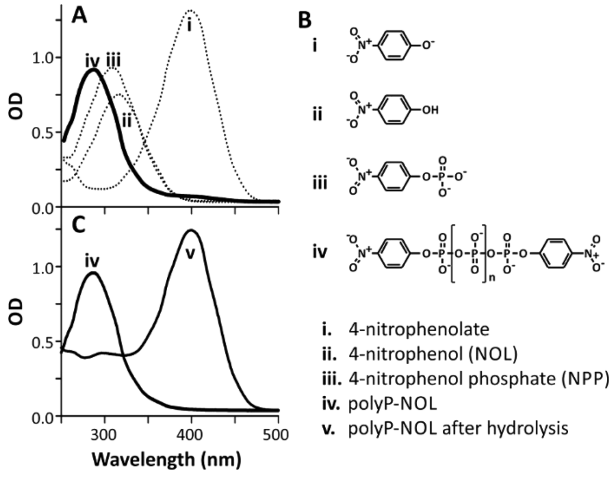

Figure 2. Product analysis and NOL substitution series using UV−vis spectroscopy. (A) Absorbance spectra of NOL substitution series with (B) the accompanying compounds' chemical structures. Each compound (except (ii)) was brought to a final concentration of 150 μM in alkaline conditions (1.5 M Tris-HCl buffer pH = 8.8, final) and scanned spectrally; NOL (ii) was scanned under acidic conditions. Absorbance maxima were the following: 398 nm (i), 317 nm (ii), 310 nm (iii), and 285 nm (iv). (C) Absorption spectra of polyP end-labeled with NOL, before (iv) and after (v) acid hydrolysis (1 M HCl for 1 h at 100 °C) followed by alkalization to pH 8.8.

released only when the last phosphate is removed from the substrate.

Endopolyphosphatase Digestion of PolyP-NOL and PolyP-MU. Covalent modification of polyP on both ends protects polyP against exopolyphosphatase (CIAP) digestion (Table 1). We therefore reasoned that two-stage assays for endopolyphosphatase activity could be devised using polyP that is completely labeled on both ends with chromophore or fluorophore. Digestion by exopolyphosphatase should be possible only after the action of endopolyphosphatase has exposed free polyP ends. In such an assay one could employ either sequential or simultaneous digestion with endo- and exopolyphosphatases. Accordingly, polyP-NOL was predigested to completion with SAP to eliminate singly labeled molecules, after which the polyP-NOL was repurified. We then used this SAP-treated polyP-NOL in a two-stage endopolyphosphatase assay in which we first digested the substrate with either Nudt3 (a hydrolase with known endopolyphosphatase activity[12]) or Nudt2 (another nudix hydrolase that cleaves dinucleotide polyphosphates, "Np$_n$Ns", but whose endopolyphosphatase activity was not known) and then monitored product release during digestion with CIAP. Figure 4 shows that few dye molecules from SAP-treated polyP-NOL were released upon incubating the substrate with either endopolyphosphatase (Nudt2 or Nudt3) or exopolyphosphatase (CIAP) alone. However, polyP-NOL was readily hydrolyzed by CIAP following pretreatment with either Nud2 or Nudt3. Additionally, this experiment demonstrated that Nudt2 has endopolyphosphatase activity (Figure 4B).

The efficiency of polyP labeling with MU was usually greater than that with NOL (Table 1), so predigestion of polyP-MU (Figure 5A) with SAP was typically not required before using this substrate to detect endopolyphosphatase activity. Figure 5B shows the reaction curves for two-stage assays of polyP-MU digestion with Nudt2 followed by CIAP. Neither Nudt2 nor CIAP alone released significant MU, while polyP-MU was efficiently digested by CIAP after incubation with Nudt2.

This experiment also demonstrates the amount of CIAP required for maximal rates of product release. Figure 5C shows

dx.doi.org/10.1021/bm500872g | Biomacromolecules XXXX, XXX, XXX−XXX

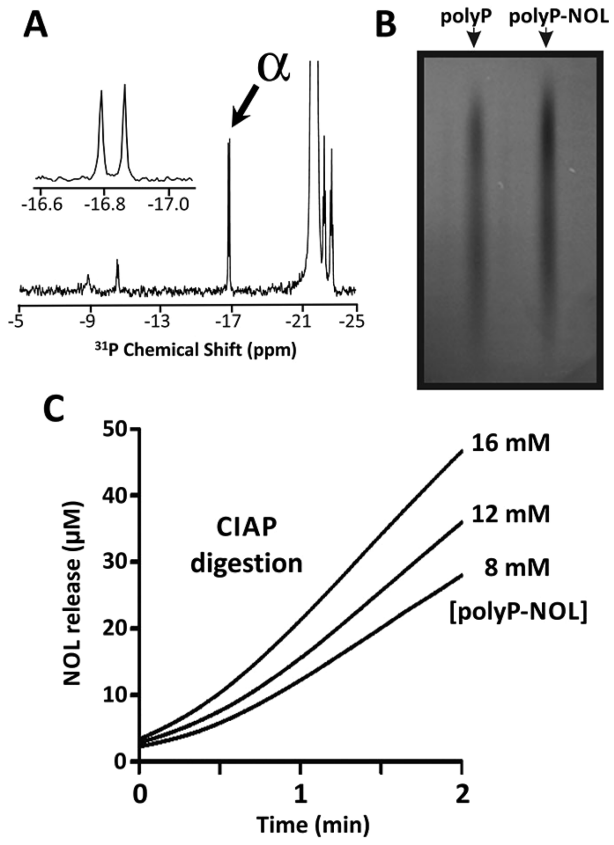

Figure 3. Analysis of polyP end-labeling with NOL. (A) 1D ^{31}P spectrum of polyP-NOL highly labeled at both ends. The alpha phosphate peak, indicated by an arrow, is resolved as a doublet (inset) upon axis expansion. (B) Comparison of polyP and polyP-NOL resolved by gel electrophoresis and detected by DAPI negative staining. (C) Enzymatic degradation of varying concentrations of incompletely end-labeled polyP-NOL (8 to 16 mM phosphate) by CIAP, with NOL release detected spectrophotometrically at 400 nm.

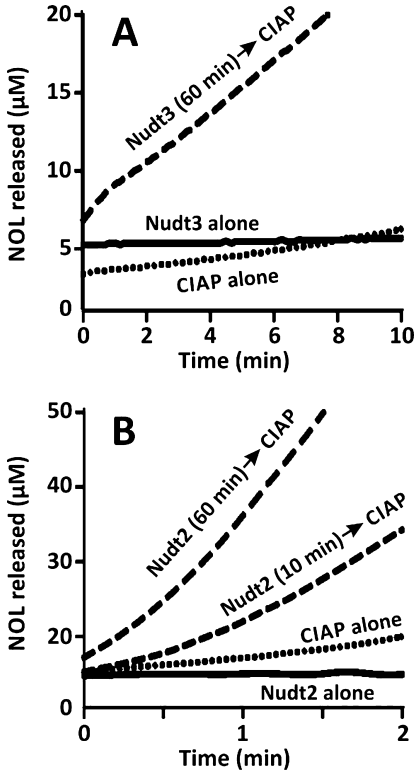

Figure 4. Sequential digestion of doubly end-labeled polyP-NOL with endopolyphosphatases and exopolyphosphatases. In both panels, doubly end-labeled polyP-NOL was first incubated with or without endopolyphosphatase (Nudt2 or Nudt3) for 10 or 60 min at 37 °C. Exopolyphosphatase (120 U/mL CIAP) was then added to the indicated samples and NOL release was quantified over time. (A) Treatment with 850 nM Nudt3. (B) Treatment with 250 nM Nudt2.

a much shorter time course of the second stage of this two-stage assay, using saturating levels of CIAP. We tested Nudt1 (a nudix hydrolase known to cleave Ap_3A but not long-chain Np_nN molecules) in a similar two-stage assay, but under the various conditions we used, the enzyme did not support MU release by CIAP (data not shown). We also examined a one-stage assay employing polyP-MU incubated simultaneously with CIAP plus varying concentrations of Nudt2. We found limited product release with CIAP alone but robust product release by the combination of CIAP and Nudt2 (Figure 5D).

DISCUSSION

This study had two goals: expand the covalent coupling chemistry for polyP, allowing for facile linkage of alcohols to the terminal phosphates of polyP via phosphoester bonds; and use this chemistry to develop high-throughput methods for detecting and quantifying the enzymatic digestion of polyP. We now report that the water-soluble cross-linker, EDAC, can be used to efficiently generate phosphoester linkages between alcohols and the terminal phosphates of polyP. We utilized this coupling chemistry to generate new chromogenic and fluorogenic substrates for detecting the enzymatic hydrolysis of polyP, based on phosphoester end-labeling of polyP with NOL or MU, respectively. Additionally, with our polyP substrates, we were able to monitor and distinguish endo- and exopolyphosphatase activities in real time.

Previously, we reported that EDAC could be used efficiently to couple compounds with primary amines to the terminal phosphates of polyP via phosphoramidate linkages, and this chemistry has allowed us to link a variety of probes to polyP;[13] for example, we used this method to biotinylate polyP, which we then employed to detect and quantify interactions between polyP and blood clotting proteins.[21,22] Although phosphoramidate linkages are relatively stable under neutral and alkaline conditions, the linkages are highly acid-labile.[23] It would be advantageous, therefore, to be able to efficiently link the terminal phosphates of polyP to organic compounds via phosphoester linkages, which, unlike phosphoramidate linkages, resist acid hydrolysis at physiological temperatures.[23] A previous study used combinations of carbodiimides (other than EDAC) in conjunction with polyP and alcohols in anhydrous organic solvents to generate phosphoester linkages to polyP; however, the reactions also caused substantial polyP hydrolysis to much shorter polyP chains and the apparent formation of cyclic and branched polyP adducts (which are unstable in aqueous solution).[24] In this report we identified aqueous coupling conditions for EDAC-mediated formation of phosphoester linkages to polyP that resulted in labeling just the terminal phosphates and that did not appreciably shorten the polyP chains.

Full-length polyP capped on either end with chromogenic or fluorogenic dyes was used to detect phosphatase activity. PolyP-

dx.doi.org/10.1021/bm500872g | Biomacromolecules XXXX, XXX, XXX−XXX

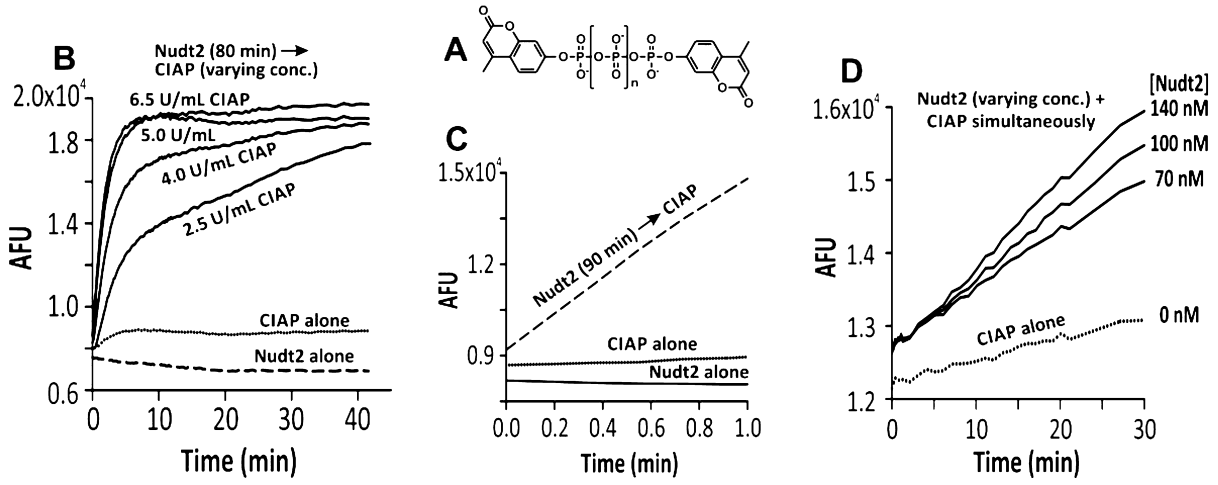

Figure 5. Digestion of polyP-MU by mixtures of endo- and exopolyphosphatases. (A) Structure of doubly end-labeled polyP-MU. (B) Sequential digestion of doubly end-labeled polyP-MU with endopolyphosphatase and exopolyphosphatase. PolyP-MU was first incubated with or without endopolyphosphatase (250 nM Nudt2) for 80 min at 37 °C, after which varying concentrations of exopolyphosphatase (CIAP) were added to the indicated samples and the increase in fluorescence (AFU) was quantified over time. (C) Sequential digestion of doubly end-labeled polyP-MU, first, with or without 250 nM Nudt2 for 90 min at 37 °C, after which 5 U/mL CIAP was added to the indicated samples and fluorescence was quantified over time. (D) Simultaneous digestion of polyP-MU with the indicated concentrations of Nudt2 and 55 U/mL CIAP, during which fluorescence was quantified over time.

NOL preparations that were incompletely labeled on both polyP ends were useful substrates for detecting exopolyphosphatase activity, which released free NOL upon the complete hydrolysis of the singly end-labeled polyP. On the other hand, polyP-NOL and polyP-MU preparations that were fully labeled on both polyP ends were highly resistant to exopolyphosphatase digestion, and this property was used as the basis of a two-stage assay in detecting endopolyphosphatase activity. In such assays, endopolyphosphatase digestion creates free polyP ends which are then substrates for exopolyphosphatase (CIAP) digestion, which in turn releases free dye from polyP-NOL or polyP-MU.

Not surprisingly, assays using the fluorogenic substrate, polyP-MU, could be conducted using lower substrate concentrations than those using the chromogenic substrate, polyP-NOL, owing to the greater sensitivity of fluorescence-based detection methods; however, assays using fluorogenic substrates require more specialized equipment and sample handling than do simple chromogenic assays, prompting us to develop both types of substrates in this study.

We constructed a two-stage assay to demonstrate the activity of a known endopolyphosphatase (Nudt3), and to demonstrate that another nudix hydrolase (Nudt2) also exhibits endopolyphosphatase activity. Nudt3, sometimes called DIPP1, or simply DIPP, is a nudix-type enzyme with multiple known in vitro substrates: capped mRNA, oxo-8-dGTPase, inositol pyrophosphates, dinucleotide polyphosphates, and inorganic polyphosphate (reviewed by McLennan[25]). Many nudix-type phosphatases are clinically important enzymes and their overexpression can be markers of disease. Nudt2 (Apah1), for example, is an Ap_4A hydrolase that, when overexpressed in breast cancer, correlates with poor prognosis.[26] In addition to processing Ap_4A, Nudt2 can hydrolyze long-chain Np_nNs such as Ap_6A. We hypothesized that this nudix enzyme, though previously not described as having endopolyphosphatase activity on inorganic polyP, might be able to cleave polyP and that we might detect this cleavage using our substrates in conjunction with CIAP. This was confirmed with our novel substrates. Like Nudt2, the human short-chain exopolyphosphatase, h-prune, is also implicated in tumor survival,[7] again providing a connection between alterations in polyP degradation and human health.

It should also be noted that the substrates only release a signal (free dye) when the last phosphate of the polyP chain is removed by an exopolyphosphatase. While this reaction was efficiently catalyzed by CIAP, other exopolyphosphatases might digest polyP to very short chains but not completely to monophosphate and therefore would not be expected to release the dye from these substrates. Such enzymes could be studied using these substrates in sequential assays employing CIAP.

We anticipate that the utilization of chromogenic and fluorogenic polyP substrates will aid further inquiry into how polyphosphates are turned over enzymatically. For example, an additional class of enzymes that could conceivably be studied using these substrates are kinases that utilize polyP as a substrate/phosphate donor. Also important is the development of a method for making stable ester linkages to the ends of polyP. Applications for such phosphoester linkages could include attaching polyP to surfaces, fabricating polyP-containing nanoparticles, and attaching fluorescent probes to polyP, in addition to creating the chromogenic and fluorogenic substrates for polyP-degrading enzymes reported here.

■ CONCLUSIONS

Using carbodiimide-mediated chemistry, we selectively esterified the terminal phosphates of inorganic polyP polymers with various alcohols. In a proof-of-principle experiment, we used methanol in esterification reactions and confirmed the product through 1D and 2D ^{31}P, ^{1}H, and ^{13}C NMR analyses. We also showed that polyP could be similarly end-labeled with chromogenic or fluorogenic alcohols to form adducts. These adducts were shown to be useful substrates for polyP-degrading enzymes, allowing us to monitor enzyme activity spectrophotometrically in real time; furthermore, we used these substrates to identify a new function for the clinically significant enzyme,

dx.doi.org/10.1021/bm500872g | Biomacromolecules XXXX, XXX, XXX−XXX

Nudt2. The chemistry and substrates developed in this work are likely to be useful for synthetic and clinical applications.

AUTHOR INFORMATION

Corresponding Author

*E-mail: jhmorris@illinois.edu. Telephone: (217) 265-5424. Fax: (217) 265-5290.

Notes

The authors declare no competing financial interest.

ACKNOWLEDGMENTS

We thank Dr. M. Burke for helpful discussions about chemical synthesis and Dr. A. Jahromi for help with recrystallization. This work was supported in part by grant R01 HL047014 from the National Heart, Lung and Blood Institute of the NIH, and by Award WQ81XWH-11-2-0021 from the U.S. Army Medical Research and Materiel Command. The U.S. Army Medical Research Acquisition Activity, 820 Chandler Street, Fort Detrick, MD 21702−5014 is the awarding and administering acquisition office. The contents of this article do not necessarily reflect the position or the policy of the Government, and no official endorsement should be inferred.

REFERENCES

(1) Rao, N. N.; Gomez-Garcia, M. R.; Kornberg, A. *Annu. Rev. Biochem.* **2009**, *78*, 605−647.

(2) Moreno, S. N.; Docampo, R. *PLoS Pathol.* **2013**, *9* (5), e1003230.

(3) Kulakovskaya, T. V.; Vagabov, V. M.; Kulaev, I. S. *Process Biochem.* **2012**, *47* (1), 1−10.

(4) Morrissey, J. H.; Choi, S. H.; Smith, S. A. *Blood* **2012**, *119* (25), 5972−5979.

(5) Azevedo, C.; Saiardi, A. *Biochem. Soc. Trans.* **2014**, *42* (1), 98−102.

(6) Lorenz, B.; Schröder, H. C. *Biochim. Biophys. Acta* **2001**, *1547* (2), 254−261.

(7) Tammenkoski, M.; Koivula, K.; Cusanelli, E.; Zollo, M.; Steegborn, C.; Baykov, A. A.; Lahti, R. *Biochemistry* **2008**, *47* (36), 9707−9713.

(8) Ruiz, F. A.; Lea, C. R.; Oldfield, E.; Docampo, R. *J. Biol. Chem.* **2004**, *279* (43), 44250−44257.

(9) Moreno-Sanchez, D.; Hernandez-Ruiz, L.; Ruiz, F. A.; Docampo, R. *J. Biol. Chem.* **2012**, *287* (34), 28435−28444.

(10) Wat, J. M.; Foley, J. H.; Krisinger, M. J.; Ocariza, L. M.; Lei, V.; Wasney, G. A.; Lameignere, E.; Strynadka, N. C.; Smith, S. A.; Morrissey, J. H.; Conway, E. M. *Blood* **2014**, *123* (5), 768−776.

(11) Smith, S. A.; Mutch, N. J.; Baskar, D.; Rohloff, P.; Docampo, R.; Morrissey, J. H. *Proc. Natl. Acad. Sci. U. S. A.* **2006**, *103* (4), 903−908.

(12) Lonetti, A.; Szijgyarto, Z.; Bosch, D.; Loss, O.; Azevedo, C.; Saiardi, A. *J. Biol. Chem.* **2011**, *286* (37), 31966−31974.

(13) Choi, S. H.; Collins, J. N.; Smith, S. A.; Davis-Harrison, R. L.; Rienstra, C. M.; Morrissey, J. H. *Biochemistry* **2010**, *49* (45), 9935−9941.

(14) Smith, S. A.; Choi, S. H.; Davis-Harrison, R.; Huyck, J.; Boettcher, J.; Reinstra, C. M.; Morrissey, J. H. *Blood* **2010**, *116* (20), 4353−4359.

(15) Gailani, D.; Broze, G. J., Jr. FXI and the contact system. In *Metabolic and Molecular Basis of Inherited Disease*; Scriver, C., Beaudet, A., Sly, W., Valle, D., Childs, B., Kinzler, K., Vogelstein, B., Eds.; McGraw-Hill: New York, 2001; Vol. *8*, pp 4433−4453.

(16) Damle, S. P.; Krishnan, P. S. *Arch. Biochem. Biophys.* **1954**, *49* (1), 58−70.

(17) Delaglio, F.; Grzesiek, S.; Vuister, G. W.; Zhu, G.; Pfeifer, J.; Bax, A. *J. Biomol. NMR* **1995**, *6* (3), 277−293.

(18) Smith, S. A.; Morrissey, J. H. *Electrophoresis* **2007**, *28* (19), 3461−3465.

(19) Otera, J.; Nishikido, J. Reaction of alcohols with carboxylic acids and their derivatives. In *Esterification: Methods, Reactions and Applications*, 2nd ed.; Wiley-VCH Verlag GmbH & Co. KGaA, 2010; pp 3−157.

(20) Jordan, S. W.; Cronan, J. E., Jr. *J. Bacteriol.* **2003**, *185* (5), 1582−1589.

(21) Choi, S. H.; Smith, S. A.; Morrissey, J. H. *Blood* **2011**, *118* (26), 6963−6970.

(22) Smith, S. A.; Choi, S. H.; Collins, J. N.; Travers, R. J.; Cooley, B. C.; Morrissey, J. H. *Blood* **2012**, *120* (26), 5103−5110.

(23) Duclos, B.; Marcandier, S.; Cozzone, A. J. *Methods Enzymol.* **1991**, *201*, 10−21.

(24) Glonek, T.; Kleps, R. A.; Van Wazer, J. R.; Myers, T. C. *Bioinorg. Chem.* **1976**, *5* (4), 283−310.

(25) McLennan, A. G. *Cell. Mol. Life Sci.* **2013**, *70* (3), 373−385.

(26) Oka, K.; Suzuki, T.; Onodera, Y.; Miki, Y.; Takagi, K.; Nagasaki, S.; Akahira, J.; Ishida, T.; Watanabe, M.; Hirakawa, H.; Ohuchi, N.; Sasano, H. *Int. J. Cancer* **2011**, *128* (8), 1770−1782.

Article

pubs.acs.org/Biomac

Size-Controlled Synthesis of Granular Polyphosphate Nanoparticles at Physiologic Salt Concentrations for Blood Clotting

Alexander J. Donovan,[†] Joseph Kalkowski,[†] Stephanie A. Smith,[‡] James H. Morrissey,[‡] and Ying Liu*[,†,§]

[†]Department of Chemical Engineering, University of Illinois at Chicago, Chicago, Illinois 60607, United States

[‡]Department of Biochemistry, University of Illinois at Urbana−Champaign, Urbana, Illinois 61801, United States

[§]Department of Biopharmaceutical Sciences, University of Illinois at Chicago, Chicago, Illinois 60607, United States

Supporting Information

ABSTRACT: Size-controlled granular polyphosphate (PolyP) nanoparticles were synthesized by precipitation in aqueous solutions containing physiological concentrations of calcium and magnesium. We demonstrate using dynamic light scattering (DLS) that the solubility is correlated inversely with PolyP chain length, with very long chain PolyP (PolyP1000+, more than 1000 repeating units) normally found in prokaryotes precipitating much more robustly than shorter chains like those found in human platelet dense granules (PolyP80, range 76−84 repeating units). It is believed that the precipitation of PolyP is a reversible process involving calcium coordination to phosphate monomers in the polymer chain. The particles are stable in aqueous buffer and albumin suspensions on time scales roughly equivalent to catastrophic bleeding events. Transmission electron microscopy images demonstrate that the PolyP nanoparticles are spherical and uniformly electron dense, with a particle diameter of 200−250 nm, closely resembling the content of acidocalcisomes. X-ray elemental analysis further reveals that the P/Ca ratio is 67:32. The granular nanoparticles also manifest promising procoagulant effects, as measured by *in vitro* clotting tests assaying contact pathway activity.

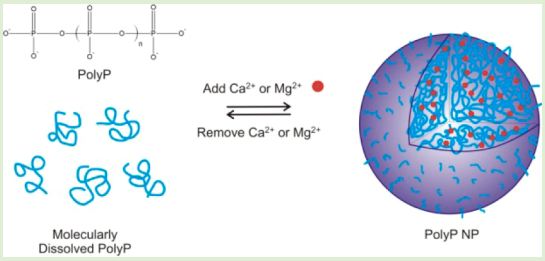

INTRODUCTION

Inorganic polyphosphate (PolyP) is an anionic linear polymer composed of orthophosphate subunits found in a broad array of organisms, ranging from the simplest prokaryotes to the most complex mammals including humans.[1] Dating from evolution's primordial stages, PolyP exhibits a diversity of functions depending upon its environment and polymer length, including highly regulated cellular tasks such as biofilm formation,[2] pathogen virulence,[3] cell motility,[4] quorum sensing,[5] transmembrane ion conductance,[6,7] metal chelation,[8] blood coagulation,[9−14] and energy storage.[15] PolyP's chemical simplicity despite its ubiquity, age, and biological versatility suggests that its precipitation into condensed granules may play a part in its myriad of biochemical tasks. Present across nearly all phylogenetic taxa are acidic subcellular storage compartments containing large quantities of PolyP.[16] Acidocalcisomes are acidic intracellular compartments found in prokaryotes that contain extremely high levels of ionized alkali earth and transition metal cations. Electron microscopy has revealed that these structures are electron dense, and elemental analysis confirms the presence of phosphate-containing compounds.[17] Ruiz et al. recently showed that this structure is conserved through the evolutionary tree to humans in the form of dense granules in human platelets.[18]

PolyP precipitates could wield different procoagulant effects than the molecularly dissolved polymer, possibly serving as an anionic contact "surface" for activation of FXII like kaolin and collagen.[19] Alternatively, these bodies could have evolved in evolution's early stages merely as condensed stores of large concentrations of PolyP for later downstream cellular functions requiring rapid nonlinear responses. PolyP has been known for approximately a century to reversibly bind to calcium, magnesium, iron, copper, zinc, barium, and other metals.[20] The calcium concentration within the platelet dense granules is as high as 2.2 M,[21] and the dissociation constants for Ca^{2+} and Mg^{2+} have even been quantified.[22]

Although successful synthesis of aluminum PolyP nanoparticles has been reported, the established synthetic routes require harsh organic solvents and intensive separation processes and lead to inadequate size control.[23] Momeni et al. investigated polyphosphate gels, or "coacervates," for potential utilization as hemostatic agents and examined the chelation of Ca^{2+}, Ba^{2+}, and Sr^{2+} to PolyP glasses of varied polymer lengths and its effects on solution pH and chain degradation of the PolyP solution.[24,25] However, systematic measurements of PolyP precipitation into particles with controlled sizes have never been reported. Moreover, the potential downstream therapeutic potential of PolyP precipitation has not been adequately addressed in the literature.

Herein, we show that the precipitation of inorganic PolyP into granular nanostructures is based on polymer length, with very long polymer lengths condensing much more robustly

Received: July 17, 2014
Revised: September 26, 2014
Published: September 30, 2014

than shorter chains like those found in human platelet dense granules. Furthermore, these condensed PolyP granules are stable in aqueous buffer and albumin suspensions on the same time scale as catastrophic bleeding events and possess potent procoagulant function, when assaying for activation of the contact pathway. Precipitation of inorganic PolyP in aqueous calcium and/or magnesium could potentially serve as a facile therapy to mitigate the deleterious effects of serious trauma via the delivery of high concentrations of PolyP stores locally to bleeding sites to rapidly induce coagulation.

EXPERIMENTAL SECTION

Materials and Reagents. Tris(hydroxymethyl)aminomethane, $CaCl_2 \cdot 6H_2O$, $MgCl_2 \cdot 6H_2O$, NaCl, KCl, and bovine serum albumin (BSA) were purchased from Sigma-Aldrich (St. Louis, MO). Water was deionized to 18.2 MΩ-cm (Nanopure II, Barnstead, Dubuque, IA). Citrated, pooled normal plasma was purchased from George King Biomedical (Overland Park, KS). L-α-Phosphatidylcholine (PC), L-α-phosphatidylserine (PS), and Avanti Mini-Extruder with 200 nm pore diameter polycarbonate membrane were purchased from Avanti Polar Lipids (Alabaster, AL). All materials were purchased at standard grades and used as received. PolyP80 (76−84 repeating units), PolyP250, (100−390 repeating units), PolyP305 (242−383 repeating units), and PolyP1000+ (more than 1000 repeating units) was size fractionated via preparative electrophoresis as previously described[14] or by differential isopropanol precipitation of heterogeneous long chain PolyP. Natriumpolyphosphat P70 (BKGP70, 20−125 repeating units, mode ∼45) was purchased from BK Guilini GmbH (Ludwigshafen am Rhein, Germany). PolyP concentrations are given throughout in terms of the concentration of phosphate monomer (monoP).

PolyP Nanoprecipitation. Aqueous size-fractionated PolyP was micropipetted into 8 mM Tris·HCl, pH 7.4 solutions containing combinations of the following: 1.2 mM, 5.0 mM, or 7.5 mM $CaCl_2$; 0.4 mM $MgCl_2$; 4.35 mM KCl; and 150 mM NaCl. The nanoparticles were then vortexed for 5 s. Precipitation was characterized by dynamic light scattering (DLS) (Brookhaven NanoDLS, Brookhaven, NY).

Determination of PolyP Solubility. The measurements of PolyP solubility are similar to the procedure used to determine the critical micelle concentration (CMC) of surfactants, copolymers, and phospholipids using DLS. PolyP samples were prepared as described above and injected into the DLS, beginning at exceedingly low concentrations (typically 100 nM to 1 μM monoP), where the scattering count rate resembled that of molecularly dissolved PolyP. The PolyP concentration was slowly titrated up until the scattering count rate increased and the correlation function was a well-behaved exponential decay on the baseline, suggesting that the PolyP sample was supersaturated. The scattering count rate was then plotted against the logarithm of the monoP concentration, producing a plot with two clear regimes representing: (1) molecularly dissolved PolyP and (2) precipitated PolyP. A linear regression was then performed on each regime and the point of intersection was found, which was defined as the solubility concentration. For consistency, all measurements were done on low laser intensity.

PolyP Nanoparticle (NP) Stability. *Stability in Aqueous Buffer.* NPs were synthesized using PolyP250 (125 μM) in either 1.2 mM or 5 mM $CaCl_2$ buffered with 8 mM Tris·HCl, pH 7.4 as discussed previously. Immediately after vortexing, particle size was characterized by DLS using at least a 1 min scattering time every 5 min for 1 h at room temperature.

Stability in BSA Suspensions. A solution of BSA (70 mg/mL) containing 8 mM Tris·HCl, pH 7.4 was prepared both with and without 2.5 mM $CaCl_2$ the day before experiments were conducted. PolyP250 (125 μM) was nanoprecipitated in 5 mM $CaCl_2$, 8 mM Tris·HCl, pH 7.4, and the particle diameter was determined immediately by DLS. The PolyP NPs were then mixed 1:1 (v:v) with the BSA suspensions. The resulting BSA and $CaCl_2$ concentrations were thus 35 mg/mL and 1.25 mM, respectively. Particle size was measured using DLS every 5 min for 1 h and subsequently every 30 min until 3 h had elapsed. The dispersion viscosity was calculated to be 1.2 cP,[26] and the refractive index was kept the same as water (1.331).

Transmission Electron Microscopy. *Sample Preparation.* PolyP250 (125 μM) was nanoprecipitated in 5 mM $CaCl_2$, 8 mM Tris·HCl, pH 7.4 as described above. The sample (10 μL) was micropipetted onto a 300-mesh carbon-coated Formvar grid (Structure Probe Inc., West Chester, PA) and allowed to dry in air for 10 min. The remaining liquid was wicked away with a Kim wipe and the process was repeated two more times to increase particle density and minimize aggregation. The sample was viewed in a JEOL JEM-1220 transmission electron microscope (JEOL, Japan).

X-ray Microanalysis. PolyP250 NPs (10 μL) were micropipetted onto a 300-mesh Holey Formvar carbon grid. The sample was dried for 15 min and examined in a JEOL JEM-3010 transmission electron microscope (JEOL, Japan).

Preparation of Large Unilamellar Vesicles (LUV). LUVs (200 nm) of PC to PS (80:20 molar ratio) were made by extrusion.[27] Briefly, 158 μL of 10 mg/mL L-α-PC and 42 μL of 10 mg/mL L-α-PS dissolved in chloroform were pipetted into a glass scintillation vial and dried under argon gas. The resulting lipid film was then placed under vacuum for an additional 1 h to remove any residual chloroform. The lipid cake was subsequently rehydrated with 1 mL Tris buffer, pH 7.4 and passed through an extruder with a polycarbonate membrane with 200 nm pore size 11 times to generate monodisperse LUV. Liposome diameter and polydispersity were verified by DLS.

Clotting Assays. Clotting was evaluated using a microplate-based assay as previously described[9] with minor modifications. The citrated plasma was prewarmed to 37 °C for 20 min, and PolyP was nanoprecipitated at room temperature and evaluated by DLS before proceeding with the assay. Wells contained 50 μL of citrated pooled normal plasma, 50 μL of PolyP NPs in 5 mM $CaCl_2$, 8 mM Tris·HCl, pH 7.4, and coagulation was initiated with 50 μL of 25 mM $CaCl_2$, 75 μM LUV, 8 mM Tris·HCl, pH 7.4. Final excess free calcium was estimated to be 4.72 mM. LUVs containing a small amount of phosphatidylserine (∼20 mol %) were added in contact activation assays, because the prothrombinase complex, consisting of Factor Va and Factor Xa, assembles on negatively charged phospholipid membranes in the presence of calcium. In the absence of negatively charged phospholipids, thrombin formation would be significantly hindered. Absorbance was read at 405 nm at room temperature on a Finstriments Microplate Reader (MTX Lab Systems Inc., Vienna, Virginia) every minute for 30 min. The sigmoidal absorbance traces were fitted to a standard Boltzmann growth function in Origin Pro 8.6 (OriginLab Corp., Northampton, MA). The *x*-coordinate of the inflection point (parameter x0) was defined as the time at which clotting occurred.

RESULTS AND DISCUSSION

In this study, the solubilities of PolyP of differing polymer lengths were first investigated by employing DLS. Analogous to determining the critical micelle concentration of a surfactant, the light scattering count rate begins to markedly increase when PolyP begins to precipitate into NPs. The scattering intensity of very long chain PolyP (PolyP1000+, similar to the long chains in prokaryotes) in aqueous solutions containing various concentrations of mono- and divalent cations is shown in Figure 1A. PolyP precipitated in the presence of divalent metal cations at biologically relevant concentrations (5 and 1.2 mM $CaCl_2$ and 1.2 mM $CaCl_2$ + 0.4 mM $MgCl_2$); however, monovalent cations exerted far less precipitative effects than their divalent counterparts. At 5 mM $CaCl_2$, concentrations typical of conventional clotting assays, PolyP nanoprecipitated much more easily than at physiological concentrations (1.2 mM $CaCl_2$). K^+ at normal physiological concentration does not statistically change the scattering intensity profile, while Na^+ at a relatively high ionic strength of 150 mM combined with 5 mM $CaCl_2$ causes the scattering intensity to increase at a

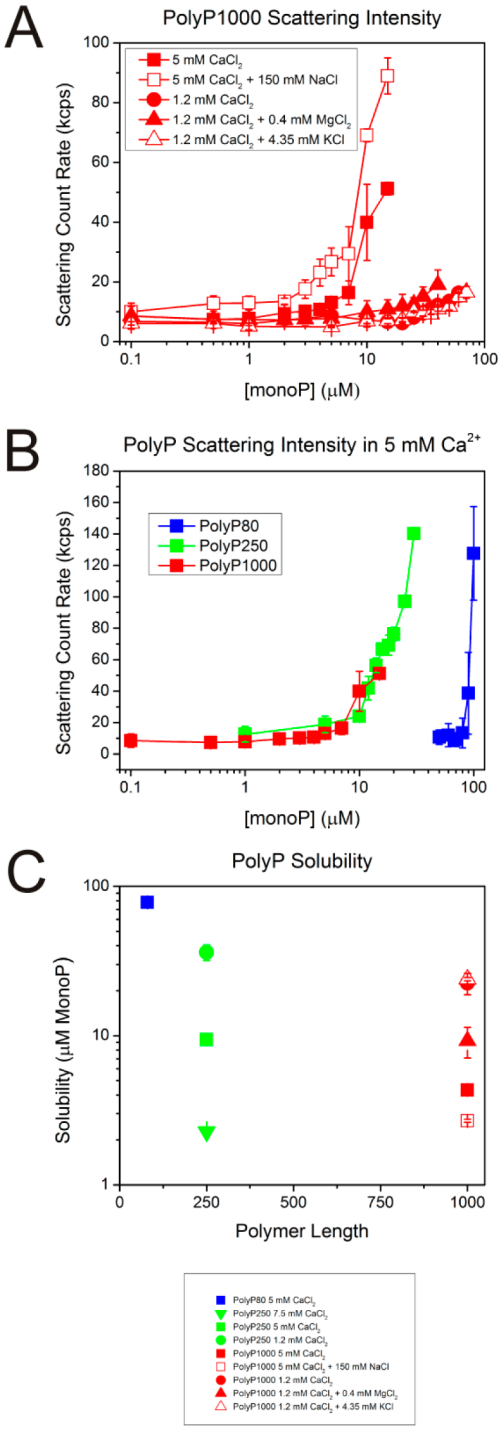

Figure 1. Solubility of PolyP as determined by DLS. (A) The precipitative effects of different metal cations on very long chain PolyP. Divalent metal cations such as Ca^{2+} and Mg^{2+} cause PolyP1000+ to robustly nanoprecipitate at physiological concentrations, as evidenced by the steep rise in the scattering intensity count rate, whereas monovalent cations such as Na^{+} and K^{+} at biologically relevant concentrations exert negligible effects on the polymer's solubility. (B) 5 mM $CaCl_2$ wields divergent precipitative effects on PolyP depending on the polymer length. PolyP1000+ precipitates most robustly with a steep rise in scattering intensity at 4.3 μM monoP concentration. PolyP250 is more soluble than PolyP1000+, with the count rate increasing near 9.4 μM. Platelet-size PolyP (PolyP80) is more soluble than both very long- and intermediate-chain length PolyP, with the scattering intensity markedly increasing at a monoP concentration almost a magnitude higher than PolyP250. (C) Solubility of PolyP of different polymer lengths. PolyP's solubility in various aqueous salt solutions buffered with 8 mM Tris·HCl, pH 7.4 plotted against polymer length in monoP units. There is a strongly nonlinear relationship, with very long chains (i.e., PolyP1000+) being much more readily precipitated than shorter polymers, e.g., polyP80. Divalent metal cations like Ca^{2+} and Mg^{2+}, which are known to chelate strongly to phosphate-containing compounds, exert precipitative effects at biologically relevant concentrations, while monovalent ions such as Na^{+} and K^{+} induce little or no significant effects on PolyP's solubility.

modestly lower monoP concentration. Ca^{2+} and Mg^{2+} function synergistically to promote nanoprecipitation. The solubility in 1.2 mM $CaCl_2$ + 0.4 mM $MgCl_2$ is more than 60% lower than in 1.2 mM $CaCl_2$ alone.

Nanoprecipitation was also a function of polymer length, with very long chains precipitating much more robustly than intermediate-length PolyP (PolyP250) or platelet-size polyP (PolyP80) at 5 mM $CaCl_2$ (Figure 1B). The solubility for each precipitative condition was determined by finding the intersection of the two linear regressions representing molecularly dissolved PolyP and PolyP NP regimes as plotted in Figure 1C. The solubilities for PolyP1000+ and PolyP250 at 5 mM $CaCl_2$ were 4.3 and 9.4 μM, respectively, while platelet-sized PolyP's solubility at the same condition was about 78 μM. Although not measured, it is safe to assume that PolyP80s solubility concentration is at or above 78 μM in 1.2 mM $CaCl_2$. Upon platelet activation, the concentration of PolyP in whole blood can reach up to 2−7 μM,[14] which suggests that platelet PolyP likely exerts its procoagulant effects while remaining largely molecularly dissolved. However, the next experiments demonstrate that PolyP nanoparticles exhibit dilution hysteresis, keeping open the possibility that condensed PolyP precipitates remain in NP format after secretion from activated platelets, despite being below the thermodynamic solubility limit. In addition, the local concentration of secreted PolyP could be orders of magnitude higher than 2−7 μM inside platelet-rich thrombi.

The solubility of platelet-sized PolyP in 5 mM $CaCl_2$ as a function of pH was also investigated. PolyP is stored intracellularly under mildly acidic conditions (~pH 5.4) together with extremely concentrated levels of calcium cations, serotonin, and pyrophosphate under the tight regulation of a H^{+}-ATPase pump in human platelet dense granules.[18] Given that this is the case in prokaryotic organisms as well, one could speculate that PolyP may be more easily precipitated under acidic conditions. However, at least for platelet-sized PolyP, the solubility is nearly identical at both mildly acidic and basic conditions (see Supporting Figure S5 and Supporting Table S3 in the Supporting Information).

PolyP250 was chosen as a paradigmatic polymer to study nanoparticle stability. First, nanoparticle growth kinetics were examined in an aqueous buffer containing biologically relevant concentrations of ionic calcium for 1 h, a time scale approximating a traumatic bleeding event and the half-life of PolyP in plasma or serum.[9] PolyP250 was nanoprecipitated in 8 mM Tris·HCl, pH 7.4 with 1.2 mM and 5 mM $CaCl_2$ (Figure 2A). Particle aggregation behavior follows power law kinetics, typical of metastable colloidal dispersions. Initial particle diameters were 169 and 58 nm for 5 mM and 1.2 mM $CaCl_2$, respectively. This suggests that the phosphate/calcium

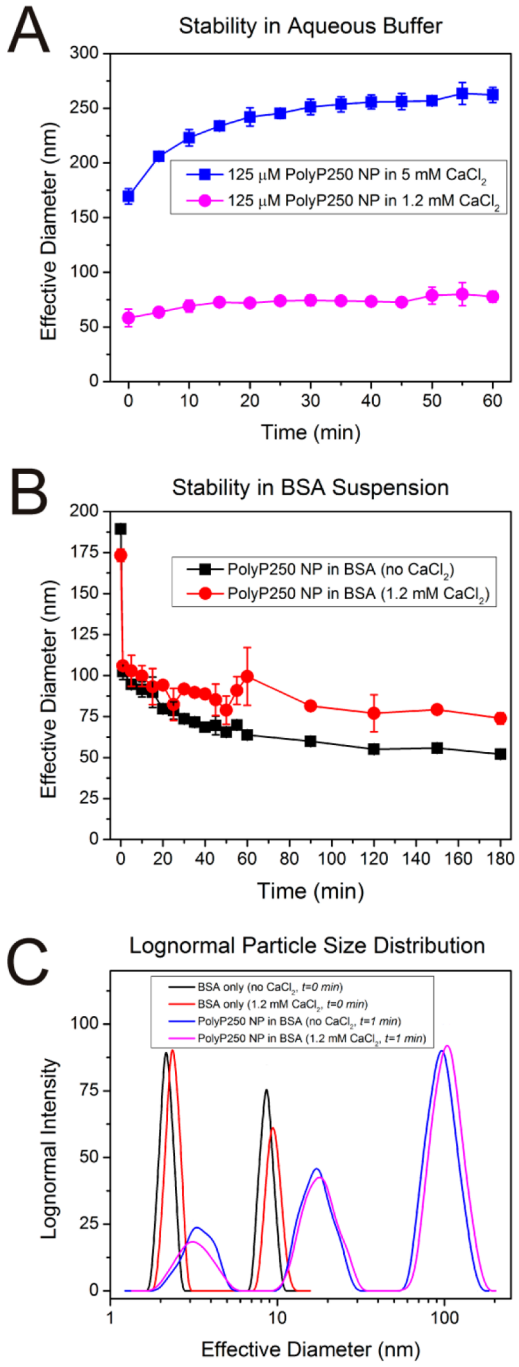

Figure 2. PolyP nanoparticle stability. (A) PolyP250 nanoparticle stability in aqueous buffer. 125 μM PolyP250 was nanoprecipitated in 8 mM Tris·HCl, pH 7.4 containing 1.2 mM or 5 mM $CaCl_2$. Average effective diameter was assessed every 5 min for 1 h, a typical time scale for a bleeding event. At 5 mM $CaCl_2$, the initial particle diameter was 169 nm and slowly grew to be approximately 260 nm after 1 h. At 1.2 mM $CaCl_2$ the particles were initially 58 nm and steadily increased to ~80 nm. The growth behavior of both suspensions appears to follow power-law kinetics typical of many metastable colloidal dispersions. (B) PolyP250 nanoparticle stability in suspensions containing BSA. 125 μM PolyP250 was precipitated in aqueous buffer containing 5 mM $CaCl_2$ as described previously and then mixed 1:1 (v:v) with 70 mg/mL BSA suspension buffered to pH 7.4 with or without 1.2 mM $CaCl_2$. Final BSA and $CaCl_2$ concentrations were 35 mg/mL and 1.2 mM, respectively. In both cases, the PolyP250 NPs shrank from approximately 170−180 nm before mixing with the BSA solution to 100 nm immediately after mixing with the BSA solution. This was not due to changes in dispersion viscosity or multiple scattering effects (confirmed by more measurements presented in the Supporting Information, Table S1). After 3 h, the PolyP NPs in BSA without $CaCl_2$ equilibration shrank to approximately 50 nm in diameter, while the NPs in the BSA equilibrated with 1.2 mM $CaCl_2$ were roughly the same size (~80 nm). It is hypothesized that BSA may be initially forming a complex with PolyP (the rapid shrinkage upon addition to the suspension) and then competitively binding Ca^{2+}, unless it has been pre-equilibrated. (C) Lognormal size distributions for (1) BSA suspension without Ca^{2+} pretreatment; (2) BSA suspension with 1.2 mM $CaCl_2$; (3) immediate addition of PolyP 250 NPs in 35 mg/mL BSA without $CaCl_2$ pre-equilibration; and (4) immediate addition of PolyP 250 NPs in 35 mg/mL BSA with 1.2 mM $CaCl_2$.

ratio may be the major driving force in the thermodynamic equilibrium of PolyP nanoprecipitation. Stoichiometry and PolyP supersaturation ratio as it relates to nanoparticle formation will be discussed systematically below. The stability of PolyP1000+ NPs precipitated at mildly acid conditions was also examined (see Supporting Figure S3 in the Supporting Information), resembling the environment in acidocalcisomes. The growth behavior manifests power law kinetics identical to physiologic pH. However, the scattering count rate remains more stable.

Aqueous buffer is only a poor approximation of the environment in circulation as it lacks many of the proteins and peptides that contribute to hemostasis and that regulate pH and plasma ionic strength. In addition to examining the nanoparticle growth behavior in aqueous buffer, stability was also investigated in Tris-buffered suspensions containing 35 mg/mL BSA to better approximate the conditions found in human serum. Serum albumin is the most abundant protein in circulation. It binds to a myriad of pharmaceuticals and foreign substances,[28] tightly regulates serum pH,[29] and robustly and competitively binds to metal cations,[30−35] most notably Ca^{2+}, Zn^{2+}, and Cu^{2+}. Because of BSA's functionality, two conditions were considered for PolyP250 NP stability: (1) BSA not pre-equilibrated with $CaCl_2$ and (2) BSA pre-equilibrated with 1.2 mM $CaCl_2$. Briefly, 125 μM PolyP250 NPs were nanoprecipitated in 5 mM $CaCl_2$ as described previously and mixed 1:1 (v:v) with the BSA suspensions. The particle size evolution was then monitored for 3 h (Figure 2B). At both salt conditions, the particles immediately shrank from 170 to 180 nm to approximately 100 nm when they were added to the BSA suspensions. The shrinkage is too rapid to suggest that this is due to enzymatic degradation. Moreover it is not an artifact of multiple scattering or changes in dispersion viscosity (see the Supporting Information, Table S1). PolyP250 NPs in BSA not pretreated with $CaCl_2$ continued to shrink to ~50 nm after 3 h, whereas the PolyP250 NPs in BSA pre-equilibrated with 1.2 mM $CaCl_2$ maintained approximately the same particle diameter, with the final size after 3 h being ~80 nm. It is conjectured that serum albumin may extract Ca^{2+} from the PolyP-Ca^{2+} complex. However, much further study is needed to prove this claim conclusively.

Figure 2C shows the log-normal particle population for the following conditions: (1) BSA without Ca^{2+} pre-equilibration; (2) BSA with 1.2 mM $CaCl_2$ pre-equilibration; (3) immediate addition of 125 μM PolyP250 NPs to BSA not pre-equilibrated with Ca^{2+}; and (4) immediate addition of PolyP250 NPs to BSA pre-equilibrated with 1.2 mM $CaCl_2$. BSA without PolyP in the presence or absence of calcium displayed two peaks. The

dx.doi.org/10.1021/bm501046t | Biomacromolecules 2014, 15, 3976−3984

first peak centered around 3 nm represents the hydrodynamic diameter of the BSA monomer. The second peak at approximately 15 nm constitutes multimeric BSA. The hydrodynamic radius has been previously reported in the literature to be 3.42 nm.[36] Quasielastic light scattering data demonstrates that the BSA monomer is a prolate ellipsoid. BSA dimerizes side-to-side, with significant overlap, leading to the dimer being less than twice the size of the monomer.[37]

Addition of $CaCl_2$ has minimal effects on the size distribution of the BSA protein. The particle populations representing conditions 3 and 4 show that there is an additional peak with a mean diameter of approximately 100 nm. This peak must be the effective diameter of the PolyP250 NPs. Moreover, the middle peak representing the BSA dimer has shifted to the right, further evidence that PolyP may be interacting directly with BSA and forming an adduct mediated by calcium. The striking discrepancy in the hydrodynamic diameter of the PolyP NPs in aqueous buffer and in BSA suspension deserves special scrutiny. Further study is needed to measure PolyP-Ca^{2+} binding constants at these conditions to corroborate the hypothesis that the evolution in PolyP particle diameter, characterized first by a steep drop and then a gradual shrinkage over a time scale of hours, is due to a competitive equilibrium process governed by the differential Ca^{2+} binding affinities of BSA and PolyP.

The initial effective diameter of the PolyP granular NPs was systemically investigated against the polymer's supersaturation ratio at three different calcium concentrations: 1.2 mM (free calcium concentration in human plasma), 5 mM (calcium concentration in *in vitro* coagulation assays), and 7.5 mM. Figure 3A shows the particle size plotted against monoP concentrations up to 1 mM for intermediate-length PolyP (PolyP250). PolyP precipitated in 5 mM $CaCl_2$ at monoP concentrations of 250 μM or greater had to be diluted with more Tris-buffered 5 mM $CaCl_2$ solution before being characterized by DLS (PolyP NP diameter is hysteretic after dilution; see the Supporting Information, Table S2). No trends between particle diameter and monoP concentration are manifest at first glance until the monoP concentration is divided by the solubility of PolyP250 at the given calcium concentration and plotted nondimensionally as the supersaturation ratio, as in Figure 3B. At low to moderate superaturation ratios (~1−50) the particle size is only a function of the calcium concentration.

After it was established that the solubility of PolyP250 was 9.4 μM in 5 mM $CaCl_2$, 8 mM Tris·HCl, pH 7.4, a sample well above the solubility concentration (in this case 30 μM) was diluted progressively with more 5 mM $CaCl_2$ to decrease the PolyP concentration and keep the calcium concentration constant, and the scattering intensity was measured after each dilution. As can be seen in Figure 3C, the system exhibits hysteresis: the count rate remains much higher even below the solubility concentration despite a thermodynamic driving force for some of the particles to resolubilize. Evidence that PolyP NP formation manifests dilution-dependent hysteresis has potentially profound ramifications: for example, a bolus of condensed PolyP could be delivered to a trauma site at locally high concentrations and be dispersed further downstream in the circulation without losing its NP format due to its hysteretic behavior, maintaining its associated biological functionality as a procoagulant and proinflammatory agent. However, in human plasma other mechanisms may come into play, such as binding of PolyP to membrane-associated proteins on vessel walls

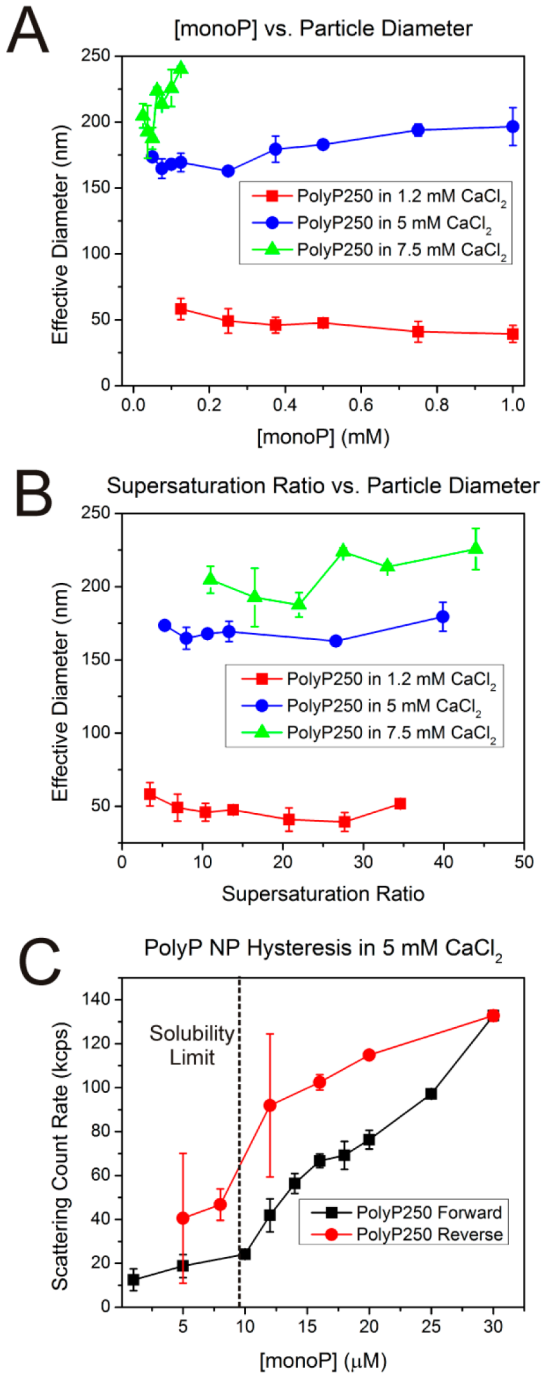

Figure 3. PolyP NP effective diameter as a function of supersaturation ratio. (A) PolyP250 NP initial effective diameter versus monoP and Ca^{2+} concentrations. Initial PolyP250 NP sizes were measured with up to 1 mM monoP concentration at three different calcium concentrations: 1.2, 5, and 7.5 mM Ca^{2+}. No trends are manifest except for a dependence on calcium concentration. (B) PolyP250 NP initial effective diameter as a function of supersaturation ratios and Ca^{2+} concentrations. When the monoP concentrations are divided by the solubility of PolyP250 at the respective calcium concentrations, it appears that at moderate supersauration ratios (~1−50), the PolyP particle diameter is only a function of the calcium concentration. (C) PolyP NP solubility hysteresis. The 30 μM PolyP250 was nanoprecipitated in 5 mM $CaCl_2$, generating a supersaturated colloidal dispersion of PolyP250 NPs. The suspension was then serially diluted with 5 mM $CaCl_2$, 8 mM Tris·HCl, pH 7.4 in order to decrease monoP concentration, while maintaining constant [Ca^{2+}]. As is evident from the reverse solubility curve (shown in red above), the

dx.doi.org/10.1021/bm501046t | *Biomacromolecules* 2014, 15, 3976−3984

Figure 3. continued

scattering intensity remains elevated, even approaching PolyP250s solubility (9.4 μM) in 5 mM $CaCl_2$ despite a thermodynamic driving force for resolubilization. This suggests that PolyP colloidal dispersions manifest hysteresis, a characteristic that may have profound ramifications for potential downstream therapeutic usage of PolyP NPs as clotting agents.

adjacent to thrombi, which may prevent PolyP NPs from being convected away from the wound site, thereby curtailing a potentially disastrous or even fatal scenario.

We have found that PolyP exerts its most robust procoagulant effects at roughly the 10−500 μM when assayed at 5 mM $CaCl_2$.[14] Indeed, this concentration range almost exactly corresponds to a supersaturation ratio of 1−50 for PolyP250 at 5 mM Ca^{2+}. However, at physiological calcium concentration, the particle diameter for this polymer length is roughly constant between 36 μM and 1.8 mM. One could speculate that organisms have specifically developed techniques to store and condense PolyP in subcellular compartments such as acidocalcisomes and platelet dense granules in a controlled manner by exploiting PolyP's roughly constant particle diameter at low to moderate supersaturation ratios. Upon secretion, these PolyP precipitates could potentially serve as concentrated stores of the polymer for biochemical processes requiring rapid, nonlinear, or threshold-switchable behavior such as coagulation or quorum sensing.

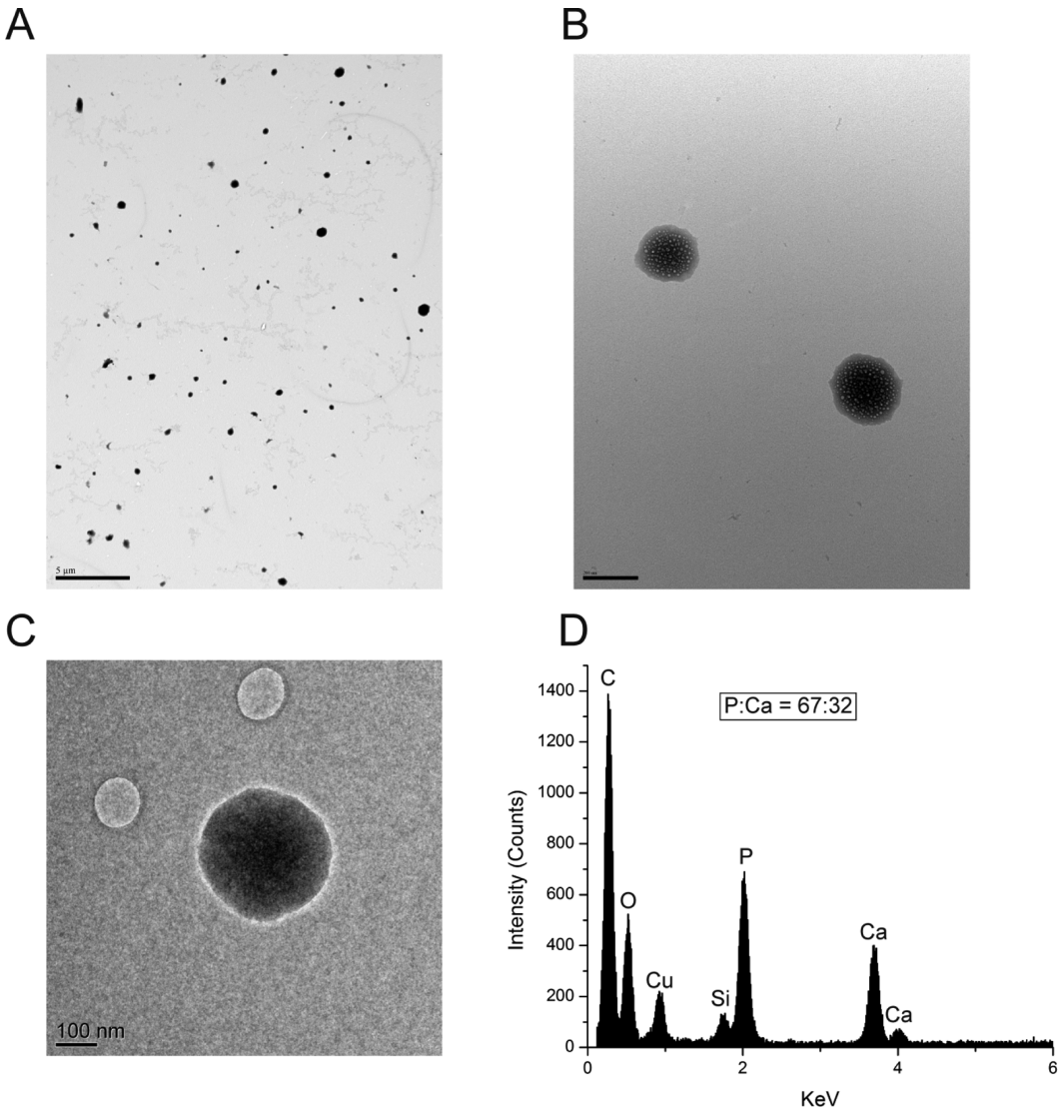

Figure 4. PolyP NP morphology, structure and elemental composition. (A) PolyP forms monodisperse particles in solution. The 125 μM PolyP250 was precipitated in 5 mM $CaCl_2$, 8 mM Tris·HCl, pH 7.4. PolyP250 forms monodisperse particle populations in the presence of 5 mM $CaCl_2$. Scale bar: 5 μm. (B) PolyP NPs appear spongy after prolonged electron beam exposure just like acidocalcisomes and platelet dense granules. Even though PolyP250 NPs are uniformly electron dense, after sustained exposure to the electron beam, white spots begin to appear so that the particles appear like round sponges or porous balls. This same phenomenon was also observed in Ruiz et al.'s investigation[18] of PolyP-containing dense granules in platelets. (C) A granular PolyP250 nanoparticle. A single PolyP 250 NP is shown at higher magnification revealing that the granule is roughly spherical and approximately 200−250 nm in diameter, in good agreement with DLS data. Scale bar: 100 nm. (D) Elemental composition of the synthetic PolyP250 NPs. Copper, carbon, and silicon are from the grid. The ratio of the phosphorus to the calcium peak is 67:32. Ruiz et al. performed the equivalent analysis with human platelet dense granules, and their resulting X-ray microspectrum is quasi-identical, except for the presence of a small K peak.[18] However, potassium was not used here for PolyP nanoprecipitation.

dx.doi.org/10.1021/bm501046t | *Biomacromolecules* 2014, 15, 3976−3984

Transmission electron microscopy was used to examine the PolyP particle structure, elemental composition, and morphology. Figure 4A is an electron micrograph taken at low magnification with a large population of PolyP250 NPs, showing that the granules are spherical in shape and relatively monodisperse, despite the presence of some larger aggregates. The particle diameter is a function of the calcium concentration; inevitably, some aggregation is bound to occur during the drying process and grid preparation. When the particles undergo substantial exposure from the electron beam, the PolyP250 NPs develop white spherical spots, resulting in the granules resembling round sponges or soccer balls, despite their uniform electron density as seen in Figure 4B. Indeed, Ruiz et al. has shown using TEM that PolyP bodies in acidocalcisomes and human platelet dense granules also appear spongy after bleaching with the electron beam, resembling the PolyP NPs synthesized here.[18]

Figure 4C shows a single PolyP250 nanoparticle at high magnification. The PolyP granule is spherical and approximately 200−250 nm in diameter, corroborating DLS data. Figure 4D is an X-ray microspectrum of the particle in part C showing its elemental composition. Copper, carbon, and silicon are from the grid. It is very typical for X-ray microspectra to have small peaks (∼1−2%) of Si and alkali earth metals arising from the detector itself or, more rarely, from silicon-containing oils deposited on the Formvar grids during the manufacturing process. In fact, a small Si peak was also observed in the X-ray microanalysis of human platelet dense granules in the past.[18] The P/Ca ratio is 67:32. Ruiz et al., in their investigation of human platelet dense granules, also determined the elemental composition of the PolyP bodies, yielding very similar results.[18] The P/Ca was 1.76 with trace amounts of K^+. However, dense granules are mildly acidic subcellular compartments, which may lead to a different P/Ca stoichiometry, and platelets contain substantial cellular stores of potassium.[38] Potassium was not used here to precipitate PolyP into synthetic PolyP granules.

Smith et al. demonstrated that PolyP is a potent activator of the contact pathway of coagulation, and its activity is related nonlinearly with its polymer length,[14] with long polymers being more robust activators than shorter chains, which exert their effects at different points in the cascade such as via acceleration of FV activation and alteration of fibrin clot architecture and morphology. Figure 5B shows a schematic representation of the intrinsic pathway of coagulation and the points in which PolyP exerts its effects. It is well accepted in the literature that anionic "surfaces" such as collagen, glass, or kaolin are required to form the primary complex consisting of FXII (Hageman Factor) and its activation partners, plasma prekallikrein and high molecular weight kininogen (HMWK).[19] However, countless other soluble substances serve as scaffolds for the (auto)activation of FXII. Examples include ellagic acid, lipopolysaccharides, dextran sulfate, and phospholipids.[39] It has been reported previously that there exists a threshold molecular weight for activation of the intrinsic pathway for polystyrene polymers and dextran derivatives, with contact activity for both polymer types rising sharply ∼25 000 Da.[40] Others have communicated that the threshold molecular weight for dextran sulfate is as low as 10 000 Da.[41] Nonetheless, the mechanism by which PolyP acts on FXII has yet to be clearly elucidated.

Previous studies assaying the procoagulant effects of PolyP were performed under conditions where the polymer would presumably exist in its molecularly dissolved state. Typically, PolyP was incubated together with pooled normal plasma

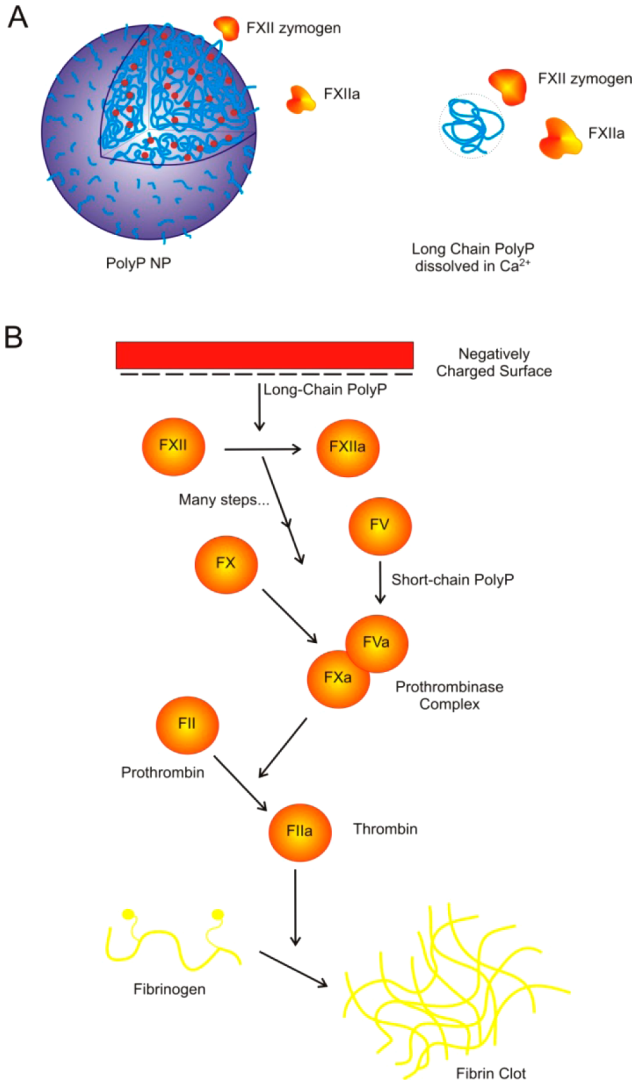

Figure 5. PolyP NPs as contact activators. (A) Possible mechanisms by which PolyP exerts its contact pathway activity. PolyP could serve as a surface for FXII activation as a colloidal particle like kaolin (left) or as a soluble anionic polymer like dextran sulfate (right) with a threshold molecular weight needed to elicit a conformational change in the FXII zymogen. (B) Schematic of the intrinsic pathway of blood coagulation. A negatively charged surface serves as the site for assembly of the primary complex consisting of FXII, kallikrein, and high molecular weight kininogen. Long-chain PolyP is able to support activation of the contact pathway, while shorter polymer lengths (like those in human platelets) are weak contact activators. PolyP also exhibits procoagulant effects further downstream in the final common pathway of blood clotting.

(PNP) for 3−5 min prior to recalcification. Since the plasma is citrated, there would be very little ionic calcium available to chelate PolyP, and thus no calcium-dependent precipitation would take place. The activation of contact enzymes and the generation of FXIIa are calcium-independent; therefore, prior studies investigating PolyP's contact activity are confined to an examination of the polymer in the absence of calcium-dependent precipitation. Moreover, plasma contains countless proteins and peptides such as serum albumin which may prevent or hinder its precipitation after recalcification. Because of PolyP's role in the early stages of natural selection, predating the arrival of polypeptides and quite possibly serving as the

dx.doi.org/10.1021/bm501046t | Biomacromolecules 2014, 15, 3976−3984

precursor to deoxyribonucleic and ribonucleic acid, it is only natural that PolyP would serve as the paradigmatic anionic scaffold for plasma and cytosolic proteins, emerging as a favored binding partner for peptides with cationic amino acid residues.

Figure 6 shows the clotting time of PolyP molecules or nanoparticles when assaying for contact activity using citrated

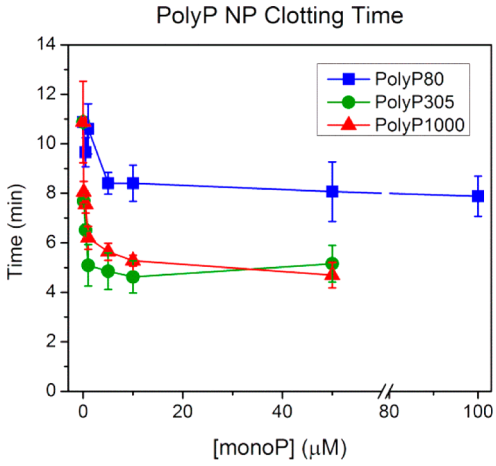

Figure 6. Initiation of the contact pathway by PolyP based on polymer length and concentration. Clotting time of PolyP is plotted as a function of monoP concentration from 0 to 100 μM. PolyP was added to 5 mM $CaCl_2$, 8 mM Tris·HCl, pH 7.4 at concentrations above and below its solubility. The presence of precipitated PolyP was monitored by DLS before addition to plasma. Intermediate- and very long-chain length PolyP (PolyP305 and PolyP1000+) are clearly more robust contact activators than platelet-sized PolyP (PolyP80). The concentration dependence on clotting time for PolyP305 and PolyP1000+ are identical, suggesting that a "saturating condition" has been established.

PNP. The polyphosphates (PolyP80, PolyP305, and PolyP1000+) were first added to 5 mM $CaCl_2$, 8 mM Tris·HCl, pH 7.4 at three times the final assay concentration and characterized by DLS (data not shown). Once the PolyP was incubated with the calcium solution, it was added to the PNP and immediately recalcified to initiate coagulation. Platelet-size PolyP (PolyP80) weakly shortened time to clot formation, saturating near 10−50 μM monoP. PolyP305 and PolyP1000+, on the other hand, were robust contact activators, drastically reducing clotting times even at submicromolar concentrations. Interestingly, the clotting activities of the two longer polymer sizes are quasi-identical (the error bars overlap for every concentration except one).

These data suggest that platelet PolyP only weakly promotes the activation of FXII, with the reduction in clotting time deriving mostly from effects on the final common pathway of clotting. On the other hand, the longer polymer sizes are large enough to serve as scaffolds for primary complex formation after treatment with calcium. One possibility is that there is a threshold polymer length (molecular weight) (as was previously reported for polystyrene and dextran sulfate) needed to exert the conformation change on the FXII zymogen (or to recruit a sufficiently high local surface density of FXII and its activators) as shown in Figure 5A. Interestingly, PolyP305's molecular weight is approximately 24 kDa, corroborating past results on threshold contact activation measured using polystyrene and dextran sulfate polymers. The fact that the concentration dependence is identical for PolyP305 and PolyP1000+ also suggests that the nanoparticle solubility is not the threshold condition for contact pathway activation for polymers over the threshold size, as PolyP1000+'s solubility is approximately 2-fold lower in 5 mM $CaCl_2$. If the solubility were the limiting condition, then PolyP1000+'s clotting time would drop at ∼4 μM, whereas PolyP305's would drop at ∼9 μM. However, there are several important caveats that limit the completeness of this analysis: (1) PolyP NPs have been shown to exhibit dilution-dependent hysteresis; (2) the solubility of PolyP in plasma or serum with its diversity of proteins and peptides and additional polyvalent cations such as Mg^{2+}, Cu^{2+}, Zn^{2+}, Mn^{2+}, and Fe^{2+}/Fe^{3+} (see Supporting Figures S2 and S4 in the Supporting Information) could be vastly different than in aqueous buffer containing only calcium; and (3) the effect of citrate and other calcium chelators such as EDTA on PolyP nanoparticle stability has yet to be investigated.

The zeta potential of the PolyP NPs was determined to be between −15 and −20 mV independent of particle diameter and polymer length (see Supporting Tables S4 and S5 in the Supporting Information). The negative surface charge of PolyP precipitates could therefore conceivably support autoactivation of Factor XII or recruitment of its activators, plasma prekallikrein, and high molecular weight kininogen independent of polymer molecular weight, discounting other factors that would influence PolyP NP stability in human plasma mentioned above.

Regardless of the physical interpretation, the fact remains that PolyP precipitation under aqueous conditions at physiologic salt concentrations is a facile means to synthesize large amounts of condensed PolyP granules similar in structure to human platelet dense granules for potential downstream uses such as a biocompatible procoagulant agent.

CONCLUSION

Herein, we demonstrate the size-controlled synthesis of monodisperse PolyP NPs at physiological concentrations of calcium and magnesium. The solubility is related nonlinearly to the polymer length, with very long-chain PolyP precipitating much more facilely than platelet PolyP. Further, the NP size is only a function of the calcium concentration across a wide supersaturation range. The granules are stable for at least an hour in aqueous buffer solutions, displaying typical power-law growth kinetics and are stable in BSA suspensions for 3 h.

The PolyP NPs possess promising procoagulant activity. Given that the PolyP particles are stable on the same time scale as a catastrophic bleeding event raises the question that PolyP's powerful procoagulant effects on the intrinsic pathway may be related to its precipitation into micron or submicron granular particles serving as negatively charged surfaces for FXII activation. The facile, size-controlled synthesis of these particles in the laboratory serves as a foundation for the future development of targeted procoagulant nanotechnologies exploiting PolyP precipitation to mitigate the effects of a diversity of bleeding phenomena such as internal hemorrhage and hemophilia in a minimally invasive manner.

ASSOCIATED CONTENT

Supporting Information

Scattering intensity of PolyP250 in 7.5 mM $CaCl_2$, 8 mM Tris·HCl, pH 7.4. Determination of any multiple scattering effects in BSA suspensions containing PolyP250 NPs. PolyP250 NP diameter hysteresis after dilution with more 5 mM $CaCl_2$. PolyP1000+ precipitation and log-normal particle size dis-

dx.doi.org/10.1021/bm501046t | Biomacromolecules 2014, 15, 3976−3984

tribution in 5 mM $MgCl_2$, 8 mM Tris·HCl, pH 7.4. Stability of PolyP1000+ NPs in acidic and basic conditions. Particle size distribution of PolyP1000+ NPs in Fe^{2+}/Fe^{3+}. Scattering intensity of platelet-sized PolyP as a function of monoP concentration at acidic and basic conditions. Solubility of PolyP as a function of molecular weight and pH. Zeta potential and particle effective diameter as a function of polymer length in 5 mM $CaCl_2$, pH 7.4. Zeta potential and particle effective diameter of PolyP at various precipitating conditions. This material is available free of charge via the Internet at http://pubs.acs.org.

AUTHOR INFORMATION

Corresponding Author

*Phone: +1(312) 996-8249. Fax: +1(312) 996-0808. E-mail: liuying@uic.edu.

Author Contributions

Experiments were conducted by A.J.D and J.K. and were designed and interpreted by Y.L., A.J.D, J.K., S.A.S., and J.H.M. Polyphosphates were prepared by S.A.S. The manuscript was composed by A.J.D. and Y.L. with editorial contributions from S.A.S. and J.H.M. All authors have given approval to the final version of the manuscript.

Notes

The authors declare no competing financial interest.

ACKNOWLEDGMENTS

The authors would like to extend their gratitude to Dr. Alan Nicholls and Linda Juarez of the UIC Research Resource Center for their excellent technical assistance with transmission electron microscopy characterization. The study was sponsored by the U.S. Army Medical Research and Material Command (Grant WQ81XWH-11-2-0021). The U.S. Army Medical Research Acquisition Activity, 820 Chandler Street, Fort Detrick MD 21702-5014 is the awarding and administering acquisition office. The contents of this article do not necessarily reflect the position or the policy of the government, and no official endorsement should be inferred.

REFERENCES

(1) Morrissey, J. H.; Choi, S. H.; Smith, S. A. *Blood* **2012**, *119* (25), 5972−5979.
(2) Shi, X. B.; Rao, N. N.; Kornberg, A. *Proc. Natl. Acad. Sci. U.S.A.* **2004**, *101* (49), 17061−17065.
(3) Kim, K. S.; Rao, N. N.; Fraley, C. D.; Kornberg, A. *Proc. Natl. Acad. Sci. U.S.A.* **2002**, *99* (11), 7675−7680.
(4) Rashid, M. H.; Rao, N. N.; Kornberg, A. *J. Bacteriol.* **2000**, *182* (1), 225−227.
(5) Brown, M. R. W.; Kornberg, A. *Proc. Natl. Acad. Sci. U.S.A.* **2004**, *101* (46), 16085−16087.
(6) Reusch, R. N.; Huang, R. P.; Bramble, L. L. *Biophys. J.* **1995**, *69* (3), 754−766.
(7) Fleischer, B.; Xie, J. P.; Mayrleitner, M.; Shears, S. B.; Palmer, D. J.; Fleischer, S. *J. Biol. Chem.* **1994**, *269* (27), 17826−17832.
(8) Kornberg, A.; Rao, N. N.; Ault-Riche, D. *Annu. Rev. Biochem.* **1999**, *68*, 89−125.
(9) Smith, S. A.; Mutch, N. J.; Baskar, D.; Rohloff, P.; Docampo, R.; Morrissey, J. H. *Proc. Natl. Acad. Sci. U.S.A.* **2006**, *103* (4), 903−908.
(10) Smith, S. A.; Morrissey, J. H. *Blood* **2008**, *112* (7), 2810−2816.
(11) Muller, F.; Mutch, N. J.; Schenk, W. A.; Smith, S. A.; Esterl, L.; Spronk, H. M.; Schmidbauer, S.; Gahl, W. A.; Morrissey, J. H.; Renne, T. *Cell* **2009**, *139* (6), 1143−1156.
(12) Choi, S. H.; Smith, S. A.; Morrissey, J. H. *Blood* **2011**, *118* (26), 6963−6970.
(13) Smith, S. A.; Morrissey, J. H. *J. Thromb. Haemost.* **2008**, *6* (10), 1750−1756.
(14) Smith, S. A.; Choi, S. H.; Davis-Harrison, R.; Huyck, J.; Boettcher, J.; Rienstra, C. M.; Morrissey, J. H. *Blood* **2010**, *116* (20), 4353−4359.
(15) Kornberg, A. *J. Bacteriol.* **1995**, *177* (3), 491−496.
(16) Docampo, R.; de Souza, W.; Miranda, K.; Rohloff, P.; Moreno, S. N. J. *Nat. Rev. Microbiol.* **2005**, *3* (3), 251−261.
(17) Docampo, R.; Moreno, S. N. J. *Parasitol. Today* **1999**, *15* (11), 443−448.
(18) Ruiz, F. A.; Lea, C. R.; Oldfield, E.; Docampo, R. *J. Biol. Chem.* **2004**, *279* (43), 44250−44257.
(19) Renne, T.; Schmaier, A. H.; Nickel, K. F.; Blomback, M.; Maas, C. *Blood* **2012**, *120* (22), 4296−4303.
(20) Jensen, T. E.; Baxter, M.; Rachlin, J. W.; Jani, V. *Environ. Pollut. A* **1982**, *27* (2), 119−127.
(21) Holmsen, H.; Weiss, H. J. *Annu. Rev. Med.* **1979**, *30*, 119−134.
(22) Bonting, C. F. C.; Kortstee, G. J. J.; Boekestein, A.; Zehnder, A. J. B. *Arch. Microbiol.* **1993**, *159* (5), 428−434.
(23) Monteiro, V. A. D.; de Souza, E. F.; de Azevedo, M. M. M.; Galembeck, F. *J. Colloid Interface Sci.* **1999**, *217* (2), 237−248.
(24) Momeni, A.; Filiaggi, M. J. *J. Non-Cryst. Solids* **2013**, *382*, 11−17.
(25) Momeni, A.; Filiaggi, M. J. *Langmuir* **2014**, *30* (18), 5256−5266.
(26) Einstein, A. *Ann. Phys.* **1906**, *19* (2), 289−306.
(27) Mui, B.; Chow, L.; Hope, M. J. *Methods Enzymol.* **2002**, *367*, 3−14.
(28) Sjoholm, I.; Ekman, B.; Kober, A.; Ljungstedtpahlman, I.; Seiving, B.; Sjodin, T. *Mol. Pharmacol.* **1979**, *16* (3), 767−777.
(29) Van Slyke, D. D.; Hastings, A. B.; Hiller, A.; Sendroy, J. *J. Biol. Chem.* **1928**, *79* (2), 769−780.
(30) Pedersen, K. O. *Scand. J. Clin. Lab. Inv.* **1972**, *30* (1), 89−94.
(31) Pedersen, K. O. *Scand. J. Clin. Lab. Inv.* **1972**, *29* (4), 427−432.
(32) Pedersen, K. O. *Scand. J. Clin. Lab. Inv.* **1971**, *28* (4), 459−469.
(33) Foghandersen, N. *Clin. Chem.* **1977**, *23* (11), 2122−2126.
(34) Pedersen, K. O. *Scand. J. Clin. Lab. Inv.* **1972**, *29* (1), 75−83.
(35) Masuoka, J.; Saltman, P. *J. Biol. Chem.* **1994**, *269* (41), 25557−25561.
(36) Axelsson, I. *J. Chromatogr.* **1978**, *152* (1), 21−32.
(37) Squire, P. G.; Moser, P.; O'Konski, C. T. *Biochemistry* **1968**, *7* (12), 4261−4272.
(38) Zieve, P. D.; Gamble, J. L., Jr.; Jackson, D. P. *J. Clin. Invest.* **1964**, *43*, 2063−2069.
(39) Samuel, M.; Pixley, R. A.; Villanueva, M. A.; Colman, R. W.; Villanueva, G. B. *J. Biol. Chem.* **1992**, *267* (27), 19691−19697.
(40) Corretge, E.; Nigretto, J. M. *Thromb. Res.* **1990**, *59* (3), 463−473.
(41) Silverberg, M.; Diehl, S. V. *Biochem. J.* **1987**, *248* (3), 715−720.

Angewandte Chemie, In Press

Clotting activity of polyphosphate functionalized silica nanoparticles **

Damien Kudela,* Stephanie A. Smith, Anna May-Masnou, Gary B. Braun, Alessia Pallaoro, Chi K. Nguyen, Tracy T. Chuong, Sara Nownes, Riley Allen, Nicholas R. Parker, Hooman H. Rashidi, James H. Morrissey,* and Galen D. Stucky*

Abstract: We present a silica nanoparticle (SNP) functionalized with polyphosphate (polyP) that accelerate the body's natural clotting process. SNPs initiate the blood clotting system's contact pathway; short-chain polyP accelerates the common pathway via rapid formation of thrombin. This enhances the overall blood-clotting system, both by accelerating fibrin generation and by facilitating the regulatory anticoagulation mechanisms essential for hemostasis. Analyzing the clotting properties of bare SNPs, bare polyP, and polyP-functionalized SNPs in plasma, demonstrates that attaching polyP to SNPs to form polyP-SNPs creates a substantially enhanced synergistic effect that lowers clotting time and increases thrombin production at low concentrations when compared to bare SNPs or polyP alone. PolyP-SNP even retains its clotting function at ambient temperature. The polyP-SNP system has the potential to significantly improve trauma treatment protocols and outcomes in hospital and prehospital settings.

Controlling hemorrhage is a major focus in the treatment and stabilization of many trauma patients. Uncontrolled blood loss accounts for nearly 50 % of all battlefield deaths, despite the fact that less than 5 % of soldiers who subsequently reach a hospital die of their wounds.[1] In civilian hospitals, 15-25 % of trauma deaths occur as a result of hemorrhage.[2] These data suggest that treatment should be focused on stopping bleeding prior to hospital arrival. Management of bleeding is currently aimed at volume resuscitation and surgical intervention to limit blood loss.[3] However, these measures, in many instances, do not address the source or mechanism of the bleeding and ultimately can limit the possible options to control it, especially in the prehospital setting.

Currently, there are three major approaches for controlling prehospital hemorrhage. The oldest method employs mechanical devices that compress the wound to minimize the area through which blood can escape the damaged vessel.[4] Agents such as kaolin or chitosan enhance coagulation (Scheme 1) through activation of either the contact pathway or platelet adhesion. Kaolin and chitosan are useful as field therapeutics for management of external hemorrhage and are widely utilized by military forces as a first-response treatment.[5] Unfortunately, use of these agents may be associated with further damage to some body tissues.[6] Furthermore, these compounds cannot be administered systemically and therefore lack utility for internal injuries with an intrinsic non-compressible hemorrhage.

Recombinant human Factor VIIa (rFVIIa) is currently licensed for the management of bleeding episodes in patients with hemophilia (hemophilia A or B and acquired hemophilia), congenital factor VII deficiency, Glanzmann thrombasthenia, and certain cases of warfarin overanticoagulation. Off-label use of rFVIIa is also commonly seen in certain other hemorrhagic conditions.[7] Although anecdotal reports of clinical response abound, a significant number of concerns regarding safety remain, due to the thrombotic complications that have been reported.[7] Field use is also limited because of drug storage requirements and the extreme cost of recombinant protein medication.[8]

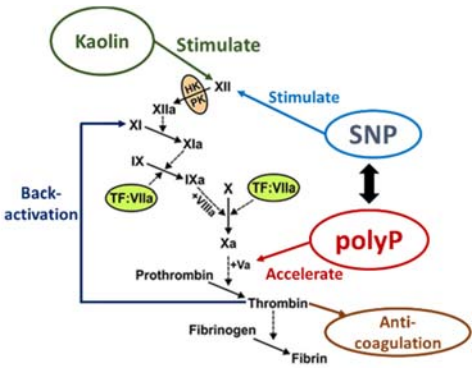

Scheme 1. Simplified coagulation cascade. SNP surface induces the activation of FXII, while short-chain polyP enhances the rates of activation of FV and FXI leading to an earlier thrombin burst. Rapid thrombin generation

Damien Kudela, Anna May-Masnou, Alessia Pallaoro, Chi K. Nguyen, Sara Nownes, Tracy Chuong, Riley Allen, Prof. Galen D. Stucky
Department of Chemistry and Biochemistry,
University of California, Santa Barbara
Santa Barbara, CA 93106, USA
E-mail: dkudela@chem.ucsb.edu, stucky@chem.ucsb.edu
Stephanie A. Smith, Prof. James H. Morrissey
Department of Biochemistry, College of Medicine
University of Illinois at Urbana-Champaign
Urbana, IL, 61801 USA
E-mail: jhmorris@illinois.edu
Anna May-Masnou
Departament d'Enginyeria Química
Universitat de Barcelona
c/ Martí i Franquès, 1-11, 08028, Barcelona, Catalunya, Spain
Gary B. Braun
Sandford-Burnham Medical Research Institute
10901 North Torrey Pines Road, La Jolla, CA 92037, USA
Nicholas R. Parker
Department of Mechanical Engineering
University of California, Santa Barbara
Santa Barbara, CA 93106, USA
Prof. Hooman H. Rashidi
Department of Pathology & Laboratory Medicine
University of California, Davis
Sacramento, CA 95817, USA
Prof. Galen D. Stucky
Materials Department
University of California, Santa Barbara
Santa Barbara, CA 93106, USA

[**] This work was funded by the U.S. Army Medical Research and Material Command under Contract Number WQ81XWH-11-2-0021, by the U. S. Army Medical Research & Materiel Command and the Telemedicine & Advanced Technology Research Center under Contract Number W911NF-10-2-0114, and by NIH grant R01 HL047014. The MRL Shared Experimental Facilities are supported by the MRSEC Program of the NSF under Award No. DMR 1121053; a member of the NSF-funded Materials Research Facilities Network. A.M.-M. thanks the Spanish MINECO for financial support within the framework of the project number CTQ2011-29336-C03-02.

Supporting information (SI) for this article: experimental details describing the synthesis and characterization of all new compounds as well as clotting assays conducted.

leads to back-activation of FXIa, accelerating the coagulation cascade, as well as facilitating increased activity in the anticoagulation pathway, which is designed to limit the spread of coagulation to uninjured vessels. Kaolin acts only to activate FXII via the intrinsic pathway.

The ideal agent to control non-compressible hemorrhage in the prehospital setting would have the following properties: (1) long shelf-life and stability in weather extremes, (2) reasonable cost, (3) promote key functions of the blood clotting system at the injury site including coagulation, regulatory anti-coagulation and fibrin formation,(4) lack of off-target adverse effects. Such an agent could initiate treatment during the transport phase when the patient is at the greatest risk for exsanguination. We propose that targeted short-chain polyphosphate-laden silica nanoparticles (polyP-SNPs) have the potential to fulfill these requirements.

Because it accelerates rather than initiates endogenous coagulation enzyme production, short-chain polyP is a reasonable candidate for the management of hemorrhage.[9] Delivery of a polyP payload on a nanoparticle carrier could potentially be optimized to target the site of injury while minimizing the impact on the systemic circulation. Effective targeting and control would in theory minimize the risk of thrombotic complications that limit procoagulant therapy. In addition to the potential for better biosystem safety, the cost of production is low for polyP (as compared to that of recombinant proteins). Upon attachment to inorganic oxides, polyP also has the potential for long-term stability under a variety of storage conditions.

In response to an injury, human platelets secrete short-chain polyP of approximately 60-100 monomers. Platelet-secreted polyP has a variety of wound-healing therapeutic effects, including enhanced activation of factors XI and V, which ultimately leads to enhanced factor X activity, and limitation of the activity of tissue factor pathway inhibitor, which results in accelerated thrombin generation.[10] The clot strength and character can be measured and evaluated using common clinical assays such as thromboelastography (TEG) since the incorporation of polyP also impacts clot structure and leads to resistance to fibrinolysis.[11] Due to a ~90 minute half-life in plasma, the procoagulant effects are temporally limited.[10-12] This endogenous metabolism of polyP offers much better biocompatibility than currently available agents such as kaolin, which are not metabolized.

While long-chain polyP is a potent activator of the contact pathway, short-chain polyP molecules such as those released from platelets have relatively poor capacity to activate factor XII.[9] We employed relatively short-chain polyP for these studies in order to maximize the enhancement of downstream coagulation enzymatic steps (common pathway), while minimizing the ability to activate the contact pathway.

As noted above, in the in vivo trauma environment, platelets serve as a polyP delivery agent, secrete procoagulants and clotting factors that promote blood coagulation, and initiate the formation of a clot-dissolving enzyme that degrades blood clots during the healing process. In our studies following up on the extensive research originally carried out by the Morrissey group,[9-12] we use free polyP as a benchmark. In the research we report here, delivery agent bifunctionality is introduced by using silica nanoparticles as a procoagulant carrier for the polyP.

Silica is generally considered to be a non-toxic material, and it is often used in drug delivery studies.[13] However, due to its negative surface charge, silica is also a contact activator.[5a,14] Consequently, the ideal construction of a polyP-bearing silica nanoparticle would shield the silica from exposure to the systemic circulation, with targeting and exposure of the silica carrier surface and polyP at the site of internal hemorrhage. Current materials used for treating external hemorrhage generally contain particles in the micrometer range, which are too large to easily traverse capillaries and unsuitable for use as intravenous therapeutics.[15] We consequently developed an approach for the synthesis of 50 - 100 nm diameter particles (Fig. 1L, Table 1).[5a,15]

In order to attach the highly anionic polyP to an oxide, we followed the model of Lorenz et al. who used zirconia, which like silica has a negative surface potential, as the scaffold for applications in protein separation and purification.[16] This strategy of attachment exploits the Lewis acid properties of an oxide surface to bind polyP, overcoming the electrostatic repulsion.[17]

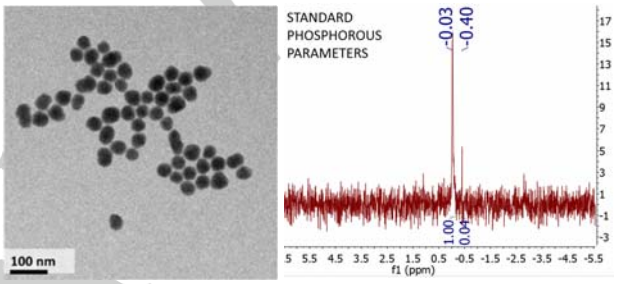

Figure 1. (Left) TEM images of polyP-SNPs; (Right) ^{31}P NMR spectrum of digested polyP-SNPs shows evidence of phosphorous.

^{31}P NMR and surface charge change qualitatively demonstrated polyP attachment. PolyP-SNPs were digested in acid to break down polyP into phosphate monomers. ^{31}P NMR tests on the digested sample detected the presence of phosphorous. The change in surface charge also suggested the presence of polyphosphate in undigested polyP-SNP (Table 1, SI Fig. 2). At physiological pH in phosphate buffered saline solution (PBS), both SNPs and polyP display a negative surface charge. In deionized water, the SNP surface charge ranged from -15 to -25 mV (Table 1, SI Fig. 2R). In simulated body fluid (SBF) at physiological pH, SNPs had a surface charge of -50 to -60 mV. PolyP is negatively charged at physiologic pH due to a pKa1 between pH 1-2 (for all internal phosphates) and pKa2 between pH 7.2 and 8.2 (for the two terminal phosphates).[18] Upon functionalization of polyP to the SNP surface, the zeta potential of the polyP-SNP decreased from -20 to -30 mV to roughly -40 to -50 mV in water, confirming the attachment of the polyP. In SBF, both particles exhibited a strongly negative charge below -45 mV.

In order to quantify the amount of polyP loaded on the surface, the digested phosphate solutions were measured using both a malachite green assay and inductively coupled plasma atomic emission spectroscopy (ICP-AES). Malachite green identified concentrations of 56, 26, and 23 nmol PO_3/mg SNP. ICP-AES determined the 26 nmol PO_3 sample had 29.6 nmol PO_3/mg SNP. Assuming each polyphosphate chain has 70 phosphate monomers, these values suggest that 100 – 200 polyphosphate molecules are attached to each silica nanoparticle.

Table 1. The zeta potential and surface charge of the particles change when dispersed in water or phosphate buffered saline solution, pH 7.4.

Compound, Medium [a]	Zeta Potential (μV)	Size (nm)
SNP, H_2O	-24.4 ± 0.3	55.97 ± 2.19
SNP, PBS	-52.5 ± 2.1	74.00 ± 6.24
PolyP-SNP, H_2O	-44.3 ± 0.3	53.79 ± 1.75
PolyP-SNP, PBS	-52.0 ± 3.2	78.18 ± 2.86

By not using tissue factor to initiate clotting, we focused our clotting assays on the intrinsic or contact activation pathway. Negatively charged particles are expected to activate the contact pathway, such as the aluminosilicate kaolin (QuikClot® Combat Gauze™) used to activate the contact pathway for external injuries.[4,5a] Because it is a poor clot initiator, polyP attachment shields SNPs in the systemic circulation, which is beneficial for use to control haemorrhage intravenously. We measured the impact of both bare SNPs and polyP-SNPs on clot time using thromboelastography (Fig. 2T, SI Fig. 4, 5) on pooled normal plasma (PNP). Both particles decreased the time to initial clot formation (R) in a concentration-dependent manner, with polyP-SNP being more potent at concentrations below 0.5 mg/mL. The clot time reported in figures 2 and 4 refers to the time to initial clot formation, which is key in illustrating how polyP-SNP successfully accelerates clotting. The agent used did not affect the overall clot size formed, only the time required to reach peak clot size. However, polyP has previously been shown to improve overall clot formation, in part by limiting the effect of fibrinolysis.[11-12]

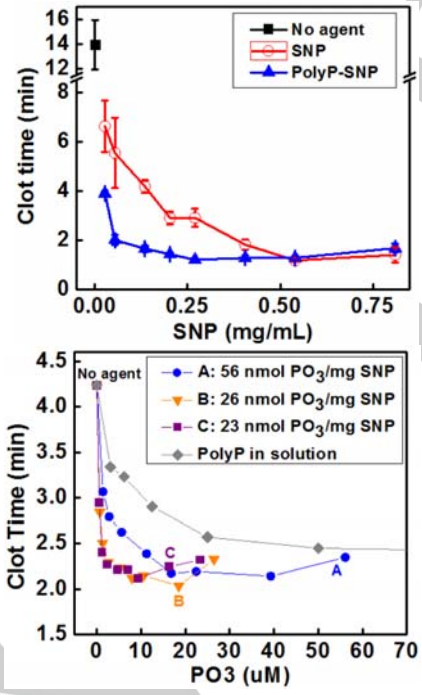

Figure 2. (Top) PolyP-SNP cuts clot time (R value using TEG) roughly in half versus SNP below 0.3 mg/ml. (Bottom) PolyP loaded onto silica lowers clot time compared to bare polyP when measured by fibrometry.

Next we evaluated the procoagulant activity of polyP-SNPs formed with differing loads of polyP. The ability to promote coagulation was measured by adding polyP-SNP or polyP in solution to PNP. Coagulation was evaluated by measuring time to clot formation on a fibrometer (Fig. 2B). In comparing polyP payload, polyP-SNPs were more potent at activating the contact pathway than polyP in solution.

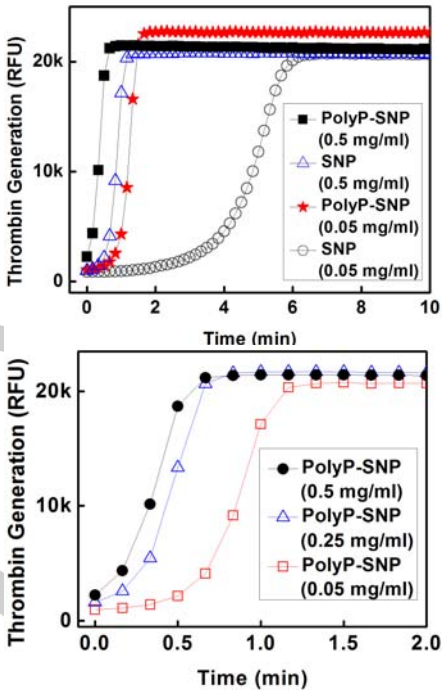

Figure 3. (Top) Thrombin generation is more rapid with polyP-SNP than bare SNP. (Bottom) polyP-SNPs are able to generate a rapid thrombin burst even at low concentrations. Thrombin generation is measured using a thrombin-sensitive fluorescent dye.

In order to further explore the relative activities of our materials, we evaluated the ability of the materials to generate thrombin, the terminal enzyme of the coagulation cascade and the primary determinant of the rate of fibrin formation.[9a] PolyP-SNP again substantially outperformed its bare counterpart (Fig. 3T).

We next evaluated whether polyP-SNPs were able to enhance the generation of downstream coagulation enzymes (common pathway). We eliminated any potential impact on contact activation by utilizing factor XII-deficient plasma and initiating coagulation using a small amount of relipidated tissue factor (LTF, 63 pM). As expected, bare SNPs did not shorten thromboelastography clot time in this system (Fig. 4T). In contrast, the time to physical clot formation was shortened by polyP-SNP. This indicates that the polyP is accessible for binding to the relevant downstream coagulation proteins. Additionally, this response could also be evaluated and measured in the clinical setting by comparing certain pre and post bleed coagulation tests such as prothrombin time (PT), partial thromboplastin time (PTT) and factor Xa that are readily available in most clinical settings.

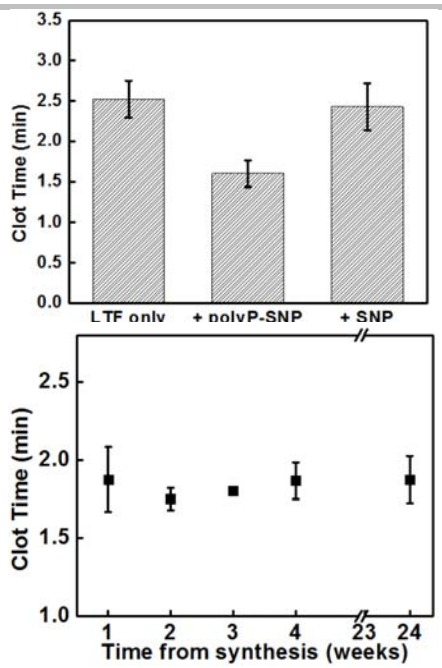

Figure 4. (Top) Adding PolyP-SNP to LTF shortens clot time in FXII-deficient plasma compared to LTF only or LTF + SNP. LTF required to initiate clotting. (Bottom) PolyP-SNP suspended in aqueous solution retains its procoagulant function after weeks of storage at ambient conditions.

One of the problems facing emergency medical personnel is that current intravenous treatments have a significantly short half-life at ambient temperature. Even pure polyP nanoparticles remain stable for hours.[9b] In comparison, attaching polyP to silica greatly enhanced the stability and procoagulant function of polyP from hours to weeks. After bench-top storage at room temperature in both powder and aqueous suspensions, polyP-SNP clotting times remained constant for weeks (Fig. 4B). The strong negative surface charge of polyP-SNPs also minimized aggregation in aqueous suspensions over the same time period. Injectable drugs with long-term shelf-life can be used by emergency medical personnel prior to hospital arrival without concern that the particles will degrade without refrigeration. This suggests that the polyP-SNP system may be the first prehospital intravenous injection designed to treat internal injuries by accelerating the clotting system at bleeding sites.

In this study, we successfully attached polyP to the surface of small-diameter SNPs and demonstrated that these polyP-SNPs are more potent than bare SNPs at promoting coagulation, likely due to polyP's ability to accelerate the common pathway for active clotting processes. PolyP-SNPs, like polyP in solution, are able to enhance downstream coagulation reactions resulting in a shorter time to clot formation. Even after long-term storage at regular room temperature, the polyP-SNP system retained its procoagulant ability. The polyP-SNP construct is consequently promising as a prohemostatic agent. While the studies reported here described polyP-SNPs, other polyP-bearing nanoparticles that are intrinsically non- or anti-contact activating are also under investigation by our group. Further exploration of methods to limit contact activation *in vivo* will be necessary for use as a systemic agent.

Keywords: hemorrhage • polyphosphate • silicates • nanoparticles • trauma

[1] a) J.B. Holcomb, N. R. McMullin, L. Pearse, J. Caruso, C. E.Wade, L. Oetjen-Gerdes, H. R. Champion, M. Lawnick, W. Farr, S. Rodriguez, F. K. Butler, *Ann. Surg.* **2007**, *245*, 986–991; b) R. F. Bellamy, *Mil. Med.* **1984,** *149*, 55–62; c) H. R. Champion, R. F. Bellamy, C. P. Roberts, A. J. Leppaniemi, *Trauma* **2003**, *54*, S13-S19.

[2] R. Pfeifer, I. S. Tarkin, B. Rocos, H.-C. Pape, *Injury* **2009**, *40*, 907–911.

[3] P. I. Johansson, J. Stensballe, *Transfusion* **2010**, *50*, 701–710.

[4] B.S. Kheirabadi, I. B. Terrazas, M. A. Hanson, J. F. Kragh Jr., M. A. Dubick, L. H. Blackbourne, *J. Trauma. Acute. Care. Surg.* **2013**, *74*, 1260-1265.

[5] a) S. E. Baker, A. M. Sawvel, N. Zheng, G. D. Stucky, *Chem. Mater.* **2007**, *19*, 4390-4392; b) D. Johnson, B. Gegel, J. Burgert, J. Gasko, C. Cromwell, M. Jaskowska, R. Steward, A. Taylor, *ISRN Emergency Medicine.* **2012**, *2012*, 927678.

[6] a) B. G. Kozen, S. J. Kircher, J. Henao, F. S. Godinez, A. S. Johnson, *Acad. Emerg. Med.* **2008**, *15*, 74–81; b) Y. Li, A. M. Sawvel, Y.-S. Jun., S. Nownes, M. Ni, D. Kudela, G. D. Stucky, D. Zink, *Toxicol. Res.* **2013**, *2*, 136–144; c) P. D. Bowman, X. Wang, M. A. Meledeo, M. A. Dubick, B.S. Kheirabadi, *J. Trauma* **2011**, *71*, 727-732.

[7] J. F. Barletta, C. L. Ahrens, J. G. Tyburski, R. F. Wilson, *J. Trauma* **2005**, *58*, 646–651.

[8] P. M. Mannucci, M. E. Mancuso, E. Santagostino, *Blood*. **2012**, *119*, 4108-4114.

[9] a) S. A. Smith, S. H. Choi, R. Davis-Harrison, J. Huyck, J. Boettcher, C. M. Rienstra, J. H. Morrissey, *Blood* **2010**, *116*, 4353–4359; b) A. J. Donovan, J. Kalkowski, S. A. Smith, J. H. Morrissey, Y. Liu, *Biomacromolecules.* **2014**, DOI: 10.1021/bm501046t

[10] S. A. Smith, J. H. Morrissey, *J. Thromb. Haemost.* **2008**, *6*, 1750–1756.

[11] S. A. Smith, J. H. Morrissey. *Blood.* **2008**, *112*, 2810-2016.

[12] S. A. Smith, N. J. Mutch, D. Baskar, P. Rohloff, R., Docampo, J. H. Morrissey, *Proc. Natl. Acad. Sci. U.S.A.* **2006**, *103*, 903–908.

[13] a) V. Cauda, H. Engelke, A. Sauer, D. Arcizet, C. Brauchle, J. Radler, T. Bein, *Nano Lett.* **2010**, *10*, 2484–2492; b) D. Tarn, C. E. Ashley, M. Xue, E. C. Carnes, J. I. Zink, C. J. Brinker, *Acc. Chem. Res.* **2013**, *46*, 792-801.

[14] J. Margolis, *J. Exp. Biol.* **1961**, *39*, 249–258.

[15] N. Singh, A. Karambelkar, L. Gu, K. Lin, J. S. Miller, C. S. Chen, M. J. Sailor, S. N. Bhatia, *J. Am. Chem. Soc*. **2011**, *133*, 19582-19585.

[16] B. Lorenz, Marmé, S., Müller, W. E. G., Unger, K., Schröder, H. C, *Anal. Biochem.* **1994**, 216, 118–126.

[17] W.-C. J. Wei, S.-C. Wang, F.-Y. Ho, *J. Am. Ceram. Soc.* **1999**, *82*, 3385–3392.

[18] A. Lee, G. M. Whitesides, *Anal. Chem.* **2010**, *82*, 6838-6846.

[19] a) T. Myles, T. H. Yun, S. W. Hall, L. L. K. Leung, *J. Biol. Chem*. **2001**, *276*, 25143-25149; b) Y. Xiao, A. A. Lubin, A. J. Heeger, K. W. Plaxco, *Angew. Chem. Int. Ed.* **2005**, *44*, 5456–5459.

Entry for the Table of Contents

COMMUNICATION

Current hemorrhage treatments are designed to clot upon exposure to blood. Safety concerns over the spread of therapeutics to healthy vessels limit such use. The use of agents such as polyphosphate that accelerate rather than initiate clotting (figure) have the potential to retain efficacy while minimizing safety concerns in treating haemorrhage.

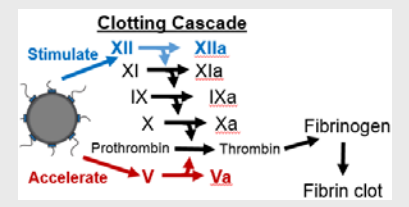

D. Kudela, S.A. Smith, A. May-Masnou, B. Braun, A. Pallaoro, C.K. Nguyen, T. Chuong, S. Nownes, R. Allen, H.H. Rashidi, N.R. Parker, J.H. Morrissey and G.D. Stucky

Page No. – Page No.

Clotting activity of polyphosphate functionalized silica nanoparticles